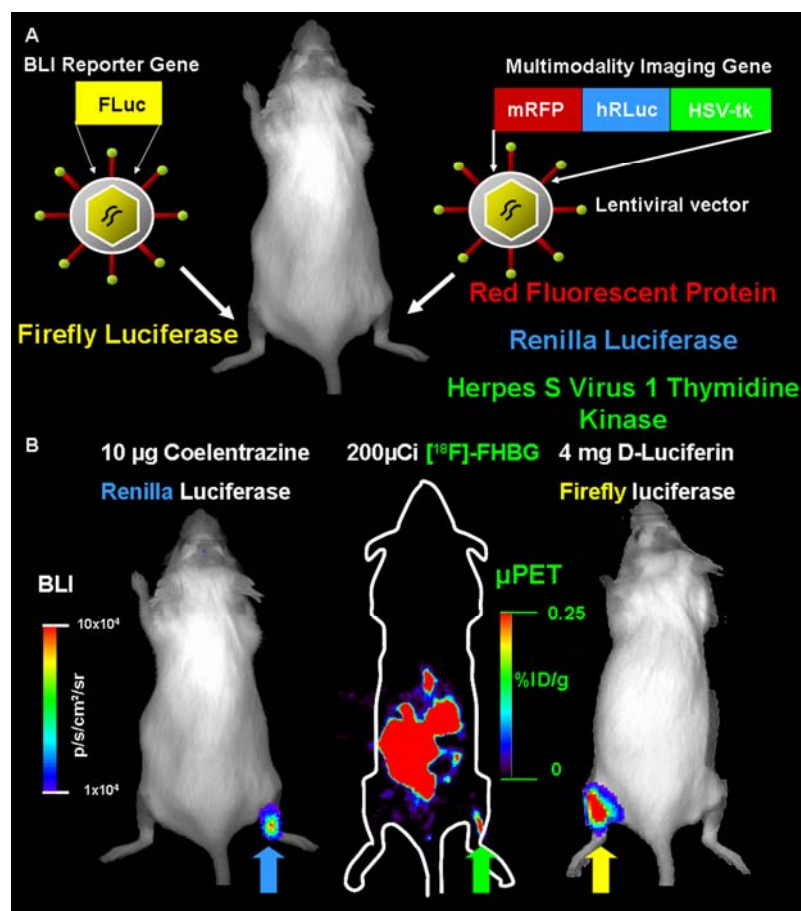


Molecular Imaging of Lentiviral Vector-Mediated Reporter Gene Expression with Positron Emission Tomography and Bioluminescence Imaging



Christophe Deroose

Promotor: Prof. Dr Ir Luc Mortelmans
Co-Promotor: Prof. Dr Zeger Debyser
Co-Promotor: Prof. Dr Veerle Baekelandt

Thesis submitted in fulfillment of the requirements for the degree of
"Doctor in Medical Sciences"
Leuven, 2007



Katholieke Universiteit Leuven

Faculteit Geneeskunde

Departement Medisch Diagnostische Wetenschappen,

Afdeling Nucleaire Geneeskunde &

Departement voor Moleculaire en Cellulaire Geneeskunde,

Afdeling Moleculaire Geneeskunde

**Molecular Imaging of Lentiviral Vector-Mediated
Reporter Gene Expression with Positron Emission
Tomography and Bioluminescence Imaging**

Christophe Deroose

Promotor: Prof. Dr Ir Luc Mortelmans

Co-Promotor: Prof. Dr Zeger Debyser

Co-Promotor: Prof. Dr Veerle Baekelandt

Thesis submitted in fulfillment of the requirements for the degree of
"Doctor in Medical Sciences"
Leuven, October 2nd 2007

Dankwoord

Modern neuroscience has learnt us that the time needed to process new information and to react upon it is about 800 to 1500 milliseconds. So when Prof. Mortelmans proposed me to defend a PhD thesis in the course of my nuclear medicine residency, I had an answer some 1520 milliseconds later... a firm yes. The extra 20 milliseconds were probably spent on a thorough assessment of this choice that would shape the coming 6 years. I had always been fascinated by the insights that science provides us and it seemed a great journey to quit being a bystander and actively participate in the effort. Prof Mortelmans has been a great guide all along the way and he has helped me through all obstacles that we encountered, be it scientific, organisational, financial, clinical or grant writing. I thank him for his expert advice and for his continuous support. I will always be grateful to him for offering me this opportunity and making it into a very satisfying experience.

My first scientific steps were performed in the lab of a truly extra-ordinary man, Prof Sanjiv "Sam" Gambhir. Although his kindness and hospitality are boundless, it will be his scientific excellence that will stay graved in my memory. The atmosphere of the Gambhir lab was an intellectual fest. Never have I met anybody who could invent so much work in so little time: one hour of discussion and I knew what to do in the next few months. The fried ants was my most original meal in Sam's company and the fishing trip hunting for a new red luciferase was the nicest field work. But the most precious thing was the continuous teaching of scientific method and reasoning, the art of interpreting results and most of all the critical spirit that is so crucial for scientific research. I would also like to express my gratitude to Aruna Gambhir who has been a very kind and gentle host on many occasions. Thanks for this wonderful time!

Terug in België kon ik voor mijn wetenschappelijk werk terecht in het lab van mijn co-promotoren, Profs Zeger Debyser en Veerle Baekelandt. Vanaf mijn eerste gesprek met Zeger – nog voor ik naar Californië vertrok - was ik onder de indruk van het enthousiasme waarmee ons voorstel onthaald werd en ik was dan ook dolgelukkig dat ik een co-promotor (en bijhorend lab) gevonden had. De periode in jullie lab was een prachtige ervaring. Jullie enthousiasme en gedrevenheid stuwden de steeds groter wordende groep vooruit. Wetenschappelijke excellentie was het doel, maar zonder de menselijke kant weg te cijferen. Van brainstorm tot labweekend, van labvergadering tot IWT oefensessie, altijd was er tijd voor een humoristische noot in het werk. Bedankt voor de ondersteuning, het vertrouwen, het geloof in de projecten en jullie inzet.

I want to thank the members of my jury, Prof. Serge Goldman, Prof. Roland Hustinx, Prof. Koen Van Laere and Prof. Thierry Vandendriessche for the critical reading and the opportunity to improve this manuscript.

Many people in the Gambhir lab have helped me both on a scientific level and with the life outside the lab. Thanks, Zac Walls, for the patient teaching of cell culture and molecular biology techniques, the book chapter we spent so many evenings writing, the many "24" episodes and my worst sun burn ever on our Sierra Nevada ski trip. He also learnt me to appreciate the specific "couleur locale" of cities hosting scientific congresses. Andy Loening helped me a lot with visualisation software, critical discussions and finally by

taking me in as a roommate. Shahriar Yaghoubi, it was great to benefit from your guidance and to have you as a friend. Pritha Ray and Abhijit De, thanks for the help with the TK assays, the DNA constructs, the lentiviral cell transductions and my first tumor inoculations. Paulmurugan Ramasamy, I would like to thank you for your help with the cloning of the constructs. John Min and Frank Berger, thanks for introducing me to the digital autoradiography world. Patrick Chow, thanks for explaining the CT scanner and programming the desired reconstruction algorithms. Judy Edwards and Waldemar Ladno, thanks for your help with the tracer injections and the PET scans. David Stout, you were always available for helping me with imaging hardware, developing mobile anesthesia carts, archiving problems and most importantly for getting me slots on the microPET. Prof. Arion Chatzioannou, thanks for your guidance with the multiple physical aspects of the combined PET/CT imaging. Manish Patel and Ian Chen, thanks for hanging around in the lab so late at night, it was great to have some company and to go for midnight meals. Joe Wu, Meera Iyer, Junie Hildebrandt, Tarik Massoud, Xiaoman Lewis and Globalakrishnan Sundaresan, thanks for all your help and discussions. Thanks also to Prof. Anna Wu and her lab members Tove Olafsen and Vania Kenanova.

The move to Stanford brought some other people on the radar that have helped me throughout this PhD. First of all, thanks to Virginie, at the time my future sister-in-law. You brought a good mix of healthy food, Belgian friends and evening decompression into my stay. Tim Doyle and Dirk Mayer, thanks for the “happy imaging” support. Murugesan Subarrayan and Zhen Cheng, thanks for the many tracer syntheses. Maaïke Schipper and Paramanaban Padmanabhan, thanks for the discussions. Olivier Gheysens, ook al was je er maar een maand, het was zowel op als naast het werk één van de meest intense. Bedankt voor de altijd boeiende gesprekken.

De MolVirGenners hebben een cruciale rol gespeeld eens ik terug in België was. Ik ben hun allen zeer dankbaar voor de aangename sfeer in het lab, de vele antwoorden bij alle mogelijke en onmogelijke problemen die ik ondervonden heb, de onbaatzuchtige hulp die ik zo vaak gekregen heb.

Veerle Reumers, het was een plezier om met jou zo intens samen te werken. Jouw handigheid bij het opereren van de muizen, jouw werklust en jouw enthousiasme zijn een doorslaggevende factor geweest voor het Leuvens BLI project. Ondanks jouw enthousiasme was jij de grootste criticus van ons werk en na de vele discussies over de data kon ik gerust zijn: als Veerle overtuigd is kunnen we er mee naar buiten komen.

Rik Gijsbers, bij jou kon ik steeds terecht voor een vraagje over de vectoren of over de meest obscure details in om het even welk moleculair biologisch protocol. Bedankt voor alle FACS stalen en voor de ontelbare keren dat jij back-up wou spelen voor mijn cellen. Abdelilah Ibrahim, bedankt voor jouw hulp om de imaging core mee uit te bouwen en voor alle hulp met de cellen toen ik opnieuw in de kliniek werkte. Chris Van Den Haute, bedankt voor de hulp met de RT-PCR en andere procedures. Het weekendwerk was altijd een stuk aangenamer als je ook in het lab was. Martine Geraerts, bedankt voor jouw hulp in de wondere wereld van de neurale stamcellen.

Bedankt ook aan Bénédicte Van Maele, Jan De Rijck, Linos Vandekerckhove, Frauke Christ, Wannes Thys, Jaan Toelen, Melissa McNeely, Katrien Busschots, Melanie Gerard, Isabelle Nefkens, An Nijs, Myriam Witvrouw, Barbara Van Remoortel, Jelle Hendrix, Arnout Voet, Christiane Duportail, Koen Bartolomeeusen, Linda Vercammen, Erwin Lauwers, Kirsten Paesen, Nadia Beelen, Anke Vanderperren, Bavo Heeman, Barbara Podessu, Bruno Hoste, Sarah Schreurs, Jessica Meuis, Vladislav Cucak en Peter Bogaerts en Veronique Daniels, Jean-Marc Taymans, Kristel Eggermont en Nam-Joo Van Der Veken.

Frea Coun, Martine Michiels, Sofie Willems, Irina Thiry en Lies Dekeyser wil ik nog eens in de bloemetjes zetten voor alle vectoren die ze hebben gemaakt en voor de excellente technische ondersteuning.

Anke Hantson, Leen Hombrouck, Jaan Toelen, Olga Krylychkina, Greetje Vandevelde, Nathalie Wellens, het was fijn om met jullie de bureau te delen. Bedankt voor de vele discussies, de boeiende wetenschappelijke theorieën en de gezellige sfeer. Caroline Vandeputte, het was een plezier om met jou samen te werken.

Voor het radiofarmaceutisch luik heb ik de voorbije jaren een zeer vlotte en aangename samenwerking achter de rug met het laboratorium van Prof. Verbruggen en Prof. Bormans. Bedankt voor jullie hulp en enthousiasme voor ons project. Satish Chitneni, you have been a very talented and reliable radiopharmacist. You have been a crucial player in the development of the new radiotracers. It was a great pleasure working with you and eagerly waiting by the wellcounter to get the results of a day's work. Sofie Celen, bedankt voor de vlotte samenwerking voor de LacZ tracers. Ook Bert Vanbilloen, Dominique Vanderghinste en Tjibbe De Groot wens ik te bedanken voor hun hulp. Dirk Rattat, you have done a great job keeping the football team together, providing me with some useful decompression time.

Prof. Jan Balzarini wens ik te bedanken voor de vlotte samenwerking en de boeiende discussies.

Peter Vermaelen, jij ben een grote hulp geweest voor alle microPET scans die we in de loop van deze jaren uitgevoerd hebben. Bedankt hiervoor. Aan onze samenwerking bij het ontwerpen van de MoSAIC heb ik de grootste voldoening overgehouden.

Voor de beeldverwerking kon ik een beroep doen op Prof. Johan Nuyts, die steeds bereid was om onze nieuwe ideeën om te zetten in gebruiksvriendelijke software. Patrick Dupont, Stefaan Vleugels, Kristof Baete en Michel Koole, bedankt voor alle IT ondersteuning.

Alle medische stafleden van onze dienst nucleaire geneeskunde, waarvan ik Prof. Stroobants en Prof. Mottaghy nog niet vermeld heb, wens ik te bedanken voor de boeiende werkomgeving waar ik tijdens het klinisch werk heb mogen vertoeven. Ook onze technologen wens ik te bedanken voor hun dagelijkse inzet.

Mijn collega's assistenten van de dienst nucleaire geneeskunde ben ik een dikke pluim verschuldigd voor al die keren dat ze voor mij hebben ingesprongen. Lieselot Brepoels, Olivier Gheysens, Raf Verscuere, Karolien Goffin, Eduard D'Hondt, Jelle Van Riet, Sylvia Deryck, Gerard Moulin-Romsee en Alexandra De Waele, bedankt voor jullie flexibiliteit en de aangename sfeer in de dokterskamer.

Francine Reniers, Marie-Louise Vandegaer, Leen Luyts en Brigitte Verheyden: ik heb nooit gearzeld om bij jullie administratieve steun te gaan zoeken, bedankt voor al hetgeen jullie voor mij gedaan hebben.

I would like to acknowledge the institutions that have helped me with financial support during this thesis, the Fonds voor Wetenschappelijk Onderzoek – Vlaanderen (FWO) and the Belgian American Educational Foundation (BAEF) in collaboration with the King Baudouin Foundation.

Tijdens deze thesis heb ik ook het genoegen gehad om op andere wetenschappelijke projecten te werken. Hans Prenen, Wim Maes, Adriana Bastidas-Zambrano, Sarah Denayer, Julian Aragones, Prof. Peter Carmeliet, Prof. Lieve Moons, Prof. Catherine Verfaillie, Prof. Stefan Janssens, Prof. Frank Claessens en Prof. Rik Lories, bedankt voor jullie bijdrage aan mijn wetenschappelijke vorming.

We verlaten nu het domein van de exacte wetenschappen voor een ander gebied, dat van de onvoorwaardelijken. Voor jullie zijn geen experimenten nodig, er is geen bewijslast vereist, de beurzen blijven eeuwig lopen en rede is van geen tel meer, er is enkel vriendschap en liefde. Bedankt mama, papa en Binne, ik heb altijd en overal op jullie kunnen rekenen, ik besef maar al te goed wat een geluk dit is.

Mijn trouwe vrienden en lieve familie, ik heb jullie in de loop van deze thesis vaak in de steek gelaten omdat de wetenschap zijn eisen stelde, ik hoop in de toekomst meer tijd voor jullie te maken.

Je tiens aussi à exprimer ma gratitude envers mes beaux-parents qui nous ont très généreusement aidés dans tous les domaines et nous ont permis de combiner notre vie professionnelle avec l'arrivée de notre petite Emilie.

Emilie, misschien lees je dit ooit, bedankt voor alle vreugde die je uitstraalt!

Me voilà à la dernière personne que je dois remercier, ma femme Isabelle. Je pourrais dire... Oh ! Dieu !... bien des choses en somme... En variant le ton, ... mais malheureusement, la place est limitée à cet endroit. Merci d' avoir eu la gentillesse de me soutenir quand j'étais aux Etats-Unis, même si cette séparation n'était pas facile pour nous. Je te remercie pour ton soutien contre vents et marées, pour ta foi en moi quand les cellules et souris ne faisaient pas ce qu' elles devaient, pour ta patience quand les expériences au labo avaient une fois de plus débordé de quelques heures, pour les weekends où je te désertais pour nourrir mes cellules au labo. Merci pour ton inspiration et pour la joie que tu me donnes chaque jour. Tu m' as donné une magnifique petite fille qui a comblé bien plus que mes attentes les plus optimistes. C'est à toi que je dédie ce travail.

Brussel, September 2007

Table of Contents

<i>Dankwoord</i>	<i>1</i>
<i>Table of Contents</i>	<i>5</i>
<i>Abbreviations</i>	<i>9</i>
Chapter 1: General Introduction	13
1. Imaging Modalities	14
1.1. Radionuclide Imaging Techniques	15
1.1.1. Single Photon Emission Computed Tomography (SPECT)	15
1.1.2. Positron Emission Tomography	16
1.2. Magnetic Resonance Imaging and Spectroscopy	16
1.2.1. Magnetic Resonance Imaging (MRI)	16
1.2.2. Magnetic Resonance Spectroscopy (MRS)	17
1.3. Optical Imaging Strategies	17
1.3.1. Fluorescence Imaging	18
1.3.2. Bioluminescence Imaging	18
2. Reporter Gene Concept and Existing Imaging Reporter Genes	19
2.1. Radionuclide Imaging Techniques	20
2.1.1. The Herpes Simplex Virus Thymidine Kinase Reporter System	20
2.1.2. Other Enzymatic Reporter Genes	22
2.1.3. Receptor Reporter Genes	22
2.1.4. Transporter Reporter Genes	23
2.2. Optical Imaging Techniques	25
2.2.1. Bioluminescence Imaging Reporter Genes	25
2.2.2. Fluorescence Imaging Reporter Genes	27
2.3. Magnetic Resonance Techniques	28
2.3.1. Magnetic Resonance Spectroscopy Reporter Genes	28
2.3.2. Magnetic Resonance Imaging Reporter Genes	30
3. Vectors for Gene Transfer	32
3.1. Oncoretroviral Vectors	34
3.2. Lentiviral Vectors	34
3.2.1. Molecular Biology of Lentiviral Vectors	35
3.2.2. Lentiviral Vector Biosafety	36
3.2.3. Improvements in Lentiviral Vector Design	37
3.2.4. Applications of Lentiviral Vectors	39
3.3. DNA Containing Viral Vectors	40
3.3.1. Adenoviral Vectors	40
3.3.2. Adeno-Associated Viral Vectors	40
3.3.3. Herpes Simplex Virus Type-1 Vectors	42
3.4. Non-Viral Vectors for Gene Delivery	42
3.4.1. Physical Methods	43
3.4.2. Chemical Methods	43
Chapter 2: Objectives	45
Chapter 3: Materials & Methods	47
1. Radiotracer Synthesis	47
2. Cell Culture and Lentiviral Vector Production	48
2.1. Cell Lines and Culture Conditions	48
2.2. Lentiviral Vector Transfer Plasmid Construction	49
2.3. Lentiviral Vector Production	50
2.4. Cell Transduction	51
3. Detection of Reporter Gene Expression	51

3.1.	Western Blot	51
3.2.	Flow Cytometry Analysis of eGFP Expression	52
3.3.	Bioluminescence Measurement in Living Cells	52
3.4.	<i>In Vitro</i> Firefly and <i>Renilla</i> Luciferase Activity Assay	52
3.5.	Herpes Simplex Virus type 1 Thymidine Kinase Activity Assay	53
4.	Cell Experiments	53
4.1.	Radiotracer Uptake Experiments	53
4.2.	High Pressure Liquid Chromatography (HPLC)	54
5.	Creation of Animal Models	54
5.1.	Inoculation of Lentiviral Vector in Mice and Rats	55
5.2.	Inoculation of Tumor Cells	55
6.	Small Animal Imaging Procedures	56
6.1.	<i>In Vivo</i> Bioluminescence Imaging of Firefly Luciferase Activity and Image Analysis	56
6.2.	<i>In Vivo</i> Bioluminescence Imaging of <i>Renilla</i> Luciferase Activity and Image Analysis	57
6.3.	Combined Positron Emission Tomography – Computed Tomography Procedure	57
6.4.	Image Fusion and Quantitative Analysis	58
6.5.	Positron Emission Tomography Imaging	59
7.	Ex vivo Confirmation Studies	59
7.1.	Histology and Stereological counting	59
7.2.	<i>Ex-Vivo</i> Brain Bioluminescence Imaging	60
7.3.	<i>Ex-Vivo</i> Xenograft Analysis	60
8.	Statistical Analysis	61
Chapter 4: Results		63
1.	Noninvasive Monitoring of Long-Term Lentiviral Vector-Mediated Gene Expression in Rodent Brain with Bioluminescence Imaging	63
1.1.	BLI Imaging Allows Quantification of Luciferase Expression in LV-Transduced Cells	66
1.3.	Characterization of the BLI Signal After Stereotactic Injection of LV-Fluc into the Mouse Striatum	69
1.4.	The Localisation of the BLI Signal Reflects the Anatomical Site of Injection	70
1.5.	BLI Allows Quantification of Luciferase Activity <i>In Vivo</i>	73
1.6.	Imaging of Long-Term Lentiviral Vector-Mediated Luciferase Expression in the Mouse Brain	73
1.7.	The BLI Signal Reports Expression of a Transgene of Interest	76
1.8.	BLI Detects Luciferase Expression in the Rat Substantia Nigra	78
1.9.	BLI can Detect Migration of Endogenous Neural Stem Cells from the Subventricular zone to the Olfactory Bulb	78
2.	Multimodality Imaging of Tumor Xenografts and Metastasis in Mice with Combined Micro Positron Emission Tomography, Small Animal Computed Tomography and Bioluminescence Imaging	83
2.1.	Establishment of a Fused MicroPET-CT Imaging Strategy	84
2.2.	[¹⁸ F]-FDG MicroPET-CT is Capable of Monitoring Growth of Tumor Xenografts	85
2.3.	[¹⁸ F]-FDG MicroPET-CT Detects Pulmonary Melanoma Metastases	86
2.4.	[¹⁸ F]-FHBG MicroPET-CT and Bioluminescence Imaging of Systemic Melanoma Metastases	87
2.5.	[¹⁸ F]-FHBG MicroPET-CT is More Sensitive than [18F]-FDG MicroPET-CT for Detection of Systemic Metastases	90
3.	Validation of Varicella Zoster Virus Thymidine Kinase as a Novel Reporter Gene for PET	97
3.1.	Uptake Kinetics of Radiolabeled BCNAs in Stably Transduced 293T Cells	100
3.2.	High Pressure Liquid Chromatography Shows Presence of Polar Metabolites in VZV-tk Expressing Cells	101
3.5.	Thymidine Blocks Uptake of Radiolabeled BCNAs in Stably Transduced 293T Cells	102
3.6.	Variable Intracellular Retention of Radiolabeled BCNAs	104
3.7.	The Accumulation of Radiolabeled BCNA Reflects the LV Titer	104
3.8.	Radiolabeled BCNAs Do Not Accumulate in Cells Expressing an HSV1-sr39TK-Containing Fusion Protein	106
3.9.	MicroPET Imaging of Accumulation of 4-[¹⁸ F]-FEP-BCNA in VZV-tk Expressing Prostate Cancer Xenografts	107
Chapter 5: General Discussion & Perspectives		115

<i>Summary</i>	123
<i>Samenvatting</i>	125
<i>Curriculum Vitae</i>	127
<i>Publication List</i>	129
<i>References</i>	133

Abbreviations

%ID/g	% injected dose per gram
[¹⁸ F]-FDG	2-deoxy-2-[¹⁸ F]fluoro-D-glucose
[¹⁸ F]-FES	16α-[¹⁸ F]fluoroestradiol
[¹⁸ F]-FESP	(3-(2'-[¹⁸ F]-fluoroethyl)-spiperone
[¹⁸ F]-FHBG	9-(4-[¹⁸ F]-fluoro-3-[hydroxymethyl]butyl)guanine
[¹⁸ F]-FMT	[¹⁸ F]fluoro-L- <i>m</i> -tyrosine
3-[¹¹ C]-MP-BCNA	3-(2'-deoxy- <i>b</i> -D-ribofuranosyl)-6-(3-[¹¹ C]methoxyphenyl)-2,3-dihydrofuro[2,3- <i>d</i>]pyrimidin-2-one
3-[¹⁸ F]-FEP-BCNA	3-(2'-deoxy- <i>b</i> -D-ribofuranosyl)-6-(3-[¹⁸ F]fluoroethoxyphenyl)-2,3-dihydrofuro[2,3- <i>d</i>]pyrimidin-2-one
3F	Triple fusion gene (hRL_mRFP_HSV1-sr39tTK)
4-[¹¹ C]-MP-BCNA	3-(2'-deoxy- <i>b</i> -D-ribofuranosyl)-6-(4-[¹¹ C]methoxyphenyl)-2,3-dihydrofuro[2,3- <i>d</i>]pyrimidin-2-one
4-[¹⁸ F]-FEP-BCNA	3-(2'-deoxy- <i>b</i> -D-ribofuranosyl)-6-(4-[¹⁸ F]fluoroethoxyphenyl)-2,3-dihydrofuro[2,3- <i>d</i>]pyrimidin-2-one
5-FC	5-fluorocytosine
5-FU	5-fluorouracil
8-[³ H]-PCV	8-[³ H]-penciclovir
AADC	aromatic L-amino acid decarboxylase
AAV	adeno-associated virus
Ad	adenovirus
ADP	adenosine diphosphate
AK	arginine kinase
AP	anteroposterior
ATP	adenosine triphosphate
BBB	blood-brain-barrier
BCNA	bicyclic pyrimidine nucleoside analogues
BLI	bioluminescence imaging
bp	base pair
CAR	Coxsackie-adenovirus receptor
CBRed	click beetle luciferase
CCD	charge-coupled device
CD	cytosine deaminase
cDNA	complementary DNA
CEST	chemical-exchange saturation transfer
CF10	10 layer cell factory
CK	creatine kinase
CMV	cytomegalovirus
CNS	central nervous system
CNT	concentrative nucleoside transporter
cPPT	central polypurine tract
CT	computed tomography
D2R	dopamine receptor type 2
DAB	diaminobenzidine
DAT	human dopamine transporter
DMEM	Dulbecco's modified Eagle's medium
DV	dorsoventral
<i>E. coli</i>	<i>E. coli</i>
ECL+	enhanced chemiluminescence plus
eGFP	enhanced green fluorescent protein
EMCV	encephalomyocarditis virus
ENT	equilibrative nucleoside transporter
FCS	fetal calf serum
FDA	food and drug administration

FAIU	2'-fluoro-2'-deoxy-5-iodo-1-β-D-arabinofuranosyl-5-iodouracil
FLI	fluorescence imaging
Fluc	firefly luciferase
FMT	fluorescence molecular tomography
GABA	gamma-aminobutyric acid
GFP	green fluorescent protein
Gluc	<i>Gaussia</i> luciferase
GP	globus pallidus
hER	human estrogen receptor
hERL	ligand binding domain of the hER
HIV-1	human immunodeficiency virus type 1
HLB	hydrophilic-lipophilic balanced
hNET	human norepinephrine transporter
hNIS	human sodium iodide symporter
hOAT1	human renal organic anion transporter 1
HPLC	high pressure liquid chromatography
hRL	humanized Renilla luciferase
HRP	horseradish peroxidase
hSSTR2	human somatostatin receptor subtype 2
HSV1-sr39tTK	truncated mutant HSV1-tk
HSV1-tk	herpes simplex virus type 1 thymidine kinase (gene)
HU	Hounsfield units
HVS1-TK	herpes simplex virus type 1 thymidine kinase (protein)
IP	intraperitoneal(ly)
IRES	internal ribosome entry element
ITR	inverted terminal repeat
K/X	ketamine/xylazine
L	lateral
LacZ	β-galactosidase gene from <i>E. coli</i>
LDLr	low-density lipoprotein receptor
LRP	lysine-rich protein
LTR	long terminal repeat
LV	lentiviral vector
MDR1	multi-drug resistance protein 1
MIBG	meta-iodobenzylguanidine
MION	monocrystalline iron oxide nanoparticles
MR	magnetic resonance
mRFP	monomeric red fluorescent protein
MRI	magnetic resonance imaging
mRNA	messenger RNA
MRP	multidrug resistance-associated protein
MRS	magnetic resonance spectroscopy
n	number
NIR	near-infrared
nu/nu	nude mouse
OB	olfactory bulb
p/s	photons per second
p/s/cm²/sr	photons per second per centimeter square per steradian
PBS	phosphate-buffered saline
PCR	polymerase chain reaction
PD	Parkinson's disease
PET	positron emission tomography
Pgp	P-glycoprotein
polyP	inorganic polyphosphate
PRG	PET reporter gene
PRP	PET reporter probe
PRRT	peptide receptor radiotherapy
PVDF	polyvinylidenedifluoride
RCL	replication competent lentivirus
Rluc	<i>Renilla</i> luciferase
RNA	ribonucleic acid
ROI	region of interest
RP-HPLC	reverse phase high pressure liquid chromatography

RT	reverse transcriptase
S/MAR	scaffold/matrix attachment region
SCID	severe combined immunodeficiency
SD	standard deviation
s.e.m	standard error of the mean
SIN	self-inactivating
SN	substantia nigra
SPECT	single photon emission computed tomography
Str	striatum
SUV	standardized uptake values
SVZ	subventricular zone
TFF	tangential flow filtration
TfR	transferrin receptor
TU	transducing unit
USPIO	ultrasmall superparamagnetic iron oxide particles
V-ATPase	vacuolar H ⁺ -ATPase
VSVg	vesicular stomatitis virus glycoprotein
Vtc	vacuolar transporter chaperone
VZV	varicella zoster virus
VZV-tk	varicella zoster virus thymidine kinase
WPRE	woodchuck hepatitis virus posttranscriptional regulatory element
β-gal	β-galactosidase

Chapter 1: General Introduction

This introduction is part of a manuscript entitled “*Seeing genes at work in the living brain with non-invasive molecular imaging*” by Deroose CM, Reumers V, Debyser Z and Baekelandt V that will be published in Current Gene Therapy.

Biomedical sciences are currently undergoing a metamorphosis in the way research is being conducted. For more than half a century, since the seminal paper defining disease at the molecular level [1], single molecules have been at the center stage of biomedical hypothesis driven research and have been studied *in vitro*, in cells, and finally in model organisms with invasive techniques. Although this single molecule approach has been very successful in discovering the causes and mechanisms of many diseases leading eventually to therapies, this approach is reductionist by definition and does not allow to comprehend the full complexity of human health and disease. Two major technological changes are reshaping the research field and changing this single molecule-based paradigm. The first technological revolution is the “omics” revolution, driven by the knowledge of several hundreds of full length genomes and by techniques allowing quantification of thousands of parameters in parallel, including mRNA and proteins. Integration of all these parameters in mathematical models of the cell and the organism allows to study the organism at the system level in the so-called field of systems biology [2]. A second major change is a shift from *in vitro* and cellular experiments towards the study of intact living organisms. Biological responses consist of changes in expression levels of multiple genes and regulatory RNA species, post-translational modifications of proteins and activation or inhibition of biological pathways that reside within a cell or that depend on the interplay between different cell types, some of which reside within a single tissue and others that are recruited from other tissues by the biological process. In the brain this is exemplified by the complex array of projections of different brain regions that are intricately interconnected and that cannot be reduced to the properties of a single cell. Although the study of biological samples such as fixed tissue slices reveals precious information, there is always a sampling bias present based on preconceived notions of the temporal kinetics of the pathophysiological process studied. The emergence of the field of molecular imaging has made it possible to study these processes in living and intact organisms. Molecular imaging is a novel field of biomedical science that studies the visual

representation, localisation and quantification of molecular processes at the cellular and subcellular level within intact living organisms [3]. Many molecular processes can be visualised, including receptor density and occupancy [4], transporter and enzyme activity, gene expression [5], metabolite concentration, protein-protein interaction [6], transcriptional activity [7], signal transduction [8] and apoptosis [9, 10]. One of the most powerful and versatile targets is gene expression, that can be imaged either by the use of reporter genes or by strategies aiming to directly image mRNA levels. Imaging reporter genes are genes that encode a protein that can be easily detected and quantified by a specific imaging modality. Standard molecular biology strategies that have been optimised during the past decades allow to link a molecular event of interest to expression of a reporter gene and so they can be used to measure a multitude of biological processes. This is an advantage over traditional molecular imaging where a specific probe has to be developed and validated for each molecular event of interest. Three main categories can be broadly defined within molecular imaging [2]: direct imaging in which the activity of an enzyme, the presence of a receptor or the concentration of a metabolite are directly measured; indirect imaging, in which the biological process studied has been linked to a reporter gene whose imaging readout will reflect the process at study; functional (or tissue microenvironment) imaging that measures the impact of a molecular event on physiologic parameters such as perfusion, hypoxia, pH level, redox status, and others. Functional imaging is looking at more downstream effects of a molecular event and so it may be less specific but it integrates other responses of the organism with the event in question. Direct imaging has the advantage of truly depicting the molecular process under study but it usually requires the development of a specific imaging probe that can be time and capital consuming. Indirect imaging, once a specific probe has been developed, can be used to study many different molecular processes with relative ease. This chapter describes the basic strategies for gene expression imaging, describes ways to image mRNA levels and reporter genes and finally discusses existing and potential applications of gene expression imaging in pre-clinical and clinical research in the neurosciences.

1. *Imaging Modalities*

Many different imaging modalities have been applied to study biological processes and for some of them strategies to detect gene expression at the RNA or protein level have been developed. The basic characteristics of these techniques will be explained below. More detailed description of the techniques can be found elsewhere.

1.1. Radionuclide Imaging Techniques

Both single photon emission computed tomography (SPECT) and positron emission tomography (PET) require injection of a probe (or tracer) consisting of a radioisotope that is chemically linked to a molecule with a well characterized biological behaviour. Photons are emitted when the radioisotope decays and their detection by the imaging device allows to determine the three dimensional distribution of the radioisotope and thus of the tracer molecule. The biological properties of the tracer will determine the (patho)physiological significance of the resulting images. The sensitivity is in the picomolar range (10^{-11} to 10^{-12} mol/L) [3] so sub-pharmacological amounts of tracer can be detected. In general, these images contain little anatomical information in contrast to X-ray based computed tomography (CT). The development of combined SPECT/CT and PET/CT devices for clinical and pre-clinical imaging has compensated this weakness. One of the major strengths of this technique is the scalability from mouse to man, where the same tracer molecule can be used in a range of species.

1.1.1. Single Photon Emission Computed Tomography (SPECT)

SPECT is based on the detection of single gamma rays emitted within a living organism. By acquiring planar projection images from many different angles the three dimensional distribution of the radioisotope can be determined. The most common radioisotopes used in SPECT have half lives ranging from ~6 hours to ~8 days and so they allow to study process taking place on a moderately long timescale (up to one week). The resolution in clinical applications is between 7 and 15 mm depending on camera and collimator characteristics but in current state of the art pre-clinical scanners resolution can be as low as 0.6 mm [11]. As SPECT requires physical collimation of the incident gamma rays its sensitivity is lower than in PET by typically an order of magnitude. Another disadvantage of SPECT is the limited temporal resolution as it requires multiple planar images from different angles that are typically acquired in ~30 minutes but modern clinical systems can complete full rotations in ~1 to 2 minutes. Modern small animal devices have acquisition times that are in the 1 to 10 minutes range. A marked advantage of SPECT is the possibility to image two different radioisotopes at the same time provided they have different gamma ray energies, allowing multiplexing of two different molecular signals.

1.1.2. Positron Emission Tomography

PET is based on the utilisation of isotopes that emit positrons, the antiparticle of the electron. Upon decay of these radionuclides, the emitted positron scatters in the tissue for a distance of the order of 1 mm and then annihilates with an electron resulting in the emission of two gamma rays at an angle of ~ 180 degrees. The nearly simultaneous detection of a gamma ray by two opposite detectors within the scanner indicates an annihilation event on the line joining these detectors and this temporal collimation takes away the need for mechanical collimation. The spatial resolution of state of the art clinical scanners is around ~ 5 mm whereas preclinical scanners achieve ~ 1 to 2 mm. Advantages of PET over SPECT are its intrinsic tomographic nature allowing to obtain a high temporal resolution and the use of isotopes that can be incorporated into biological molecules with no or minimal influence on their biochemical properties (e.g. ^{11}C replacing a carbon atom or ^{18}F replacing a hydroxyl group). The major disadvantage of PET is the necessity for most of the isotopes to be generated on site by a dedicated cyclotron because of their short half life (^{11}C : ~ 20 min, ^{18}F : ~ 110 min) and the need for a subsequent elaborate radiopharmaceutical synthesis of the tracer. Recently commercial networks distributing PET tracers have been developed allowing sites without cyclotron to perform PET studies.

1.2. Magnetic Resonance Imaging and Spectroscopy

The signal in magnetic resonance (MR) based techniques is composed of radiofrequency electromagnetic waves that are emitted by atoms when they return to a basic aligned state within a magnetic field after transient perturbation by a radio frequency pulse emitted by the device. The frequency and temporal characteristics of these radio waves are dependent on the molecular and tissular composition of the depicted object. There are two main ways to process this signal: either three-dimensional visual representation of signal intensity in MR imaging (MRI) or determination of the spectral properties of the signal in MR spectroscopy (MRS).

1.2.1. Magnetic Resonance Imaging (MRI)

MRI in its most common form depicts the influence of tissue composition on hydrogen atoms within water molecules. MRI offers a very high spatial resolution (submillimeter in clinical scanners and ~ 10 to $100 \mu\text{m}$ in animal devices) with a very high tissue contrast as well as high temporal resolution that allows dynamic cardiac imaging, respiratory gating as well as dynamic bolus contrast tracking. On the other hand, the

sensitivity is typically low in the milli- to micromolar range for the most common contrast agents and amplification strategies are required to detect lower concentrations. Quantification of contrast agents can also be complicated by non-linear effects and by the use of negative contrast mechanisms. This low sensitivity and difficult quantification has hampered the development of MR reporter genes.

1.2.2. Magnetic Resonance Spectroscopy (MRS)

In MRS, the frequencies of the radio wave signal coming from a voxel of interest within the subject are analysed. Applied to a pure chemical sample, this will result in a specific spectrum of peaks and valleys. Living tissues and organisms are by definition chemically complex and so their spectra are a combination of their chemical constituents, overlapping one another and with relative intensities that reflect their intrinsic signal strength (which may vary from substance to substance) and their relative concentrations (ratios) [12]. As such, MRS is a true form of molecular imaging as it allows the three-dimensional representation of the concentration of endogenous molecules. MRS can be performed on commercially available clinical scanners and on small animals MR systems.

1.3. Optical Imaging Strategies

Two different visible light based strategies have been proposed to image gene expression in living organisms, bioluminescence imaging (BLI) and fluorescence imaging (FLI). As both techniques use light within the detection range of the human eye (~300-700 nm) or in the near-infrared (NIR) range (~700-1400nm), they suffer from scattering and attenuation by biological tissue. The absorption of photons with wavelenghts lower than 600nm causes a decrease by about a factor 10 per centimeter of tissue. This absorption is primarily caused by the hemoglobin concentration within the tissue [13]. Current research is focusing on creating probes or enzymes that emit light with wavelenghts within this so called NIR window. The main advantage of these optical imaging devices is their low cost, which has allowed their rapid dissemination within the research community and the possibility to acquire different molecular signals at the same time (multiplexing). Their main limitation is the poor tissue penetrance, limiting their translational potential for clinical use. However, as a rapid and inexpensive tool for biomedical research and for preclinical evaluation of molecular imaging strategies they have shown to be of great value.

1.3.1. Fluorescence Imaging

Fluorescence imaging is based on the excitation of a fluorophore by externally applied light (excitation photons) which results in the emission of light at a longer (less energetic) wavelength (emission photons). By using the appropriate filter sets for both the excitation and emission light, it is possible to measure only the emitted light by a highly sensitive charge-coupled device (CCD) camera. The emission light can be maximized by high intensity excitation light at the optimal absorbed wavelength. Fluorescence imaging can be done at different resolutions and depth penetrations, from intravital microscopy at around tens to hundreds micrometers to several centimeters with fluorescence molecular tomography (FMT) [14]. The use of two-photon microscopy has also greatly improved the depth at which imaging can be performed. Complicating factors for FLI are autofluorescence and photobleaching. Autofluorescence is caused by endogenous molecules different from the molecules studied that have excitation and emission wavelengths similar to the studied molecule. Spectral unmixing correction techniques and the use of molecules emitting in the NIR window can greatly reduce this autofluorescence interference. Photobleaching is the loss of the fluorescent properties of the molecule caused by exposure to the excitation light. Optimisation of the fluorescent molecule can reduce photobleaching to a minimum and optimised hardware decreases the illumination time.

1.3.2. Bioluminescence Imaging

BLI is based on the enzymatic light production resulting from the oxidation of certain molecules (called luciferins) catalyzed by substrate specific enzymes (called luciferases). This reaction requires oxygen and certain co-factors such as oxygen or energy in the form of adenosine triphosphate (ATP) that vary between different luciferases. In contrast to FLI, there is no need for excitation light. As the background light production in most species of interest is very low, BLI is capable of attaining very high signal to noise ratios, the highest of all modalities discussed. This allows very sensitive imaging of specific molecular events within a model organism up to ~2 to 3 cm depth. Resolution is depth dependent and reported values are around 2 to 3 millimeters [15]. Most BLI applications are based on genetic modification of the cell, virus or animal under study and thus are based on gene expression imaging. Notable exceptions are strategies where the luciferase enzyme has been covalently linked to either peptides [16] for non-invasive detection of tumors expressing peptide receptors or to self-illuminating quantum dots [17].

2. Reporter Gene Concept and Existing Imaging Reporter Genes

Reporter genes have been used in molecular biology for several decades. A reporter gene can be defined as a gene that encodes a protein that can be easily detected and quantified. The first reporter gene products were detected by biochemical analyses of tissue lysates (chloramphenicol acetyl transferase, β -lactamase) or of blood samples (alkaline phosphatase). The use of the β -galactosidase from the lactose operon from *E. coli* (LacZ) represented a significant advance as it allowed detection of gene expression on histological sections after application of a chromogenic substrate. The use of green fluorescent protein (GFP) cloned from the jellyfish *Aequorea victoria* [18] and later from anthozoa corals [19] has revolutionized the biomedical field as it allows detection of gene expression in living cells, in histological slices and within living animals. A whole variety of color-shifted and optimized mutants has been designed (for a review see [20]). Imaging reporter genes are genes encoding proteins that can be detected and quantified with non-invasive imaging techniques, either directly or after injection of a specific imaging probe that interacts with the protein product. An ideal reporter gene/reporter probe system would have the following characteristics (adapted from [3]):

- (1) The reporter protein should be non-immunogenic, so the gene should be preferentially present within the organism, but not expressed.
- (2) The reporter protein should not have any perturbing nor toxic effect on the cell.
- (3) The size of the reporter gene and its driving promoters should be small enough to fit into a delivery vehicle (plasmids, viral vectors), except for transgenic applications.
- (4) The half-life of the reporter protein should match the temporal dynamics of the biological process studied.
- (5) For conditional reporter proteins, the signal should be null in the absence of the activating event and its intensity should be maximal in its presence.
- (6) The reporter probe should accumulate only in those cells where the reporter gene is expressed.
- (7) No reporter probe should accumulate in cells not expressing the reporter gene.
- (8) The reporter probe should be stable *in vivo* and not be metabolized before reaching its target.
- (9) The reporter probe should rapidly clear from the circulation and background signal should not interfere with detection of specific signal.

(10) The reporter probe or its metabolites should not be cytotoxic nor perturb normal cell homeostasis.

(11) Natural biological barriers (e.g. the blood-brain-barrier) must not prevent the reporter probe from reaching its destination.

(12) The image signal should be readily quantifiable and correlate well with levels of reporter gene mRNA and protein *in vivo* over a range of several orders of magnitude.

Not surprisingly, no single reporter gene/reporter probe system meets all these criteria at present.

For most gene therapy applications the therapeutic transgene is a gene that can not be directly imaged. Several strategies have been proposed to determine expression levels of the therapeutic gene with a reporter gene: (1) co-injection of 2 vectors containing a therapeutic and reporter gene, respectively [21] (2) using 2 copies of the same promoter driving the therapeutic or the reporter gene (3) using a viral [22] or synthetic [23] internal ribosome entry element (IRES) connecting the therapeutic and reporter gene (4) using a bidirectional promoter [24] (5) using picorna virus-derived peptide 2a sequences that can link up to 4 genes in a stoichiometric 1:1 ratio [25].

2.1. Radionuclide Imaging Techniques

Radionuclide imaging was among the first techniques for which non-invasive reporter genes have been developed. There are 3 categories of proteins that have been used as reporters up to date: enzymes that will cause metabolic trapping of the reporter probe, receptors to which the receptor probe will bind and finally transporters that will actively pump the probe from the extracellular space into the cell. The enzymes and transporters have the theoretical advantage of amplifying the signal as one single protein can cause accumulation of several probes, whereas for the receptors only one probe can bind per protein.

2.1.1. The Herpes Simplex Virus Thymidine Kinase Reporter System

The paradigm reporter gene is the herpes simplex virus type 1 thymidine kinase (HSV1-tk) (note that tk denotes the gene whereas TK denotes the protein). The HSV1-tk gene was originally developed as a suicide gene because the HSV1-TK enzyme has a loosened substrate specificity compared to its human counterpart and beside thymidine (its natural substrate) it also phosphorylates a range of pyrimidine and acycloguanosine substrates. The resulting monophosphate compounds are trapped within the cell because

of the negative charge and they will be converted to di- and triphosphates by intracellular enzymes. The triphosphate compounds interfere with DNA synthesis as they are chain terminators and this perturbation of DNA synthesis leads to apoptosis. Suicide gene therapies have met with modest success, particularly for the treatment of glioblastoma multiforme [26-28]. The concept of using PET or SPECT to monitor the efficacy of gene transfer and the resulting gene expression by using radiolabeled versions of a substrate was developed in parallel with the suicide gene therapy paradigm [29, 30]. As the radiolabeled probe is administered in sub-pharmacological concentrations, the HSV1-tk expressing cells do not undergo apoptosis during imaging. Until now, more than 15 different tracers for HSV1-tk have been proposed of which the pyrimidine nucleoside analogue $^{124/131}\text{I}$ -labeled 2'-fluoro-2'-deoxy-5-iodo-1- β -D-arabinofuranosyl-5-iodouracil ($^{124/131}\text{I}$ -FIAU) [31] and the side chain radiolabeled analogue of penciclovir 9-(4- ^{18}F -fluoro-3-[hydroxymethyl]butyl)guanine (^{18}F -FHBG) [32] are the most widely used. The latter has received Food and Drug Administration (FDA) approval for initial use in gene therapy trial volunteers after preclinical demonstration of its preclinical safety [33, 34]. Optimisation of this system has been pursued by development of novel tracers, improvement of the synthesis methods of the existing tracers, kinetic modelling of dynamic PET data [35], utilisation of mutants with increased tracer affinity and decreased thymidine affinity [36] and partial truncation of the nuclear localisation signal domain of the enzyme (leading to higher cytosolic enzyme concentrations) [37]. Recently mutants without affinity for thymidine but with conserved affinity for ganciclovir were developed [38]. The HSV1-tk reporter gene has been used in many different settings: monitoring of viral and non-viral vector gene transfer efficacy, cancer cell follow-up, tracking of cellular therapies including adoptive immune therapy and stem cell transfer, imaging of protein-protein interactions [39] and clinical suicide gene therapy [26]. The capability of ablating HSV1-TK expressing cells with a prodrug that is inoffensive for native cells allows to use this gene as a safety net in gene therapy and cell therapy trials [40].

The most important shortcoming of the HSV1-tk system is that despite synthesis of more than 15 tracers, there is currently no tracer available that crosses the intact blood-brain-barrier (BBB) [33, 41]. Imaging gene expression in the brain with these viral reporter genes is not possible, except if there is pathological BBB disruption that will lead to influx of the tracer into the brain [42]. Another drawback of this system is its viral origin with potential pre-existing or acquired immune responses. Recently a similar reporter gene concept based on mitochondrial thymidine kinase type 2 and ^{124}I -FIAU has been proposed to overcome immunogenicity problems [43].

2.1.2. Other Enzymatic Reporter Genes

Some other enzymatic systems different from the thymidine kinase genes have been proposed. Of considerable interest for brain studies is the aromatic L-amino acid decarboxylase (AADC) that can be imaged with [^{18}F]fluoro-L-*m*-tyrosine ([^{18}F]-FMT) [44]. This enzyme is responsible for conversion of L-dopa to dopamine and has been pre-clinically evaluated for gene therapy trials of Parkinson's disease (PD) [45, 46]. Long-term expression of this enzyme could be detected 6 years after injection of AAV vectors in the brain of MPTP lesioned monkeys [47] and monkeys with increased [^{18}F]-FMT accumulation showed a better response to L-DOPA therapy [46]. This is an example of direct imaging of transgene expression without need for an indirect reporter gene. Because of its metabolic influence on the cells in which it is expressed this enzyme is unfortunately not suited for use as a general reporter gene.

Another enzyme that has been proposed as PET reporter is the hypoxanthine phosphoribosyl transferase gene from *E. coli* [48]. This gene mediates the transfer of a phosphoribosyl group onto xanthine derivatives resulting in metabolic trapping within the cell. The attractiveness of this system lies in the fact that xanthines rapidly cross the BBB by passive diffusion. Up to now only proof of principle studies have been performed with autoradiography of a [^{14}C]-marked xanthine that was trapped in intracerebral tumors in which the BBB was intact as shown by MRI. Unfortunately no PET or SPECT tracer has been developed that would allow *in vivo* detection of this gene.

2.1.3. Receptor Reporter Genes

The most studied PET receptor reporter gene is the human dopamine receptor type 2 (D2R) [49]. This receptor can be imaged with (3-(2'-[^{18}F]-fluoroethyl)-spiperone ([^{18}F]-FESP) and [^{11}C]-raclopride, both tracers that do cross the intact BBB. Other advantages of this gene is its human origin preventing immunogenicity and the validation of a mutant uncoupled receptor for imaging. This mutation (D2R80A) completely eliminates the normal response of this receptor to dopamine, i.e. the activation of a Gi-protein complex that leads to inactivation of adenylyl cyclase and a consequent decrease in cellular cyclic AMP levels. It is expected that in the future other reporter genes will be optimized so that the interaction with the reporter probe is maximal with minimal interaction with normal cellular function [38]. The D2R system has been used for many applications, often as a second reporter gene in conjunction with HSV1-tk [21, 50, 51]. Adenoviral vector-mediated overexpression of D2R in the rat striatum was demonstrated with PET using three different tracers by Ogawa et al. [52] and its rapid decline within less than 2 weeks was similarly

demonstrated by these authors [53]. The major limiting factor for D2R use in other preclinical brain disease models is the high endogenous D2R expression level, particularly in the striatum which causes a large background signal that will prevent detection of subtle changes of expression of the reporter gene.

Another receptor that has been validated as reporter gene is the human somatostatin receptor subtype 2 (hSSTR2). The advantages of this receptor include non-immunogenicity and widely available reporter probes for SPECT (^{111}In -Octreotide) and to a lesser extent for PET (^{68}Ga]-DOTATOC). This receptor is the subject of intensive study because it can be used for peptide receptor radiotherapy (PRRT) with ^{90}Y trium, ^{177}Lu tetium or ^{188}Re henum binding peptides [54, 55], which would also allow this receptor to be used as a suicide gene. Unfortunately these peptides do not cross the intact BBB. Proof of principle studies with gamma scintigraphy were first carried out by Zinn *et al.* who showed a 5 to 10-fold increase of radiolabeled peptide in xenografts injected with adenoviral vectors encoding hSSTR2 compared to control vectors [56] and similar results were found in follow-up studies [57-59].

An alternative to membrane receptors is the use of intracellular receptors such as the human estrogen receptor (hER). Furukawa *et al.* [60] have proposed to use the ligand binding domain of the estrogen receptor (hERL) in conjunction with the well characterised 16α - ^{18}F]fluoroestradiol (^{18}F]-FES) that has already been used in human studies and that crosses the BBB [61]. This human-derived system has lost its signal transduction capacity because the DNA binding domain of the hER is lacking. Initial cell uptake studies show almost tenfold increase of ^{18}F]-FES in transfected cells and autoradiography showed a 25% increase in tracer accumulation in mouse calf muscle electroporated *in vivo* with an hERL encoding plasmid compared to controls. It remains to be determined if the low *in vivo* tracer uptake is due to low efficiency of the electroporation or to the intrinsic properties of the hERL/ ^{18}F]-FES system.

2.1.4. Transporter Reporter Genes

Transmembrane transporter proteins combine the advantage of easy access to extracellular tracer molecules (shared with receptors) with the signal amplification of enzymes. The most studied transporter reporter gene is the human sodium iodide symporter (hNIS) gene [62]. The glycoprotein transmembrane protein hNIS is normally expressed at high levels in the thyroid and at lower levels in the salivary glands, the stomach, the lactating breast and some other tissues. It is responsible for actively transporting an iodide ion from the extracellular space into the cell against a concentration

gradient. Because normal expression of hNIS is restricted to a few organs and endogenous substrate levels are very low, a high signal to noise ratio can be expected within most of the body. Furthermore, a wide range of iodine isotopes is available for *in vitro*, animal (^{125}I) and clinical (^{123}I , ^{124}I and ^{131}I) applications for SPECT as well PET. The most commonly used isotope in nuclear medicine, $^{99\text{m}}\text{Tc}$, can also be used to visualize hNIS expression in pertechnetate form at low cost. By using high doses of ^{131}I , an ablative dose of beta emission can be administered to hNIS expressing cells. This treatment is standard for differentiated thyroid carcinoma and its use for other cancers is contemplated [63]. A limitation is the moderate retention of iodide or pertechnetate within non-thyroidal cells that are expressing hNIS. Strategies to improve retention by co-expression of the enzyme thyroperoxydase has encountered mild success with increased retention by a factor of ~ 3 [64]. It has been demonstrated that the extent of radioiodine uptake generally correlates with NIS protein levels within a certain range and that the transporter is efficiently trafficked to the cytoplasmic membrane [65]. Imaging within the brain is problematic with this symporter as neither iodine nor pertechnetate cross the intact BBB, limiting its use to pathological areas where BBB integrity has been compromised.

The human dopamine transporter (DAT) is a transporter that has been used to quantify adeno-associated viral vector (AAV)-mediated transduction of murine muscle with the SPECT tracer [$^{99\text{m}}\text{Tc}$]TRODAT-1 [66]. Although DAT is physiologically a transporter, it is important to realize that this tracer is an agonist that binds to the transporter but that does not undergo translocation, making this system function in practice like a receptor/ligand system. Other specific mono-amine tracers with highest affinity for DAT are available for SPECT ([^{123}I]-FP-CIT) and PET ([^{18}F]-FECNT) and all cross the intact BBB. DAT expression is almost exclusively limited to the striatum where it is presynaptically located on the projections of the dopaminergic neurons from the substantia nigra. This will result in a high background signal in normal brain similar to D2R.

The last transporter system that has been validated for reporter gene imaging is the human norepinephrine (or noradrenalin) transporter (hNET). Radioligands have been developed for this transporter because it is overexpressed in certain tumors (neuroblastoma, pheochromocytoma) and because it plays an important role in cardiac innervation. Meta-iodobenzylguanidine (MIBG) labelled with ^{123}I (SPECT) [67], ^{124}I (PET) and ^{131}I (SPECT and therapy) are commercially available and ^{11}C -labeled hydroxyephedrine [68] can also be used for PET. The hNET transporter functions as a rapid norepinephrine reuptake system near presynaptic terminals of noradrenergic cells. The hNET protein belongs to a family of Na^+/Cl^- -dependent transporter with highly

conserved hydrophobic amino acid sequences (12 or 13 transmembrane domains). Expression of hNET in mammals is almost exclusively restricted to the central and peripheral sympathetic nervous system with great signal to background ratio's. Immunogenicity is not expected because it is a human protein. Initial reports showed low retention of [¹³¹I]-MIBG [69] but using other cell lines *in vivo* uptake ratios between hNET expressing xenografts and other tissues of more than 100 have been found at late imaging time points [70]. The influence of hNET expression on the homeostasis of the cell needs to be further studied before human applications with this reporter gene can start. The aforementioned tracers are all hydrophilic and do not cross the BBB but many groups are evaluating hNET ligands that cross the BBB as this transporter is thought to be involved in many psychiatric diseases [71]. Endogenous hNET expression in the brain could be a potential confounder when using these.

The currently available reporter genes for radionuclide imaging are not satisfactory for brain use and further research in this area is warranted. Potential targets are receptors or transporters for which BBB penetrating ligands are known and that are not expressed within the brain.

2.2. Optical Imaging Techniques

2.2.1. Bioluminescence Imaging Reporter Genes

Bioluminescence imaging has been almost exclusively based on the use of a specific category of reporter genes encoding light producing enzymes called luciferases. There are currently 5 different luciferases validated for *in vivo* BLI based on 3 different biochemical pathways that all require the presence of oxygen [15]. The two luciferases from the coleoptera order, firefly luciferase (Fluc) from the North American firefly (*Photinus pyralis*) and click beetle luciferase (CBRed) from the click beetle (*Pyrophorus plagiophthalmus*), use D-luciferine (benzothiazole) and ATP as substrate. The marine luciferases *Renilla* luciferase (Rluc) from the sea pansy (*Renilla reniformis*) and *Gaussia* luciferase (Gluc) from the marine copepod (*Gaussia princeps*) use coelenterazine without need for ATP. The third biochemical pathway is dependent on decanal. It is used by the Lux luciferase that is found in bacteria such as *Photobacterium luminescens* and that consists of a five gene operon encoding a heterodimeric luciferase (Lux A and Lux B) as well as substrate regenerating enzymes. This luciferase does not need exogenous

administration of a substrate and when cloned in bacteria leads to permanently autoluminescent strains.

The most commonly used luciferase is Fluc. It is a 61 kDa protein encoded by a 1653 bp gene. It has an emission peak at 612 nm at 37°C in contrast to subphysiological temperatures where the peak shifts to the blue (560 nm at 22°C) [72]. The Fluc gene has been codon optimized for mammalian use and spurious transcription factor binding sites have been reduced. The substrate D-luciferin crosses the intact BBB although luciferin concentrations have shown to be lower in the brain than in other tissues [73]. The Fluc protein has a cellular half-life of ~2 to 3 hours [74] and so it is ideally suited for the study of dynamic processes on a timescale of several hours. Fluc is a remarkably flexible enzyme that has been split in C-terminal and N-terminal halves that have almost no activity but when brought together in close proximity regain a substantial fraction of the activity of intact Fluc. This phenomenon has been used by several groups to study protein-protein interactions [6, 75]. CBRed has the longest peak emission at 615 nm but the difference with Fluc is only 3 nm [72]. As there is no real advantage over firefly luciferase, this reporter gene has been much less utilized.

The other major luciferase enzyme is Rluc. It is a smaller protein of 36 kDa size with a peak emission of 480 nm for the native protein. This blue light is strongly absorbed by hemoglobin and so it is primarily the small part of the spectrum that has a wavelength longer than 600 nm that is available for *in vivo* detection. The Rluc substrate coelenterazine is not recognised by Fluc and reciprocally Rluc does not recognise D-luciferin, allowing almost simultaneous detection of 2 independent molecular events within the same animal [76]. Coelenterazine has a relatively short circulation time *in vivo* with some autoluminescence [77] requiring intravenous injection of the substrate followed by acquisition within the first couple of minutes after injection. Similar to Fluc, the Rluc gene has been codon optimized [78] and split reporters have been developed for protein-protein interaction studies [79, 80]. Self complementing fragments have been developed that can be used to study different cellular events such as subcellular localization of proteins, cell-cell fusion, and the evaluation of cell delivery vehicles [81, 82]. Further mutations have been added to improve the light output 5-fold [83]. As Rluc does not require ATP it can be used for extracellular applications such as detection of antigens with antibodies fused to Rluc protein [16] or for the creation of “self-illuminating” quantum dots [17]. Coelenterazine is a substrate for the multidrug resistance MDR1 P-glycoprotein (Pgp) [84] and differential expression of this protein over the course of an experiment can interfere with non-invasive detection of Rluc levels. As Pgp is a structural part of the BBB this is a complicating factor

for the use of Rluc in the brain. The other luciferase that uses coelenterazine as its substrate is Gluc. It is a small 20 kDa protein that is extracellularly secreted and that does not require ATP. It has been codon-optimized and it produces a light output 100 fold higher than Rluc [85]. Split reporters have also been designed for the detection of protein-protein interactions where its small size and high light output have allowed the development of a sensitive *in vitro* system [86]. *In vivo* experience using this luciferase is still limited and extracellular secretion might be a confounding factor in animal studies. For neurological research BLI has been used to track *ex vivo* transduced and implanted neuronal progenitor cells [87, 88], to monitor the growth of implanted [89-91] and spontaneous [92, 93] brain tumors, to determine gene expression after adenoviral vector injection in orthotopic brain tumors [94] and to monitor treatment of herpes simplex encephalitis [95]. The gene transfer studies into intracranially implanted tumors monitored gene expression only for 17 days [94]. Yoshimitsu *et al.* [96] used BLI to evaluate gene expression after intravenous injection of lentiviral vectors encoding luciferase in mouse neonates

2.2.2. Fluorescence Imaging Reporter Genes

Since its first use as a reporter of gene expression [18], the jellyfish-derived GFP has become nearly ubiquitous in molecular biology. It has allowed to inject genetically encoded specificity at the cellular and subcellular level. Many strategies have been applied to improve the intrinsic properties of this protein [97], to shift the emission wavelength [20] or to link fluorescence to specific cellular processes [98]. An other family of fluorescent proteins has been cloned from anthozoa corals [19] and has since then been further optimized (for review see [99]). Most of these proteins require oligomerization to become fluorescent although monomeric variants have been designed [100]. The chromophore of GFP is the result of the cyclization of amino acid residues 65-67 (Ser-Tyr-Gly) at the center of a β -barrel structure in the mature protein, and is generated in an oxygen dependant matter [97]. Protein folding and maturation, quaternary structure, intrinsic brightness and photobleaching are all important parameters to be taken into account when using fluorescent proteins. For *in vivo* imaging the monomeric red shifted variants such as mPlum [101] are the most interesting because of optimal penetration of the emitted light through tissue. Despite all these improvements, quantitative *in vivo* imaging using fluorescence remains challenging. It needs to be noted that GFP expression can have toxic effects under certain circumstances [102]. For instance, cardiomyocyte specific expression of GFP using the α -myosin heavy chain gene promoter resulted in a moderate-

to-severe dilated cardiomyopathy in 2 lines of transgenic mice out of a total of 4 lines [103]. The cardiomyopathy occurred in the two lines with the highest expression levels, suggesting a dose dependent effect. In an *in vivo* gene transfer study to the mouse substantia nigra, robust expression of GFP mediated by high titers of AAV8 caused neurotoxicity, including dopaminergic cell death [104]. Recently, it was shown that GFP expression can interfere with polyubiquitination, a post-translation modification that consists of attaching multiple ubiquitin molecules to a protein. There are two major forms of polyubiquitination and they differ by the site of the isopeptide bond (on lysine 48 or 63 respectively). Lys48-linked polyubiquitination targets a protein for degradation and is important for maintaining homeostatic levels of certain proteins (e.g. p53) and in certain signal transduction pathways. GFP-mediated reduction in signal transduction activity or in protein levels might be responsible for the observed cell death. GFP expression can also result in more than 2-fold changes of expression levels in some 200 genes. Finally, immune-mediated toxicity can also be of concern. Skin grafts from rats transgenic for GFP were rejected by wild type rats in less than 10 days, whereas grafts from rats transgenic for firefly luciferase were tolerated for more than 100 days [105].

2.3. Magnetic Resonance Techniques

Efforts towards the development of MR reporter genes have been pursued for more than 15 years but the field is still in an early developmental stage. The major hurdles have been the low sensitivity of detection and the pharmacokinetic behaviour of the developed probes [106]. However, recently significant progress has been made and some biological applications have been reported.

2.3.1. Magnetic Resonance Spectroscopy Reporter Genes

The first examples of reporter genes for MRS were based on genes encoding enzymes that catalyze the conversion of ATP to adenosine diphosphate (ADP), yielding a signal (change in ATP/ADP ratio) that can be measured by ^{31}P MRS. The creatine kinase (CK) gene from the mouse brain was expressed in a liver specific manner in a transgenic mouse model and non-invasive detection of gene expression could be performed [107]. This reporter gene has been used to study gene therapy strategies targeting the mouse liver with adenoviral vectors [108]. Recently, this gene was used for indirect monitoring of expression of the low-density lipoprotein receptor (LDLr) gene in transgenic mice lacking this receptor and the *in vivo* measured phosphocreatine concentration was a good

predictor of LDLr expression levels [109]. A similar strategy is based on the use of the arginine kinase (AK) gene from *Drosophila melanogaster* that besides converting ADP to ATP also produces phosphoarginine, a metabolite that is not present in vertebrate cells and that can be detected in the ^{31}P spectrum [110]. The major drawback for both CK and AK genes is the fact that they influence the energy metabolism and that the signal depends on the energetic state of the cell which can vary depending on a range of influences [106]. Furthermore the endogenous expression of CK in brain and the activation dependent changes in brain metabolism are likely to preclude this system for being used for brain studies. Another approach based on ^{31}P MRS is proposed by Ki et al. [111] who have used two yeast genes that encode part of the vacuolar transporter chaperone (Vtc) and the vacuolar H^+ -ATPase (V-ATPase) which are the major determinants of inorganic polyphosphate (polyP) accumulation in yeast. PolyP concentration can be measured in yeast cells with MRS as the authors have shown, but it remains to be determined if similar high concentrations ($\sim 120\text{mM}$) will be reached in higher organisms. Furthermore, background polyP concentrations may cause an unfavorable signal to noise ratio. A recent report using the bacterial polyphosphate kinase succeeds in detecting polyP in eukaryotic cells *in vitro* [112].

Other MRS approaches are based on the conversion of a probe or prodrug by the enzymatic activity of the reporter protein. The yeast cytosine deaminase (CD) gene catalyses the conversion of the harmless prodrug 5-fluorocytosine (5-FC) to 5-fluorouracil (5-FU), a standard clinically used chemotherapeutic drug. Using ^{19}F MRS, Stegman *et al.* [113] were able to measure conversion of 5-FC to 5-FU in mouse xenografts of human colon cancer. Another group has used genetically modified attenuated *Salmonella serovar typhimurium* species that express yeast CD as a vehicle for gene transfer to hypoxic tumours. Upon injection of the bacteria, they colonize the hypoxic tumor areas and they can convert 5-FC to 5-FU that is released to the tumor cells. MRS of this strategy allows non-invasive monitoring of gene activity within the tumors [114]. These approaches could be translated to brain studies as 5-FC does cross the BBB readily. A similar enzymatic approach has been used with β -galactosidase (β -gal) where the liberation of a glycone group from the substrate 4-fluoro-2-nitrophenyl- β -D-galactopyranoside leads to a small chemical shift of the ^{19}F MRS signal [115]. However, the amplitude of the shift depends on the pH of the cell and this might complicate applications of this approach. Furthermore, the penetration of the BBB by this compound was not studied.

2.3.2. Magnetic Resonance Imaging Reporter Genes

This same enzyme β -gal has been used as a reporter with specific activatable or “smart” probes that emit no signal in their native state but that become active after a specific molecular interaction, allowing their non-invasive detection. The gadolinium based EgaMe contrast agent contains a galactose group that prevents the gadolinium atom from interacting with the hydrogen atoms in the surrounding water molecules and thus prevents the T1 signal increase caused by this interaction. In cells expressing the lacZ gene encoding β -gal, the enzyme will cleave off the galactose group restoring the gadolinium/hydrogen interaction and thus yielding signal. This concept was demonstrated in embryos of *Xenopus laevis* with MRI after injection of EgaMe at the 2 cell stage of development [116]. Both cells were injected with probe but only one with LacZ mRNA, resulting in a mature embryo with intense signal on one half of his body as the first mitosis roughly separates the future left and right side in this species. The lack of cellular penetration of this compound has precluded its further use. A more general problem with these smart probes is the fact that in their native state the signal is not equal to zero and so image interpretation may be complicated [106].

Similar to radionuclide imaging, receptors have also been used to bind MRI contrast agents. One receptor type that has been used is the human transferrin receptor that has been engineered to achieve supraphysiological expression levels and that binds transferrin conjugated monocrystalline iron oxide nanoparticles (MION) [117, 118]. Upon binding to the receptor, the receptor/ligand complex is internalised and the MION particle is trapped in the endosomes where it will cause a significant shortening of T₂ relaxation time that can be detected by MRI. Other generic strategies have been proposed with either antibodies conjugated to ultra small superparamagnetic iron oxide particles (USPIO) that bind to a non-endogenous antigen [119] or fusion proteins containing avidin that bind biotinylated iron particles [120]. These approaches are still in the *in vitro* stage and sufficient binding and accumulation *in vivo* remain to be demonstrated. Furthermore, *in vivo* uptake of the USPIOs by macrophages might yield aspecific signal and the BBB-crossing potential of these rather large particles is doubtful.

Several strategies exploit the fact that increasing the accumulation of endogenous iron in cells yields significant MR contrast. Proof of principle of this concept was provided with overexpression models of the transferrin receptor (TfR) that binds endogenous transferrin which contains two iron atoms that will be released to the cell in the endosomes. Xenografts of TfR overexpressing fibroblasts were shown to have almost threefold higher iron content which resulted in a 25% decrease of T₂ signal. Subsequent

approaches used the human tyrosinase gene which is the rate limiting enzyme for melanin synthesis. Melanin has a high affinity for iron resulting in an iron-mediated 30% increase in T_1 signal intensity in fibroblasts and embryonic kidney cells that overexpressed tyrosinase eightfold [121]. Inducible expression of tyrosinase resulted in significant signal changes *in vitro* [122]. The use of tyrosinase might be limited by the increase in reactive oxygen species production mediated by melanin and its precursors that can result in significant toxicity. A different strategy has used the iron storage protein ferritin which can contain up to 4000 iron atoms in a crystal configuration that shields them from biochemical interaction with the cellular *milieu*. Because of the random orientation of the spins within this particle most spins cancel out with an antiparallel spin and so the net magnetic moment is coming from uncanceled spins on the surface of the crystal. Artificial (U)SPIOs have all spins aligned endowing them with a much greater (~20 to 200) magnetic moment [106]. Nevertheless, at higher magnetic field strengths ferritin can exhibit strong T_2 contrast enhancing properties as shown by Genove *et al.* [123]. Adenoviral vectors encoding both the heavy and light chain of ferritin were injected into the mouse brain and this resulted in a visible hypointensity on 11.7 Tesla T_2 and T_2^* -weighted images from 5 days to 39 days after injection. Quantification of the signal over time was not provided. Another group has shown regulatable transferrin expression in tumor xenografts with a tet-off system in which tetracycline inhibits ferritin expression [124]. Significant relaxation rate changes at 4.7 Tesla due to increased iron content were seen in the absence of tetracycline at one time point for R_1 and at all time points for R_2 but it has to be noted that these changes are small (less than 15% increase). Nevertheless, lower numbers of cells (40 times less) could be detected compared to the tyrosinase system. Co-expression of ferritin and TfR has been proposed by Deans *et al.* [125] who could show increased iron concentration and higher R_2^* values on *ex vivo* brain scans after cell transplantation. The additional value of the TfR to ferritin expressing cells was not examined so this still needs to be determined. Transgenic mice expressing ferritin under influence of specific promoters have been used to image expression in endothelial cells and in the liver of living mice [126]. Ferritin has a number of drawbacks: (i) it relies on the presence of endogenous iron but different tissues have different iron concentrations (ii) sensitivity is dependent on magnet strength and is lower at the 1.5 [125] and 3 Tesla field strengths that are clinically available (iii) transferrin does not report cell viability because when transferrin overexpressing cells die the crystal will remain for some time on site and causes signal until final metabolism (iv) in dividing cells, the iron within the ferritin molecules will be diluted, leading to decreased signal that will return to normal when the cells have replenished the transferrin to predivision levels

and this process is accompanied by non-linear effects [106] (v) ferritin is a negative contrast agent in T2 and T2*-weighted images which can complicate quantification and the relaxation rate can be influenced by other parameters than ferritin. A strong advantage of the ferritin gene is the absence of reporter probe and despite the aforementioned pitfalls it is expected that ferritin based approaches will be applied to study biological hypotheses in the near future.

A reporter system for MR that is based on proton exchange has recently been proposed. In this system, radiofrequency irradiation is used to noninvasively label agent protons that exchange with water. These chemical-exchange saturation transfer (CEST) agents produce contrast by changing the relaxation rate of water and they can be switched on and off by selectively irradiating (saturating) at the exchangeable proton resonance frequency. Rapidly exchanging amide protons in polypeptides yield CEST signal in solution and so an artificial reporter gene encoding a protein consisting of 200 lysine residues (lysine-rich protein, LRP) was developed [127]. CEST signal could be detected in cells *in vitro* and in orthotopic brain tumors in rat brain. A significant advantage of this reporter gene is the fact that the encoded protein is biodegradable so it can be used to assess cell viability.

3. Vectors for Gene Transfer

Progress in the field of virology and advances in biotechnology have allowed the development of virus-based systems that allow the transfer of genetic material to cells, the so-called viral vectors. These viral vectors can be used for basic science purposes in cell systems or in model organisms or they can be used for *ex vivo* or *in situ* gene therapy. Viral vectors are based on the fact that viruses have been selected over billions of years to infect cells, introduce their genetic material and replicate it. For the development of viral vectors, the replication potential is suppressed or made dependent on specific cellular alterations, by deleting parts of the viral genome. This results in a single round infection of the host cell without replication. The deleted genes can be replaced by a gene of interest that will be expressed in the host cell. Vectors harbour a single or double stranded DNA or RNA genome that is sheltered in a protein cage called the capsid. The latter can be surrounded by a lipid bilayer, the envelope, derived from the host cell in which the vector was produced. This envelope can carry some of the lipo- or glycoproteins from the host cell. The general concept of viral vector development is the physical separation in different

plasmids of *cis*-acting elements involved in the transfer of the vector genome from the *trans*-acting elements that encode the structural viral proteins. Transfection of all plasmids into production cells will provide these cells with all the genetic material necessary for vector production while minimizing the risk of forming infectious particles. There is however a risk of obtaining replication competent vectors by homologous recombination. Several technical design elements of the viral vectors aim to prevent homologous recombination and vector batches are tested for recombinant viruses before use. Many different viral vectors have been described and they all have their strengths and weaknesses. The choice of a particular system is mainly dependent on the desired duration of transgene expression, the size of the transgene, the target cell and biosafety issues.

The most widespread viral vectors derived from RNA containing viruses are based on retroviruses. These are a large family of viruses that are found in all vertebrates and that can be divided in three main groups: the oncoretroviruses, the lentiviruses and the spumaviruses. A retroviral vector contains two copies of a single-stranded RNA genome which is surrounded by a conical core and the envelope. Retroviruses have been the object of intense study resulting in a detailed knowledge of their genome and of their relatively straightforward replication cycle. The retroviral genome consists of three major coding domains flanked by long terminal repeats (LTR): *gag* encodes the core proteins matrix, capsid and nucleocapsid, *pol* encodes the viral enzymes reverse transcriptase (RT), integrase and protease and the *env* gene encodes the surface and transmembrane components of the envelope glycoproteins. During infection or transduction these glycoproteins will bind to a specific receptor and the viral capsid, which harbours the RNA genome, will enter the host cell through membrane fusion. In the cytoplasm, the viral RT converts the genomic RNA into double-stranded DNA, the proviral DNA. This proviral DNA is bound to different viral proteins (RT, integrase and nucleocapsid) in the so-called preintegration complex. The latter is transported to the nucleus by an ill-understood process and there the integrase enzyme will catalyze the insertion of the proviral DNA into the genome of the host cell. Cellular transcription factors will transcribe the proviral DNA from the LTRs which results in the production of new viral RNA. Translation of parts of this RNA results in production of the structural and envelope proteins and the enzymes protease, integrase and RT. The genomic RNA and newly produced viral proteins are assembled during the budding process and form a new viral particle. The expression level may vary depending on the integration site, the copy number, the promoter choice, the use of specific regulatory elements and the transgene [128]. The predilection for a specific

integration site on human chromosomes is dependent on the type of retrovirus: human immunodeficiency virus (HIV) preferentially targets actively transcribed genes whereas murine leukemia virus will be found near transcription start regions with only a weak bias towards active genes [129]. The main safety issues regarding retroviral vectors for gene therapy are the risk of insertional mutagenesis, the possibility of vector mobilization after infection of transduced cells with the parental virus and the generation of new pathogenic viruses after recombination of the vector with endogenous retroviruses in the host tissue [130].

3.1. Oncoretroviral Vectors

The oncoretroviral viruses were named after one of their characteristic features: the capacity to induce malignant transformation. The vectors are derived from viruses such as the murine leukemia virus and the Rous sarcoma virus. These vectors were the first ones used for gene transfer *in vitro* and *in vivo*, including clinical applications. They can carry an insert of up to 8000 base pairs (bp) but they can only transduce dividing cells and integrate their genome after division. The aforementioned oncogenesis is a major concern for clinical gene therapy applications. In two gene therapy trial for X-linked severe combined immunodeficiency (SCID-X1), 4 out of 20 children developed T-cell acute lymphoblastic leukemia due to insertional mutagenesis upstream of growth promoting genes, including *LMO2* [131].

3.2. Lentiviral Vectors

Lentiviruses, together with the spumaviruses, belong to the so-called complex retroviruses. Both primate and non-primate lentiviruses have been used to develop lentiviral vectors (LV) and they all transduce dividing and non-dividing cells to a similar extent. Some authors have argued that potential recombinant virus resulting from non-primate vectors would be non-pathogenic in humans, resulting in a theoretical biosafety advantage of these vectors over primate LV. Primate (simian immunodeficiency virus) and non-primate (e.g. equine infectious anemia virus and feline immunodeficiency virus) have been used, but the most widely used LV is derived from HIV-1. Lentiviral vectors (LV) transduce both dividing and non-dividing cells and ensure stable and long-term transgene expression because they integrate into the host genome [132]. Stereotactic injection of LV into the brain of mice, rats or primates generates locoregional transgenic animals that are

not affected by developmental plasticity. The contralateral side of the brain serves as an internal control. We and others have used this technology to create models of neurodegenerative diseases such as PD [133] allowing functional genomic studies and evaluation of therapeutic strategies [134]. LVs have great therapeutic potential for CNS disease since a wide range of neuronal and glial cell types are stably transduced, expression is long-term and inflammatory and immune responses are mild [135]. Pre-clinical therapeutic efficacy was achieved after local injection [136], systemic delivery [137], or by retrograde axonal transport after peripheral injection [138]. LV have been engineered to encode short hairpins as precursors of siRNA to silence gene expression by RNA interference [139]. Promising therapeutic results have been obtained for diseases caused by “toxic gain-of-function” mutations such as amyotrophic lateral sclerosis [140, 141]. The use of viral vector-mediated gene transfer into the brain is confined by the inter-individual variation of gene expression and the lack of non-invasive assessment of the location, magnitude and duration of transgene expression.

3.2.1. Molecular Biology of Lentiviral Vectors

The HIV-1 viral particle has a diameter of 110 nm and it contains two copies of a single-stranded RNA genome of 9200 bp. The genome is made up of the 3 major genes found in the simple retroviruses (*gag*, *pol*, *env*) supplemented with 6 accessory genes that encode additional regulatory genes: *tat*, *rev*, *vpr*, *vpu*, *vif* and *nef*. *Tat*, which mediates transactivation of viral transcription, and *rev*, which is responsible for nuclear export of unspliced viral RNA, are present in all lentiviruses. LV were developed in 1996 by Naldini *et al.* [132, 142] using the same strategy that was previously used for retroviral vectors. LV are produced by triple transient transfection in 293T cells using three different plasmids. The first plasmid is the packaging plasmid and it encodes the structural viral proteins from *gag* and the enzymes encoded by *pol* under control of a constitutive promoter, the human cytomegalovirus (hCMV) promoter. The packaging signal (Ψ), a *cis*-acting element responsible for incorporation of the RNA into the viral particle, and the *env* gene have both been deleted from this plasmid, so the RNA transcript is not incorporated in the LV particles. This plasmid also encodes the Rev protein. The second plasmid encodes the envelope glycoprotein of the vesicular stomatitis virus (VSVg). The third plasmid carries the transgene which can be a reporter gene or a therapeutic gene under control of an internal promoter and surrounded by *cis*-acting elements such as the packaging signal Ψ (for encapsidation), the primer binding site and terminal polypurine tract (for reverse transcription), the Rev responsive element (for nuclear export of the RNA genome) and

attachment sites at the end of the LTR (for integration). As the encapsidation signal lies within the *gag* gene, there is a small overlap between the transfer plasmid and the *gag* gene encoded on the packaging plasmid.

After triple transfection, viral vector particles bud from the produced cells into the cell culture medium. Pseudotyping the LV with VSVg stabilizes the particles allowing concentration with ultracentrifugation and provides a broad cellular tropism to the LV particles. After concentration of the LV particles, titers are typically determined by enzyme linked immunosorbent assay (ELISA) for the capsid protein p24, by reverse transcription polymerase chain reaction (RT-PCR) or by flow cytometry of cells transduced with serially diluted LV. The latter can only be used with LV encoding fluorescent proteins. Quantification is still hampered by the variation in methods which precludes comparison between different research groups and currently there are no standardised methods for quantification. Particle titer (pg p24/mL) and the transducing titer (TU/mL) are both important parameters, because impurities and variations in transduction potential can influence the efficacy of gene transfer and toxicity of the LV [143].

3.2.2. Lentiviral Vector Biosafety

The use of therapeutic vectors derived from HIV might encounter resistance because of the strongly negative connotation of this virus. Biosafety issues thus need to be addressed before this vector system can be widely used for biomedical research or clinical purposes. The transfer plasmid has thus been stripped of most viral sequences that are not strictly necessary for single round infection. The *cis*- and *trans*-acting elements were split over different plasmids. To generate replication competent lentiviruses (RCL) from these split-genome plasmids, multiple recombination events in the producer cells would be required, which is highly unlikely. In the first generation of LV, the natural HIV envelope gene was deleted and the vector was pseudotyped with VSVg. Furthermore, Ψ is deleted from the packaging plasmid and the LTRs are replaced by a heterologous promoter and a polyadenylation signal. In the second generation LVs, on top of these changes there has also been a deletion of the genes encoding the accessory proteins (Vif, Vpr, Vpu and Nef) [144]. As HIV loses its pathogenic potential in the absence of these genes, this represents an important step in biosafety as there is no source containing these genes in the producer cells or in target tissue. Third generation LV do not require the Tat protein for production as the U3 region of the 5' LTR in the transfer plasmid is replaced by a constitutive promoter [145]. The packaging plasmid does not contain the *tat* gene anymore and the Rev protein is provided by a fourth plasmid. An important biosafety measure is the

introduction of a self-inactivating (SIN) 400 bp deletion in the 3' LTR of the transfer construct. This deletion removes most of the promoter activity from the LTR and as the 3' LTR serves as template for the 5' LTR during reverse transcription, the integrated provirus will have this mutation at both LTRs. This system thus removes the LTR promoter activity which has been implicated in insertional mutagenesis in the SCID-X1 trial [146].

Another strategy to overcome the problem of insertional mutagenesis is the use of integrase deficient LVs [147]. These vectors can still transduce cells but their proviral DNA is not integrated into the host chromosome but is maintained episomally.

A number of tests for RCL can be performed. In the vector rescue assay, naïve cells are inoculated with the supernatant of cells transduced with a LV encoding a reporter gene. Detection of the reporter gene in these naïve cells is tantamount to the presence of RCL. In the Tat transfer assay on HeLa P4.2 cells, the presence of Tat producing HIV (RCL) will be visualized by LacZ reporter gene expression, since LacZ is driven by the HIV LTR in these cells. Other strategies for RCL detection are based on the repeated measurement of p24 concentration by ELISA or on the detection of RT activity in an RT assay. More sensitive tests such as quantitative PCR with primers and probes directed against the viral sequences should be routinely performed during production of LV for clinical trials [128].

3.2.3. Improvements in Lentiviral Vector Design

In recent years improvements in the design of LV have resulted in enhanced efficacy and improved specificity of these vectors. A first amelioration has been the insertion in the LV of the so-called central polypurine tract (cPPT) in the center of the HIV genome. As a result of central initiation and termination of the second strand synthesis during reverse transcription, a central DNA flap is created, which aids in the nuclear import of the preintegration complex [148]. Inclusion of this element in the LV increases the transduction efficiency and gene expression three- to tenfold because of enhanced nuclear import [149]. Other improvements have targeted the post-translational stage. The woodchuck hepatitis virus posttranscriptional regulatory element (WPRE) enhances expression levels ~five fold in different cell lines and tissues because of the increased stability of the mRNA. It has to be noted that due to an open reading frame in the WPRE a 60-amino acid fragment of the hepadnavirus X protein can be expressed and this has been linked to oncogenesis with specific LVs [150].

Pseudotyping with envelope glycoproteins allows to change the tropism of LV to target specific cell types, in line with the tropism of the original virus. It also allows to explore

transduction routes different than the ones used by HIV. Many different glycoproteins have been studied in this context [151]. For transduction of the central nervous system (CNS), VSVg enveloped vectors are mostly used. They target both astrocytes and neurons, whereas LV pseudotyped with the envelope of the lymphocytic choriomeningitis virus predominantly transduce astrocytes and neural progenitor cells [152]. Intramuscular administration of LV pseudotyped with the rabies virus envelope resulted in retrograde transport to the CNS. The envelopes from the Moloka virus, human foamy virus and amphotropic murine leukemia virus have also been studied for CNS targeting. The production of LV with varying envelopes can be difficult and stability and toxicity should be carefully evaluated.

A key issue in applying LV to clinical gene therapy trials is the regulation of transgene expression in the case of side effects. Unlike classical pharmacological treatment the therapeutic/iatrogenic effect can not be halted by simply stopping administration of the drugs, as they are continuously produced from integrated proviral DNA. One possibility is the incorporation of suicide genes that can be ablated with prodrugs that are harmless for non-transduced cells (e.g. HSV1-tk). Another approach is based on the use of regulatable promoters where expression can be up- or down-regulated upon addition or removal of a specific ligand. The best characterized system is based on a tetracycline-inducible promoter (tet-on and tet-off), but this system still maintains a low baseline expression level in conditions where expression should be turned off [153]. For some applications it is desirable to express multiple subunits of a heteromultimeric protein, to express multiple genes or to include non-therapeutic genes such as reporter genes or suicide genes. Multicistronic vectors have been developed based on different systems. A first strategy uses fusion proteins that incorporate different moieties from multiple proteins in one single protein [154, 155]. The downside of this strategy is the functional impairment that can be caused by the bulky size. Another strategy is based on the use of bidirectional promoters or incorporates two promoters within the same vector. This strategy is limited by low expression levels and a lack of space in the vector, respectively. The most frequently used system is based on a viral-derived sequence called internal ribosome entry site (IRES), a sequence in the mRNA that initiates a separate ribosomal translation of the downstream gene. This IRES sequence is placed between the two transgenes. The major limitation is the lower expression from the gene downstream from the IRES and these sequences are rather large in size (~500 bp). Another virus-derived sequence is based on the protease-independent cleavage of multigene products by 2A-peptide sequences. These highly conserved small sequences

(between 54 to 66 bp) disrupt translation and impair the normal formation of a peptide bond between the last residue of the 2A peptide and the next residue. Inclusion of this sequence between genes in LV can result in stoichiometric expression of more than two genes [25]. However, in some systems a large fraction of the expression product can remain uncleaved and the effect of the residual 2A-tag on the expressed proteins is not known [156].

Stable integration of retroviral vectors in the genome contributes in part to transcriptional gene silencing that compromises long-term gene expression [157]. The incorporation of *cis*-acting elements as insulators and scaffold or matrix attachment regions (S/MAR) has been used to reduce silencing. S/MARs are believed to bind to the nuclear matrix of genomic DNA and establish local access of transcription factors to the enhancer/promoter sequences within the domain which results in increased gene expression.

The development of stable producer cell lines has been advocated for production of clinical grade LV. However, this has been a challenging task as several HIV-derived proteins and the VSVg protein are cytotoxic. Several groups have developed inducible packaging cell lines for the stable production of LVs but all of these suffered from low vector titers. Large-scale production of LV using stable producer cells has been reported, paving the road for potential clinical applications [158].

3.2.4. Applications of Lentiviral Vectors

LVs offer the unique potential for *ex vivo* or *in vivo* introduction of any gene sequence in the genome of dividing or non-dividing cells, resulting in long-term gene expression. The potential of LVs has been mainly used in two areas. The first is basic biomedical research where they are used for up- and downregulation of gene expression and the creation of local somatic transgenic animal models. A second area is clinical gene therapy, either by overexpression of therapeutic genes or the downregulation of disease causing genes [159]. Different delivery routes can be used for delivery of therapeutic LVs. Delivery can be *in vitro* into cell lines and primary cells, *ex vivo* into primary cells isolated from patients (e.g. hematopoietic stem cells) or *in vivo*, either into blood vessels irrigating a particular organ or directly into the organ (such as stereotactic brain injections). LVs have been tested in clinical phase I trials in the context of anti-HIV gene therapy [160], thalassemia [161] and X-linked adrenoleucodystrophy.

3.3. DNA Containing Viral Vectors

3.3.1. Adenoviral Vectors

More than 50 adenoviral (Ad) serotypes have been isolated from a large range of species and tissue types. Adenoviruses are non-enveloped icosahedral viruses with a double-stranded DNA of 36.000 bp. They can infect and replicate in a wide range of tissues including the respiratory, urinary and gastrointestinal tract, the eye and the liver [162]. Extensive splicing of the viral mRNA results in the production of more than 50 proteins of which only 11 are structural virion proteins. The viral life cycle is divided in an early and late phase. The genes can be categorized in three major groups: the early genes (E1A, E1B, E2, E3 and E4), the genes of delayed transcription (IX and Iva2) and the major late transcription unit, which is processed into 5 mRNAs (L1 to L5). The E1, E2 and E4 genes encode proteins that are necessary for DNA replication, whereas the E3 protein plays a role in immune suppression. The majority of Ad serotypes interact with the Coxsackie-adenovirus receptor (CAR) and virus internalization is mediated through interaction with the cellular integrin α_v receptor [163]. The Ad genome is transported to the nucleus through the nucleopore of dividing and non-dividing cells, but the viral DNA is not integrated into the host DNA but is replicated extrachromosomally. This results in dilution of the DNA with subsequent cell division. The major hurdle for the clinical use of Ad-based vectors is the strong immune response that is observed *in vivo*, since ~50% of people have antibodies against serotypes 1, 2 and 5. The most frequently used Ad-vector is derived from serotype 5, but many other human and non-human serotypes have been described as well. The first generation of Ad vectors in which the E1 gene was replaced by a transgene induced immune responses when injected *in vivo*. In the second and third generation vectors called gutless or minimal vectors all the viral coding sequences were removed from the vector genome. Only the terminal ends consisting of the inverted terminal repeats (ITR) and the packaging sequence were retained. These gutless vectors are superior to the first generation vectors because of their high payload, reduced immunogenicity and long-term gene expression in liver, muscle and even brain [164]. The proteins necessary for viral DNA replication and packaging have to be provided in *trans* during production.

3.3.2. Adeno-Associated Viral Vectors

Adeno-associated viruses (AAV) are members of the parvovirus and up to now no single AAV has been shown to be pathogenic in humans. Nine subtypes of the virus have

been found for which the human species is the primary host. Some 80% of the population is seropositive for the most common serotype AAV2 but there is no known pathology associated with it. AAV virions are small icosahedral non-enveloped particles (20-25nm) that contain a linear single-stranded DNA genome of ~4700 bp. There are two open reading frames in this genome, *red* and *cap*, flanked by ITRs. Only the ITRs are retained in AAV vectors and they play a role in integration, packaging and replication. Four regulatory Rep proteins are required for replication and packaging. The *cap* gene encodes the three structural proteins that form the capsid (VP1, VP2 and VP3). This genomic structure has been found in most AAV serotypes currently known [165]. Infection with AAV necessitates a second helper virus that can be an adenovirus or a herpes virus. They can also replicate in cells that are under stress such as ionising radiation. When there is no permissive environment that supports AAV replication, the AAV genome can become integrated into the host cell genome to establish a latent infection. AAV vectors transduce non-dividing cells and long-term transgene expression is obtained from episomal monomers and concatamers. In the presence of viral Rep proteins (Rep 68 and 78), AAV will specifically integrate in chromosome 19 [166]. Since Rep is not encoded by AAV vectors there is only a small fraction of AAV vectors that integrate into the host genome and these integrations occur at random locations within the host genome. There is however a marked preference for integration in actively transcribed genes or near transcription start sites [167, 168]. After gene transfer, gene expression rises slowly, reaching a steady-state level after a period of weeks. This is due in part to the time needed to generate double-stranded DNA genomes by annealing of single-stranded genomes or by second strand synthesis followed by vector genome linking to form concatamers. In the production process of AAV vectors, Rep and Cap are provided in *trans* from a plasmid together with a helper virus, usually an Ad. High-titer AAV vectors can be produced but small amounts of the wild-type Ad contaminate these vector preparations. The increased knowledge of the molecular virology of AAV and Ad have led to production methods where 293 cells (which already express the adenoviral protein AdE1) are transfected with a mini-Ad plasmid that supplies the required E2A, E4 proteins and the VA RNA, without the possibility of production of infectious Ad.

AAV vectors based on the serotype 2 capsid have been the most commonly used and transduction of a wide range of tissues has been demonstrated including the brain, retina, muscle, liver and lungs. AAV transduction is greatly enhanced in the S phase of the cell cycle but cells in any stage of the cell cycle can be transduced. The major obstacles for clinical use of AAV are the limited packaging size, the possible humoral immune response against the viral capsid and the presence of circulating neutralizing antibodies

against AAV in the majority of the population. However, modifications in the viral capsid or use of capsids from different serotypes may overcome the latter problem [164].

3.3.3. Herpes Simplex Virus Type-1 Vectors

Human herpes simplex virus type 1 (HSV-1) is a large DNA virus with a double-stranded genome of 152 kb, containing more than 80 almost entirely unspliced genes. Half of these turn out to be non-essential for viral replication in cell based assays. The HSV-1 virion is 20 nm in diameter and consists of an envelope, a tegument, a capsid and the viral genome. HSV vectors can contain up to 30 kb of payload DNA. Natural infection with HSV-1 is a biphasic process with a lytic replication phase in mucosal or epithelial cells followed by a latent phase where the viral genome persists in neurons. The wild-type virus can be reactivated from its latent state under influence of a range of stressors. It is possible to construct replication defective viruses that retain the ability to establish persistent latent genomes in neurons, but that are unable to reactivate. These persistent genomes lack expression of the lytic genes but retain the ability to express latency-associated transcripts. HSV-1 based vectors can transduce non-dividing cells of a large number of cell types but they do not integrate and are maintained episomally. The neurotropic nature of this virus make it a good candidate for gene therapy for neurological diseases such as malignant glioma [169]. However, limitations to the use of these vectors are the suppression of transgene expression associated with the latency state, immune response caused by residual viral proteins expressed from the HSV-1 vector after long-term gene expression in the CNS and difficulties related to vector targeting, since the mechanism of HSV-1 attachment and entry is complex, involving multiple viral envelope glycoproteins [164].

3.4. Non-Viral Vectors for Gene Delivery

Potential problems with viral vectors such as pre-existing immunity, immunogenicity of viral proteins and insertional mutagenesis have stimulated research in gene transfer methods that are not derived from viruses. Similar to viral vectors, their main aim is to protect the DNA from nucleases, to deliver it across the plasma membrane and bring it into the nucleus. Two main approaches can be recognised: chemical methods (or synthetic gene carriers) and physical methods (using no carrier).

3.4.1. Physical Methods

Physical approaches are based on the application of a force onto cells or tissue that will induce transient defects in the cell membranes so that DNA can diffuse into the cell. The most simple physical method is local needle injection of naked DNA which results in transgene expression in organs such as muscle, liver and lung, and is devoid of toxicity. *In vivo* applications are hindered by the presence of nucleases and by various barriers to DNA that prevent it from entering the nucleus. The gene gun concept is based on bombarding tissue with DNA-laden gold particles that penetrate the tissue for several millimeters, releasing the DNA into the cells on their path. The ease of this method makes it a good candidate for DNA-based immunization. Electroporation can be used in any type of tissue in which two electrodes can be inserted and increases reporter gene expression by 2 to 3 orders of magnitude compared to naked DNA. It can result in stable expression up to one year [170]. However, the limited effective range (~1 cm) between the electrodes restricts this method to small volumes and the high voltages applied can cause tissue damage. Ultrasound can be used to transfer DNA to cells or tissues, resulting in a ~10 to 20-fold increase in gene expression over naked DNA. Ultrasound creates membrane pores allowing diffusion of DNA into the cell. The penetration of soft tissue to access the internal organs and modulation of gene delivery based on output strength, frequency and duration allow modulation of gene expression in the desired tissues. Low efficiency is still the major hurdle for this technique. Hydrodynamic gene delivery is a simple method that is based on the rapid intravenous injection of a large volume of fluid causing retrograde flow into the organs where the pressure increase will result in transient membrane defects allowing the DNA to enter the cells. This method achieves the highest efficacy of all non-viral methods: ~35% of hepatocytes can be transfected by a hydrodynamic injection of 50 µg plasmid DNA into a mouse [171]. This method has been used for delivery of many different therapeutic proteins in mice as well as small interfering RNAs and imaging constructs [24]. The challenge for this technique is the adaptation of this simple method in mice to an applicable clinical method. Direct upscaling to humans would require rapid injection of ~7.5 liter of fluid which is not tolerable, but catheter based occlusion models that have recently been developed in swine liver [172] require smaller volumes (150 ml) and might be translated to patients.

3.4.2. Chemical Methods

The other main non-viral strategy, chemical methods, is based on formulations where the DNA is packed into condensed particles with cationic lipids or polymers. These

enter the cell by endocytosis, macropinocytosis or phagocytosis and the DNA is released into the cytoplasm. Cationic lipid-mediated gene delivery is a routine technique for *in vitro* cell culture. When plasmid DNA is mixed with cationic lipids alone or with neutral helper lipids that generate liposomes, small quasi-stable particles called lipoplexes are formed. These lipoplexes can efficiently transfect cells in the absence of serum. *In vivo*, however, they tend to interact with negatively charged blood components and form large aggregates, preventing efficient DNA delivery to the cell. Epithelial barriers such as mucus or surfactant in the lung also inhibit the transfection activity of lipoplexes. After intravenous injection, expression peaks within 24 hours and declines rapidly thereafter. Toxicity of these complexes is mostly marked by an acute inflammatory response [173], which is a serious concern for clinical translation. Potential solutions of this problem are based on shielding of the lipoplex by inert polymers, but these have not been tested in the clinic yet. Cationic polymers are an alternative to lipids. A significant number of cationic polymers has been studied for gene transfer (for a review, see [174]). The most studied molecule is polyethylenimine, of which many variants (linear or branched, with or without chemical modifications) have been studied. It is a very effective agent for cell transfection and performs as well as lipoplexes for several *in vivo* applications such as pulmonary endothelium transfection. However, it is not biodegradable and is associated with toxicity of which the intensity is dependent on the molecular-weight and structure. The mechanism of DNA delivery is still insufficiently understood. Another option that has been recently explored are cationic peptides, such as peptides derived from the Tat protein encoded by HIV. Their role in clinical gene transfer remains to be defined. Hybrid systems combining lipids and polymers have also been studied and they showed lower toxicity, but at the cost of low *in vitro* and *in vivo* activity.

Despite significant progress that has been achieved recently, the majority of these non-viral methods are still less efficient than the viral methods and the latter remain the best choice for clinical studies.

Chapter 2: Objectives

Three main goals can be put forward in this work. The first goal has been the development of a non-invasive imaging strategy for the assessment of LV-mediated gene transfer to the mouse and rat brain. This work builds on the previous work performed in the labs of Drs Debyser and Baekelandt who demonstrated that LV can be used to induce long-term gene expression in the mouse and rat brain [133, 175, 176]. This data was obtained by histological study of the brain after sacrifice and we recognised that non-invasive assessment would be a powerful tool for further neurobiological studies. We hypothesized that the magnitude, duration and localisation of gene expression after stereotactic injection of LVs could be monitored with BLI in the mouse and rat brain. After we had validated BLI for this purpose we also wanted to evaluate the feasibility of non-invasive detection of the migration of neuronal precursor cells to the olfactory bulb. This latter work is based upon the pioneering finding from the Debyser lab that it is possible to transduce the endogenous neural stem cell in the mouse brain by local injection of LV [177], corroborating the initial proof of principle study by Consiglio *et al.* [178]. Again, these original findings were entirely dependent on histological data and we realized that a non-invasive method that would allow to monitor this stem cell population would be of great value for the study of the role of this intriguing cell population. We hypothesized that after *in situ* transduction of the neuronal stem cells in the subventricular zone of mice with a LV encoding firefly luciferase, we would be able to detect migration of neuronal stem cells.

A second objective has been the application of multimodality PET and BLI reporter gene imaging to monitor cancer cell trafficking. This work was the primary focus of the work in Dr Gambhir's lab. We aimed at developing an imaging strategy based on PET reporter gene imaging to study the growth of metastases in mice. At that time, the standard tool to evaluate tumor treatment were mouse xenografts whose size can be readily measured with callipers. These models are imperfect for a number of reasons, the most important being the fact that they do not take into account the interaction between the tumor and its environment which is a key process in tumor development. Particularly for metastases this has been shown to be of great importance [179]. One of the reasons why metastatic tumor models have been less used in oncological research is the variability of these models and the lack of adequate methods to monitor the growth of metastases.

Previous work in Dr Gambhir's lab had shown the value of PET reporter gene imaging to study the dissemination of leukemia [180] and we sought to expand this concept to the study of metastases from solid tumors. We hypothesized that by expressing PET and BLI reporter genes with LV in a melanoma cell line, we would be able to follow the development of melanoma metastases with reporter gene imaging. Our aim was to develop an imaging strategy combining PET, BLI and computed tomography to allow sensitive detection of metastases and to localise these lesions in three dimensions with relevant anatomical landmarks. We first sought to validate the PET/CT technique with the use of tumor xenografts. We then applied this technique to metastatic models together with BLI imaging.

The last objective of this work has been the validation of a new PET reporter gene allowing visualization of gene expression in the brain of living rodents. When this project started no PET reporter genes had been described that can detect gene expression in an intact brain with a good signal to noise ratio. For the prototype HSV1-tk gene no tracers were available that could penetrate the intact BBB, whereas the D2R system had a low signal to background ratio because of the high levels of endogenous expression in the brain. At the start of this project a newly discovered class of molecules with specific and potent action against varicella zoster virus (VZV) was available. These compounds are bicyclic nucleoside analogs (BCNAs). As some of these molecules were good candidates to cross the BBB and their mode of action required metabolic trapping by the thymidine kinase encoded by VZV (VZV-TK), we hypothesised that VZV-tk expression could be imaged by PET with the use of radiolabeled BCNAs. We first sought to determine the uptake of radiolabeled BCNAs in cell systems. We then planned to image *in vivo* expression of VZV-tk in rodent brain. In the course of the thesis, an additional goal was formulated: *in vivo* detection of gene expression in tumor xenografts which is a standard method for validation of reporter gene expression.

Chapter 3: Materials & Methods

1. Radiotracer Synthesis

Four different radiolabeled BCNAs were synthesized. The *meta*-substituted compounds 3-(2'-deoxy- β -D-ribofuranosyl)-6-(3-[18 F]fluoroethoxy-phenyl)-2,3-dihydrofuro[2,3-*d*]pyrimidin-2-one (3-[18 F]-FEP-BCNA) and 3-(2'-deoxy- β -D-ribofuranosyl)-6-(3-[11 C]methoxy-phenyl)-2,3-dihydrofuro[2,3-*d*]pyrimidin-2-one (3-[11 C]-MP-BCNA) were synthesized from a 3-(2'-Deoxy- β -D-ribofuranosyl)-6-(3-hydroxyphenyl)-2,3-dihydrofuro[2,3-*d*]pyrimidin-2-one precursor as previously described [181]. Briefly, the precursor was converted using 18 F-fluoroethylbromide or 11 C-methyl iodide as alkylating agent in the presence of cesium carbonate as base and by heating the mixture. The specific activity was 72 GBq/ μ mol and 51 to 79 GBq/ μ mol at the end of synthesis for 3-[18 F]-FEP-BCNA and 3-[11 C]-MP-BCNA respectively.

The *para*-substituted compounds 3-(2'-deoxy- β -D-ribofuranosyl)-6-4-[18 F]fluoroethoxyphenyl)-2,3-dihydrofuro[2,3-*d*]pyrimidin-2-one (4-[18 F]-FEP-BCNA) and 3-(2'-deoxy- β -D-ribofuranosyl)-6-(4-[11 C]methoxyphenyl)-2,3-dihydrofuro[2,3-*d*]pyrimidin-2-one (4-[11 C]-MP-BCNA) were synthesized from a 3-(2'-deoxy- β -D-ribofuranosyl)-6-(4-hydroxyphenyl)-2,3-dihydrofuro[2,3-*d*]pyrimidin-2-one phenol precursor as previously described (Chitneni *et al.*, personal communication). In brief, 200 μ g of this precursor in 200 μ L dimethylformamide was reacted with 18 F-fluoroethylbromide or 11 C-methyl iodide as alkylating agent in the presence of about 1 mg of cesium carbonate at 90 $^{\circ}$ C for respectively 15 and 8 min. The specific activity was 55 GBq/ μ mol and 99 GBq/ μ mol at the end of synthesis for 3-[18 F]-FEP-BCNA and 3-[11 C]-MP-BCNA, respectively.

For all tracers, the synthesis was followed by purification using semi-preparative reverse phase high pressure liquid chromatography (RP-HPLC). Chemical and radiochemical purity of both HPLC purified tracers was examined on an analytical RP C₁₈ column and was always found to be >99%. The identity of the tracers was confirmed by co-elution with authentic non-radioactive compounds after co-injection on analytical RP-HPLC, with 30% acetonitrile in 0.05 M sodium acetate buffer (pH 5.5) as mobile phase.

2-Deoxy-2-[18 F]fluoro-D-glucose ([18 F]-FDG) was synthesized by the method described by Hamacher *et al.* [182] at a specific activity of \sim 185 TBq/mmol. 9-[4-[18 F]fluoro-

3-(hydroxymethyl)butyl]guanine ($[^{18}\text{F}]$ -FHBG) was synthesized as previously described [33] with a specific activity of ~ 37 TBq/mmol.

2. Cell Culture and Lentiviral Vector Production

2.1. Cell Lines and Culture Conditions

All cells were cultured at 37°C in a humidified atmosphere containing 5% CO₂. 293T (human embryonic kidney), N2a (murine neuroblastoma) and SHSY5Y (human dopaminergic neuroblastoma) cells were maintained in Dulbecco's modified Eagle's medium (DMEM) with Glutamax (Gibco BRL, supplied by Invitrogen, Merelbeke, Belgium) supplemented with 10% heat-inactivated fetal calf serum (FCS; Harlan Sera-Lab Ltd., International Medical, Brussels, Belgium) and 1% penicillin (10000 U/ml)/streptomycin (10 mg/ml) (Gibco BRL). PC12 (rat pheochromocytoma) cells were maintained in the aforementioned medium supplemented with 1% Essential Amino Acids (Gibco BRL). GL261 (mouse glioma) cells were maintained in the aforementioned medium supplemented with 2mM glutamine (Cambrex, East Rutherford, NJ, USA) and 500 μl β -mercaptoethanol (Sigma-Aldrich, Steinheim, Germany).

N2a murine neuroblastoma cells were obtained from Dr V. Mauro (Scripps Research Institute, La Jolla, CA). B16F0 and A375M human melanoma cells were provided by Dr M. Kolodney (University of California, Los Angeles, CA). These cell lines were cultured in high glucose DMEM supplemented with 10% FCS and 1% penicillin/streptomycin solution (respectively 100 $\mu\text{g/ml}$ and 292 $\mu\text{g/ml}$). C6 rat glioma cells were provided by Dr M. Black (Washington State University, Pullman, WA) and cultured in high glucose deficient DMEM supplemented with 10% FCS, 1% penicillin-streptomycin solution, and 1% L-glutamine (100nM). The A375M cell line was previously transfected with a Firefly luciferase encoding plasmid or transduced with a second generation LV expressing the triple fusion (3F) gene hRL_mRFP_HSV1-sr39ttk (humanized *Renilla* luciferase, monomeric red fluorescent protein and truncated sr39 mutant herpes simplex virus type 1 thymidine kinase) and they are referred to as A375M-Fluc [183] and A375M-3F [154] respectively.

PC3 (human prostate cancer) cells were a gift of Dr J. Swinnen (KU Leuven) and were maintained in DMEM/F12 (1/1) medium (Gibco BRL) supplemented with 10% FCS and Gentamycin (Gibco BRL).

2.2. Lentiviral Vector Transfer Plasmid Construction

Different lentiviral transfer plasmids were constructed. The transfer plasmid encoding firefly luciferase (Fluc) was constructed as follows. The Fluc fragment was obtained by polymerase chain reaction (PCR) amplification with a Fluc forward primer (5'-CGGGATCCATGGAAGACGCCAAAAC-3') and a Fluc reverse primer (5'-TCCCCCGGGTTACACGGCGATCTTTCC-3') from CSCMV-sr39tk-IRES-Fluc (Dr. Sanjiv Sam Gambhir, Stanford University, CA). The unique restriction sites *Bam*HI and *Xma*I were added to the 5' and 3'-ends, respectively. After amplification, the Fluc PCR product was digested with *Bam*HI and *Xma*I and inserted into the transfer plasmid pCHMWS [176] to yield pCHMWS-Fluc (LV-Fluc). We also constructed a bicistronic lentiviral vector encoding eGFP and Fluc separated by an encephalomyocarditis virus (EMCV) IRES sequence [50]. The IRES-Fluc fragment was removed from CSCMV-sr39tk-IRES-Fluc using *Bsa*I and *Eco*RI and inserted into the *Pst*I and *Eco*RI site of the pBKRSV shuttle plasmid. The IRES-Fluc fragment was excised using *Xho*I and *Bss*HII and cloned into pCHMWS-eGFP, digested with *Mlu*I and *Xho*I resulting in pCHMWS-eGFP-IRES-Fluc (LV-eGFP-I-Fluc).

We also constructed a lentiviral transfer plasmid encoding varicella zoster virus thymidine kinase (VZV-tk) and β -galactosidase (LacZ). The previously described pGEX-5X-1-VZV-tk plasmid [184] was digested with *Bam*HI and *Sal*I and the VZV-tk encoding sequence was ligated in the lentiviral transfer plasmid pCHMWS_eGFP [176] that was digested with *Bam*HI and *Xho*I to yield pCHMWS_VZV-tk. The LacZ encoding sequence was digested from the pHR'-CMV-LacZ plasmid [185] with *Bam*HI and *Xho*I and was ligated in a pCHMWS_eGFP-Zeo plasmid digested with the same restriction enzymes to yield pCHMWS_LacZ. To generate transfer plasmids that include the puromycin resistance gene puromycin-N-acetyl-transferase from *Streptomyces alboniger*, pCHMWS_VZV-tk and pCHMWS_LacZ were digested with *Bam*HI & *Mlu*I and *Bam*HI & *Spe*I respectively and ligated in the pCHMWS_eGFP-IRES-Puro plasmid [186] digested with *Bam*HI & *Mlu*I and *Bam*HI & *Spe*I respectively to yield pCHMWS_VZV-tk-IRES-Puro (VZV-tk-I-P) and pCHMWS_LacZ-IRES-Puro (LacZ-I-P).

For cloning of pCHMWS_3F which encodes a fusion protein containing a truncated mutated HSV1-sr39TK, the fusion gene was amplified by PCR using AGCTCTAGATCTATGGCTTCCAAGGTGTACGACCC and

GTCGACACTAGTTCAGTTAGCCTCCCCCATCTCCC as forward and reverse primer, respectively. After purification the PCR product was digested with BglII and SpeI.

2.3. Lentiviral Vector Production

Two different production methods were used, one for low concentration vector for establishment of stable cell lines and one for highly concentrated vector used for cell and *in vivo* experiments. For both production methods, 293T cells were transiently triple transfected with a second-generation packaging plasmid lacking the *vif*, *vpr*, *vpu* and *nef* genes (pCMVΔR8.91), a plasmid encoding the VSVg envelope glycoprotein (pMDG), and the transfer plasmid. The small scale lentiviral vector productions were performed as described previously [187] except for minor changes in culture medium. One day before transfection 5×10^6 293T cells were seeded in a 10cm cell culture plate. The next day 20 µg transfer plasmid, 10µg packaging plasmid, and 5 µg envelope plasmid (encoding VSVg) were added to 700µL of a 150 mM NaCl solution. This mixture was added to 700µL of a 150 mM NaCl solution containing 1.6 mM polyethylenimine. After 15 min incubation at room temperature, the mixture was added to Optimem 0% FCS and applied to the 293T cells. The next day the medium was refreshed with Optimem 0% FCS. The supernatants were collected on day 2 and 3 post-transfection and stored at -80°C .

The highly concentrated LV was produced as described previously [188]. 293T cells were seeded in a ten-tray cell factory (CF10; Nunc A/S, Roskilde, Denmark) at 60×10^6 cells per cell factory in OPTIMEM with Glutamax supplemented with 2% FCS and 20 µg/ml gentamicin. The next day, a 56mL mixture of the three plasmids was made in 150mM NaCl: 1600µg of transfer plasmid, 800µg of packaging construct and 400µg of envelope plasmid. An equal volume of polyethylenimine solution was added slowly to this DNA mixture and the solution was incubated at room temperature for 15 min. The DNA-polyethylenimine complexes were added to 500mL OPTIMEM without FCS and added slowly to the 293T cells that were then incubated for 24 h. Supernatant was harvested 2 and 3 days post-transfection and filtered through a 0.45µm easy-flow filter (Becton Dickinson Labware, Le Pont de Claix, France). Large volumes of cell-culture supernatant were purified and concentrated by tangential flow filtration (TFF) using a Minim™, a benchtop TFF machine, with the Centramate™ LV holder (Pall, Dreieich, Germany) and a 100kDa or 300kDa Omega Screen channel-cassette according to the manufacturer's protocol. Briefly, prior to concentration of the cell-culture medium, the cassette was washed with PBS for 1 h followed by a 30 min equilibration with OPTIMEM. In total 1L of

cell-culture supernatant was collected from two CF10 (500mL of each CF10 were pooled for days 2 and 3 post-transfection) and concentrated to 15mL, resulting in a 66-fold concentration in about 2 h. To increase vector titers even more after TFF, additional centrifugation steps were performed: low-speed centrifugation (5 h, 26000 g) at 4°C in a fixed-angle rotor (Biofuge Stratos; Heraeus Instruments GmbH&Co.) and ultracentrifugation (2 h, 76000 g) at 4°C in a swinging-bucket rotor (SW55.1; Beckman). The concentrated vector was stored at -80°C.

For all vector productions the p24 concentration was determined by enzyme-linked immunosorbent assay (HIV-1 p24 ELISA kit; PerkinElmer, Milano, Italy).

2.4. Cell Transduction

For luciferase assays on transduced cells, cells were seeded in a 96-well plate at 1.5×10^4 cells per well the day before transduction. On the day of transduction, medium was replaced by DMEM containing serial dilutions of the LV and incubated for 5 hours. Five hours after transduction, medium was replaced and 48 hours after transduction the cells were assayed.

To create stable cell lines, cells were seeded in a 96-well plate (1.5×10^4 cells/well) the day before transduction. On the day of transduction, medium was replaced by DMEM containing different dilutions of LV and the cells were incubated for 48 hours. Puromycin was added to a final concentration of 1µg/mL and the cells were maintained in this condition.

For titration experiments, 293T cells were plated in triplicate in 24-well plates (10^5 cells/well) the day before transduction. On the day of transduction, medium was replaced by DMEM containing serial two-fold dilutions of the viral vector. The cells were incubated for 48 hours after which uptake studies were performed.

3. *Detection of Reporter Gene Expression*

3.1. Western Blot

Extracts of transfected or transduced cells were made using 1% SDS complemented with Complete™ protease inhibitors (Roche Diagnostics GmbH, Mannheim, Germany). Ten µg of total protein was separated on a self-cast 13.5% SDS-

polyacrylamide gel and transferred to a polyvinylidenedifluoride (PVDF) membrane (Bio-Rad, Watford, United Kingdom). The PVDF membrane was incubated first at 4°C in PBS containing 0.1% Tween20 and 5% milk powder overnight and then at room temperature for 2h with a polyclonal primary antibody against firefly luciferase (Promega), at a dilution of 1:2000. After washing in PBS+0.1% Tween20 (3x10 min), the blot was incubated at room temperature for 1h with horseradish peroxidase (HRP)-conjugated anti-goat secondary antibody. The blot was washed in PBS+0.1% Tween20 (5x10 min) and immunoreactive proteins were visualized using the enhanced chemiluminescence plus (ECL⁺) kit (Amersham Biosciences, Uppsala, Sweden).

3.2. Flow Cytometry Analysis of eGFP Expression

Cells were transduced with specific amounts of lentiviral vector as described. Two days post transduction eGFP expression was analyzed by FACS. Cells were trypsinized and subsequently fixed in 2% paraformaldehyde prior to analysis with a FACS-calibur flow cytometer (Becton-Dickinson, Franklin Lakes, NJ). The data obtained were analyzed using the CellQuestTM software package provided with the instrument.

3.3. Bioluminescence Measurement in Living Cells

Cells were plated as described previously in a 96-well plate with black tinted walls. D-luciferin (Xenogen, Alameda, CA) or coelenterazine containing medium was added to a final concentration of 150µg/L medium. After 5 minutes incubation, the cells were imaged during 1 to 5 seconds in the IVIS 100 system.

3.4. In Vitro Firefly and Renilla Luciferase Activity Assay

For cell culture experiments, the cells were lysed using 20µL of Luciferase Cell Culture Lysis Reagent (Promega) per well of a 96-well plate. They were subsequently incubated with 100µL Luciferase Assay Reagent (Promega) and luciferase activity was measured during 2 seconds in both a Luminocount luminometer (Perkin Elmer, Milan, Italy) and the IVIS system. To determine luciferase activity on brain slices, proteins were extracted from brain tissue. The tissue was first frozen at -80°C and then pulverised with tissue grinders in Luciferase Cell Culture Lysis Reagent. Samples were centrifuged at 12000 g and supernatant was collected afterwards while the pellet was discarded.

Luciferase activity was measured by incubating 20 μ L of extract in 100 μ L Luciferase Assay Reagent (Promega) and by measuring during 2 seconds in the IVIS system.

Renilla luciferase assay was performed using the Dual-Luciferase Reporter Assay System from Promega. Each of the luciferase reactions was measured in a TD 20/20 luminometer (Turner Designs, Sunnyvale, CA) for a period of 10 seconds and normalised for protein content.

3.5. Herpes Simplex Virus type 1 Thymidine Kinase Activity Assay

Cell or tumor extracts were incubated for 20 min with 8-[³H]-penciclovir (8-[³H]-PCV) to determine the formation of phosphorylated 8-[³H]-PCV. This phosphorylated 8-[³H]-PCV was trapped on a DE-81 filter (Whatman) while the parent compound was washed away. The remaining activity was counted in a Beckman LS-9000 Liquid Scintillation Counter with Biosafe II scintillation fluid. The results are reported as percent conversion of 8-[³H]-PCV in (desintegrations per minute/ μ g protein of cell or tumor extract)/(desintegrations per minute of control sample) \times 100.

4. Cell Experiments

4.1. Radiotracer Uptake Experiments

Stable 293T or PC3 cells transduced with LV-VZV-tk-I-P or LV-LacZ-I-P were counted with a Z1 Coulter[®] cell and particle counter (Beckman Coulter, Fullerton, CA) and plated in triplicate in 24-well plates (293T: 2 x 10⁵ cells/well; PC3 8 x 10⁵ cells/well). After 24 h, the medium was discarded and 250 μ L of fresh medium with HPLC-purified tracer (5 μ Ci ¹⁸fluorine tracer or 30 μ Ci of ¹¹carbon tracer) was added per well. The cells were then incubated at 37°C in a 5% CO₂ atmosphere for various durations. After incubation and removal of the medium, the cells were washed three times with 400 μ L of ice-cold phosphate-buffered saline (PBS). The cells were then lysed with 250 μ L of Cell Culture Lysis Reagent 1x solution (Promega Corporation, Madison, USA) for 10 min after which the lysate was collected, followed by a 125 μ L rinse with this same solution. The cell fractions (lysate and rinse) as well as the wash fractions (medium and PBS) were collected separately for each well and the radioactivity was measured using an automated gamma counter. The protein concentration of each cell fraction was determined using the Bio-Rad Protein Assay (Biorad, München, Germany) and a spectrophotometer (Bio Synchron -

Anthos 2010, Anthos LabTec Instruments, Austria) at 595 nm. The tracer uptake was normalized for total protein content in the cell fraction for each individual well and expressed as percentage of total radioactivity per mg protein. Uptake ratios were calculated by dividing the protein normalised activity in VZV-tk expressing cells by the protein normalised activity in LacZ expressing control cells.

The experiments with the titration series and the LV-3F transduced cells were performed similarly but uptake ratios were calculated with non-transduced control cells. For wash-out experiments, after the 3 wash steps with PBS the cells were incubated with radiotracer free medium for various time points. After this second incubation, the radiotracer-free medium was collected and the cells were washed 3 times with PBS. The cell fraction was collected as described above. The amount of tracer present in the cell fraction is reported as percentage of the total radioactivity present at time of reincubation (sum of cell fraction, tracer-free medium and second series of PBS washes).

4.2. High Pressure Liquid Chromatography (HPLC)

For RP-HPLC studies, cells were plated in a 75cm² or in 3 wells from a 24-well plate and were grown to confluency. Uptake studies were performed as described above. The cell fraction was centrifuged at 1837g for 5 min and cold reference compound for the native tracer was added to the supernatant. The mixture was passed through an Oasis[®] HLB column (Hydrophilic-Lipophilic Balanced; 4.6mm × 20mm, Waters Corporation, Milford, USA) that was preconditioned by successive washings with acetonitrile and water. After connection of the Oasis column to the HPLC, it was rinsed by pumping 6mL of water and the eluate was collected as two 3-mL fractions (fractions 1 and 2). The outlet of the Oasis column was then connected to an analytical column and eluted with 30% acetonitrile in sodium acetate buffer. Samples were collected during 1 min and counted in the gamma-counter.

5. *Creation of Animal Models*

All animal experiments were approved by the bioethical committee of the Katholieke Universiteit Leuven or the University of California, Los Angeles Animal Research Committee or the Administrative Panel on Laboratory Animal Care of the Stanford University.

5.1. Inoculation of Lentiviral Vector in Mice and Rats

Adult female NMRI mice were used. The animals were housed under 14 hour light/10 hour dark cycle with free access to food and water. For intramuscular delivery, 250 μ L of a ketamin/medetomidine mixture was injected intraperitoneally before shaving the right lower leg and making a 5mm incision in the skin. Using a 10 μ L Hamilton syringe, two μ L of LV-Fluc (180ng p24) were injected within 30 seconds into the right gastrocnemius muscle. The skin was sutured and after subcutaneous injection of 25 μ L ampicillin (200 mg/mL), a dose of 250 μ L of atipamezole antidote was administered ip. The animals were kept in individually ventilated cages until sacrifice at day 21, at which time both gastrocnemius muscles were excised and stored at -80°C. For brain injections, anaesthetized animals were placed in a stereotactic head frame (Stoelting, Wood Dale, IL). A midline incision of the skin was made and a small hole drilled in the skull in the appropriate location, using bregma as reference. The coordinates used for striatal injection were: anteroposterior (AP) 0.5, lateral (L) \pm 2.0 and dorsoventral (DV) -3.0 and -2.0 mm. Two μ L of highly concentrated vector supplemented with polybrene (4 μ g/mL) was injected at a rate of 0.25 μ L/min with a 30-gauge needle on a 10 μ L Hamilton syringe. After 4 minutes of injection (1 μ L), the needle was raised slowly in the dorsal direction over the distance indicated by the two dorsoventral coordinates. After the injection, the needle was left in place for an additional 5 minutes to allow diffusion before being slowly withdrawn from the brain. The coordinates used to target different anatomical sites are: substantia nigra: AP -3.1, L -1.2 and DV -4.0 mm; medial globus pallidus: AP -1.3, L -1.8 and DV -4.0 mm; olfactory bulb: AP 4.7, L -1.0 and DV -1.5 mm. Injections were performed similarly to the striatal injection except for the fact that there was only one injection site and that we used only 1 μ L for injection in the olfactory bulb.

Adult female Wistar rats were used in similar conditions as the NMRI mice. The animals were bilaterally injected in the substantia nigra with a total of 8 μ L vector (two injections of 2 μ L LV-eGFP-I-Fluc per side), using the following coordinates: (site 1) AP -4.8, L \pm 2.0 and DV -7.2 mm; (site 2) AP -5.5, L \pm 1.7 and DV -7.2 mm.

5.2. Inoculation of Tumor Cells

For combined microPET, microCT and BLI studies, cells were harvested after trypsinization, suspended in a solution containing 150mM sodium phosphate and 150mM

sodium chloride (pH: 7.2) (PBS) and stored on ice. All mice were anesthetized using 30 μ L of a Ketamine/Xylazine (K/X) mixture (80mg/mL and 20 mg/mL respectively) injected intraperitoneally (IP). Twelve to 16-week old male nude mice (*nu/nu*) were injected subcutaneously in the shoulder region with 1.5×10^6 N2a cells (n=3), 0.5×10^6 C6 cells (n=4) and were injected in the left cardiac ventricle with 1.5×10^6 A375M cells (n=3), A375M-3F (n=6) and 0.5×10^6 B16F0 (n=3). Eight week old beige SCID mice were injected in the lateral tail vein with 0.7×10^6 A375M-Fluc cells (n=5). The weight of the mice and the size of the tumor grafts were recorded on a regular basis and before each scan.

For validation of VZV-tk, female adult athymic nude mice (*nu/nu*) were used. The animals were housed under 14 hour light/10 hour dark cycle with free access to food and water. For inoculation into nude mice, PC3 cells stably expressing VZV-tk or LacZ were washed with PBS digested with trypsin and re-suspended in culture medium. After centrifugation, the pelleted cells were re-suspended in PBS at a concentration of 5×10^6 viable cells per 100 μ L. One hundred μ L of cell suspension was injected subcutaneously in the right (VZV-tk) or left (Lac-Z) flank of 4 nude mice. Tumour growth was assessed on a regular basis. Two orthogonal diameters were measured with a calliper and used to calculate the volume of the tumour using the ellipsoid formula $\pi/6 \times a \times b \times (a+b)/2$, where a and b are the measured craniocaudal and dorsoventral diameter respectively. The mice were imaged when the tumors reached a volume of about 250 mm³.

6. Small Animal Imaging Procedures

6.1. In Vivo Bioluminescence Imaging of Firefly Luciferase Activity and Image Analysis

The mice were imaged in an IVIS 100 system (Xenogen, Alameda, CA). Anaesthesia was induced in an induction chamber with 2.5% Isoflurane in 100% oxygen at a flow rate of 1L/min and maintained in the IVIS with a 1.5% mixture at 0.5L/min. The mice were injected with D-luciferin (126mg/kg) dissolved in PBS (15mg/ml) either by intraperitoneal or intravenous route. Subsequently, they were placed in prone position in the IVIS 100. This system consists of a cooled CCD camera (-105°C) mounted on a light tight chamber. Consecutive 1 to 5 minute frames were acquired until the maximum signal was reached or until the signal returned to background level in the pharmacokinetic

studies. Each frame depicts the bioluminescence signal as a pseudocolor image superimposed on the grey scale photographic image. The photographic and bioluminescent images were superimposed using the Living Image V 2.20 software (Xenogen Inc.) and IGOR pro image analysis software (V 4.06A, Wavemetrics, Lake Oswego, OR). The data are reported as the photon flux (p/s) and the maximum pixel in photons.s⁻¹.cm⁻¹.steradian⁻¹ (p/s/cm²/sr) from a 1.23cm² circular region of interest (ROI) around the head.

The BLI imaging in rats was performed as described above, using gas anesthesia and intravenous injection of D-luciferine at a concentration of 30mg/mL in the lateral tail vein. Quantification was performed with an 2.95cm² ellipse-shaped ROI.

6.2. In Vivo Bioluminescence Imaging of *Renilla* Luciferase Activity and Image Analysis

Each mouse was injected with 30μL K/X IP and placed in supine position. To generate the bioluminescence reaction catalyzed by *Renilla* luciferase, its substrate coelenterazine (Biotium, Inc., Hayward, CA) was injected (20μg in 100μL of a methanol 10% / PBS (pH=7.4) 90% solution). Immediately after injection in the lateral tail vein, the animal was placed supine in the Xenogen IVIS system. A photographic image and a bioluminescent image, consisting of the photon collection during one minute, were acquired successively three times. A ROI was manually drawn over the body of the mouse and the average radiance was measured in p/s/cm²/sr. The highest value of the three scans is reported.

6.3. Combined Positron Emission Tomography – Computed Tomography Procedure

Animals were fasted for a minimum of 6 hours before imaging procedures with [¹⁸F]-FDG. Animals were anesthetized using 1L/minute of 2% Isoflurane in 100% oxygen. After anesthesia the mice were injected with 200μCi [¹⁸F]-FDG or 200μCi [¹⁸F]-FHBG. After one hour to allow clearance of not specifically bound tracer the animal was injected IP with 30μL of a K/X mixture (80mg/mL and 20 mg/mL respectively) and subsequently fixed in prone position on a polystyrene bed with 6 fiducial markers. These consisted of a PCR tube filled with 2μL of iohexol (Omnipaque) and 2μCi of [¹⁸F]-FDG to allow detection by CT and PET and were positioned next to the mouse. A 10 minute static single frame scan was

acquired on the P4 MicroPET (Concorde Microsystems Inc., Knoxville, TN). Immediately afterwards the mice were transferred to the CT scanner while still being fixed to their polystyrene bed with fiducial markers. We used a microCAT small animal CT scanner (Imtek, Knoxville, TN). This system consists of a low-energy X-ray tube (X-ray energy 30-50kVp), a high-resolution phosphor screen and CCD detector with 1024 by 1024 pixels (field of view of $\sim 50 \times 50\text{mm}^2$) and a precision-motion translation stages. The detector and X-ray source rotate about a fixed bed allowing the mouse to be fixed in the same horizontal position as in the microPET system. After a booster dose of 15 μL K/X IP, the mice were positioned and two bed positions separated by 40.6mm along the longitudinal axis were scanned during 15 minutes each (190 projection images) to acquire the entire body of the mouse (total axial field of view: $\sim 90.6\text{mm}$). The total procedure took ~ 40 minutes including 2 x 5 minutes for positioning and system initialization. The images were acquired in step and shoot mode with the X-ray source set at 50kVp and 450 μA .

Image reconstruction for PET was done by filtered back projection using a ramp filter. The pixel size was 0.845 by 0.845 by 1.260mm and the resolution was $\sim 1.85\text{mm}$. For the CT images, two-dimensional slices of each bed position were reconstructed using a fan beam resorting algorithm with a standard ramp filter. Images were reconstructed on a 256x256-pixel grid where the pixel size was 70x70 μm . To reconstruct in Hounsfield units (HU), the system was calibrated using a 50mL polypropylene tube filled with water. The resolution of the reconstructed images was 200 μm . The images of both bed positions were then merged into a single whole body image dataset by discarding the 18 outer slices of each bed position and by computing a progressive weighted average of the overlapping 18 slices. No X-ray contrast medium was used in these studies.

6.4. Image Fusion and Quantitative Analysis

Both the PET and the CT datasets were imported in AMIDE software [189] version 0.8.2 (<http://amide.sourceforge.net>). “Fiducial marker points” were placed at the center of each of the images of the fiducial markers and this was done in the datasets of both modalities. Subsequently, the “fiducial marker points”, and their respective datasets, were aligned with the Alignment wizard using the Procrustes rigid body alignment algorithm. The CT images were displayed in Hounsfield Units. The PET images were converted to % injected dose per gram (%ID/g) units by (i) using a calibration constant obtained from scanning a cylinder phantom in the microPET scanner, (ii) assuming a tissue density of 1g/mL and (iii) dividing by the injected dose that was decay corrected to the start time

point of scanning. Three dimensional ellipsoidal regions of interest were drawn over the tumors and metastases. In the metastatic models, control lesions were drawn on the contralateral side or in non-pathological tissue. The mean and maximum pixel values were obtained for both the data sets. Tumor to background contrast was calculated with the %ID/g values using the formula $(\text{tumor} - \text{background}) / (\text{tumor} + \text{background})$.

6.5. Positron Emission Tomography Imaging

The PC3 tumor-bearing mice were imaged using a Focus 220 microPET® scanner (Concorde Microsystems Inc., Knoxville, TN, USA). The mice were anaesthetized with 2.5% Isoflurane in 100% oxygen at a flow rate of 1L/min and 10MBq of 4-[¹⁸F]-FEP-BCNA was administered by lateral tail vein injection. One hour after injection a 10 min static scans was acquired. Images were reconstructed using a maximum a posteriori algorithm from the vendor with 18 iterations and uniform resolution. The images were displayed in AMIDE and three-dimensional ROIs were drawn over the tumors. The mean radioactivity in the ROIs was converted to %ID/g as mentioned above. Standardized uptake values (SUVmean) were obtained by multiplying the mean %ID/g of the tumor by the weight of the animal divided by 100. The latter value corrects the %ID/g to a fractional value.

7. *Ex vivo Confirmation Studies*

7.1. Histology and Stereological counting

To assess lentiviral transduction in the brain, the mice and rats were deeply anesthetized with pentobarbital and perfused transcardially with saline followed by ice-cold 4% paraformaldehyde in PBS for 15 minutes. The brain was removed from the skull and postfixed overnight in the same fixing solution. Coronal brain sections (50µm thick) were cut with a vibratome and stored at 4°C in PBS buffer containing 0.1% sodium azide. A polyclonal antibody against firefly luciferase (Promega) was used for immunohistochemistry. The sections were treated with 3% hydrogen peroxide and incubated overnight with the primary goat anti-Fluc antibody (diluted 1:500) in 10% normal rabbit serum and 0.1% Triton X-100. The sections were then incubated in biotinylated rabbit anti-goat secondary antibody (Dako, Glostrup, Denmark), followed by an incubation with Strept-ABC-HRP complex (Dako). Detection was with diaminobenzidine (DAB), using

H₂O₂ as a substrate. A similar procedure was used to detect eGFP expression with a primary rabbit anti-eGFP body (diluted 1:10.000) and a secondary swine anti-rabbit antibody (Dako). The transduced volume was determined by stereological counting based on the Cavalieri method with Stereoinvestigator software (Microbrightfield, Magdenburg, Germany) as described previously [139].

7.2. Ex Vivo Brain Bioluminescence Imaging

To demonstrate the region of luciferase expression after intracranial injection, the mice were injected with the anesthetic mixture as described and injected in the lateral tail vein with D-luciferin (126mg/kg). Mice were placed in the IVIS and 2 consecutive scans of one minute were acquired. Immediately afterwards they were sacrificed by cervical dislocation, decapitated and the brain was dissected. The brain was placed in an acrylic brain matrix (Harvard apparatus, Holliston, MA) and sliced in 1.0mm thick coronal sections. These were imaged for 1 minute in the IVIS before removing and storing at -80°C both striata from the section emitting most light. The data are reported as the maximum pixel (p/s/cm²/sr) from the most intense slice as this value was shown to correlate best with gold standard *in vitro* measurements.

7.3. Ex Vivo Xenograft Analysis

Immediately after PET scanning the mouse was sacrificed by cervical dislocation. The VZV-tk expressing and control PC3 tumor were dissected, weighed and the activity concentration was determined by gamma counting. The tissue was frozen by immersion in isopentane/liquid nitrogen and separately cut into 10–50µm slices mounted on microscope slides with a Microm HM 550 cryotome (Microm, Walldorf, Germany). The sections were exposed over night to a high-performance phosphor screen (Packard, Meriden, CT, USA) and scanned in a Phosphor Imager Scanner (Cyclone™, Packard). The images were analysed using Optiquant software (Packard) and the activity concentration in the autoradiograms was expressed as digital light units (DLU)/mm². Tracer concentration in the VZV-tk expressing as well as control PC3 tumors was estimated by a ROI analysis of the autoradiograms from all the slices.

8. *Statistical Analysis*

Data were processed in Microsoft Excel 2000, Excel 2003 (Microsoft, Redwood, WA) or in JMP 6.0 (SAS Institute, Cary, NC). Results are expressed as mean \pm standard error of the mean (s.e.m) or mean \pm standard deviation (SD). For correlation analysis, a linear regression was performed to obtain the Pearson's correlation coefficient. For comparisons of different tracers, cell-lines, time points and titers one-way ANOVA was used with a post-hoc two-sided unpaired t-test. Comparisons of consecutive scans within the same animal and with control animals were compared using a paired and unpaired two-sided Student t-test respectively. Significance was determined at the $p < 0.05$ level.

Chapter 4: Results

1. *Noninvasive Monitoring of Long-Term Lentiviral Vector-Mediated Gene Expression in Rodent Brain with Bioluminescence Imaging*

The results of this section have been published in the article “Noninvasive monitoring of long-term lentiviral vector-mediated gene expression in rodent brain with bioluminescence imaging” by Deroose[®] CM, Reumers[®] V, Gijssbers R, Bormans G, Debysers Z, Mortelmans L and Baekelandt V in *Molecular Therapy*, 2006; 14(3):423-31.

Christophe Deroose performed cell experiments, intramuscular LV injections, *in vivo* and *ex vivo* BLI, *ex vivo* assays, data and statistical analysis.

Veerle Reumers performed vector cloning and validation, stereotactic LV injections, histology and *in vivo* and *ex vivo* BLI.

Non-invasive molecular imaging plays an increasing role in biomedical research (for a review see [3]). Bioluminescence imaging (BLI) uses the production of visible light photons during the enzymatic oxidation of luciferin by luciferase [190]. Prior to this study, BLI had not been used to detect and follow-up viral vector-mediated gene transfer into the adult mouse brain. We have previously shown that LV transduction in mouse brain results in stable transduction of neurons and astrocytes for up to 1 year [176]. We have optimized lentiviral vector constructs and production methods for brain applications [188]. Here, we evaluate the feasibility of BLI monitoring of LV-mediated gene transfer in the mouse brain. We constructed LV encoding firefly luciferase and characterized the BLI signal after stereotactic injection in the mouse brain in terms of kinetics, reproducibility, correlation with gene expression and long-term persistence. With a LV encoding green fluorescent protein linked to firefly luciferase by an internal ribosome entry site, we show that BLI can report gene expression in the brain. Finally, we provide proof-of-principle data for BLI in the adult rat brain.

Continuous neurogenesis is generally accepted to occur in the adult mammalian brain, including that of humans [191-193]. Modulation of adult neurogenesis could provide therapeutic benefits for various brain disorders (including stroke and PD) [194, 195] and is

therefore actively studied. In adult rodent brain, neurogenesis is known to occur in two different areas: the subventricular zone (SVZ) [196] of the lateral ventricle and the subgranular layer of the dentate gyrus [197]. In the dentate gyrus, neural progenitor cells migrate a short distance into the molecular layer and give rise to mature granular cells [198]. The exact role of these cells is still not clearly defined and heavily debated, with reports either suggesting a role in behavioural adaptation to environmental enrichment [199, 200] or contradicting this [201]. Other reports have suggested a role in the mediation of anxiolytic-like effects of antidepressants [202] and in the development of spatial memory [203, 204]. Neural progenitor cells from the SVZ, however, travel a longer distance towards the olfactory bulb. In the SVZ slowly proliferating astroglial-like type B cells generate actively proliferating type C cells, which in turn give rise to migrating neuroblasts or type A cells. These type A cells migrate tangentially in chains through tubular structures, forming a well-defined migratory pathway called the rostral migratory stream (RMS). Upon arrival in the OB, the progenitor cells differentiate in functioning interneurons and integrate into existing neural pathways [205]. These different cell populations can be distinguished by immunohistochemistry: type B cells are positive for glial fibrillary acidic protein (GFAP) but S100 β negative; type C cells and neuroblasts are doublecortin positive while mature interneurons are NeuN positive [191]. The turnover of neurons in the OB is believed to play a role in olfactory memory formation [206]. In human brain the analogous migration of neuroblasts to the olfactory bulb via a lateral ventricular extension was only recently demonstrated [193], albeit without clear functional role identified until now. It is well known that impaired odor discrimination is an early sign of PD and that the proliferation of progenitor cells in the SVZ and neuroblast migration is reduced in PD animal models and in PD patients [207, 208]. Altogether, the data suggest that endogenous neuronal stem cell proliferation and migration towards the OB play a physiological role in humans. It also follows that the rodent brain provides a relevant model to study migration, proliferation and differentiation of the neuronal stem cell population. Non-invasive imaging of stem cell migration in rodent brain would facilitate this research effort considerably.

We have shown before that lentiviral vectors (LVs) can be used for efficient and long-term *in vivo* marking of adult rodent neuronal stem cells (NSCs) in the SVZ. This enables histochemical detection of neural progenitor cells during proliferation, migration and differentiation [177]. Noninvasive imaging of reporter genes encoded by LV would allow direct monitoring of stem cell migration in an individual animal over time. Different imaging strategies have been proposed to follow the fate of exogenous stem cells in a living organism. Direct strategies (For a review, see [209-211]) are based on labelling cells

with molecules that generate a detectable signal such as paramagnetic iron particles for MRI [212] or radionuclides that can be detected with SPECT or PET [213-215]. Other strategies depend on stable expression of imaging reporters that will either interact with injected imaging probes or that generate an imaging signal by themselves. *In vivo* MRI tracking of labelled exogenous stem cells in animal models was done for several diseases such as stroke [216-218], multiple sclerosis [219] and brain tumors [220]. BLI has so far been used to follow the migration of exogenous, *ex vivo* labelled stem cells towards glioblastomas [88, 221] and ischemic infarcts [87, 222]. Pineda *et al.* transplanted stem cells expressing GDNF in the RMS and observed with BLI that these cells follow the natural migratory pathway and protect striatal neurons from quinolinic acid induced toxicity in a mouse model for Huntington's disease [223]. PET has been used to image the presence of multipotent adult progenitor cells in gliomas in the context of stem cell-mediated suicide gene therapy [224]. Considerably less attention has been paid to detect the fate of the different types of endogenous stem cells present in adult organisms. Nevertheless recent evidence suggests that at least part of the beneficial effects of exogenous stem cell therapy might be mediated by the endogenous stem cells in the brain. For example, it was shown that implantation of human bone marrow-derived mesenchymal stem cells into the dentate gyrus of the hippocampus of immunodeficient mice stimulated proliferation, migration, and differentiation of the endogenous neural stem cells that survived as differentiated neural cells [225]. This provides a novel paradigm for explaining the beneficial effects of mesenchymal stem cells in animals models despite low numbers of engrafted exogenous cells.

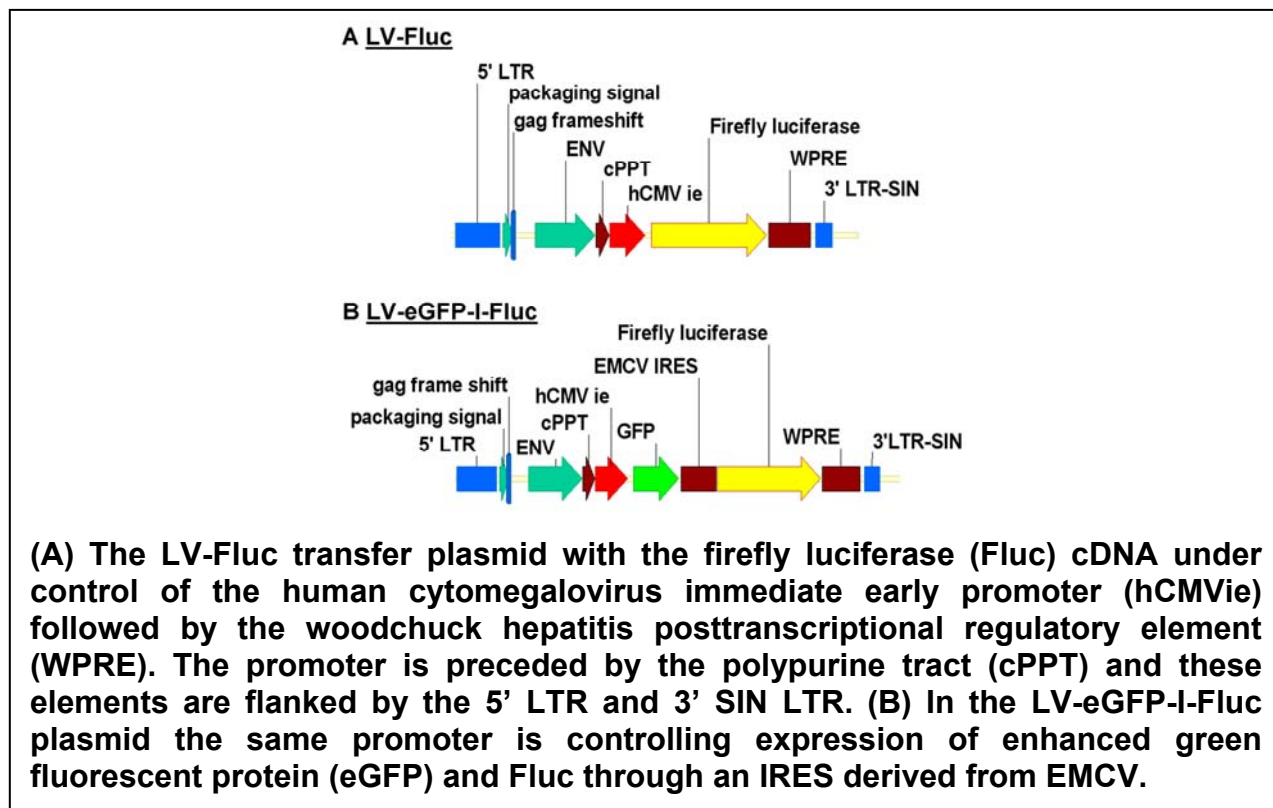
We evaluated the feasibility of detecting the migration of endogenous neuronal progenitor cells with BLI. We stereotactically injected a bicistronic LV encoding Fluc and eGFP in the SVZ to stably mark the neuronal stem cells in this region. BLI scans detected a signal from endogenous stem cells when they had migrated to the olfactory bulb.

RESULTS & DISCUSSION

1.1. BLI Imaging Allows Quantification of Luciferase Expression in LV-Transduced Cells

We created a lentiviral vector construct encoding firefly luciferase (LV-Fluc) as well as a construct encoding eGFP (enhanced green fluorescent protein) and firefly luciferase separated by the internal ribosome entry site (IRES) of the encephalomyocarditis virus (EMCV) (LV-eGFP-I-Fluc) (Figure 1).

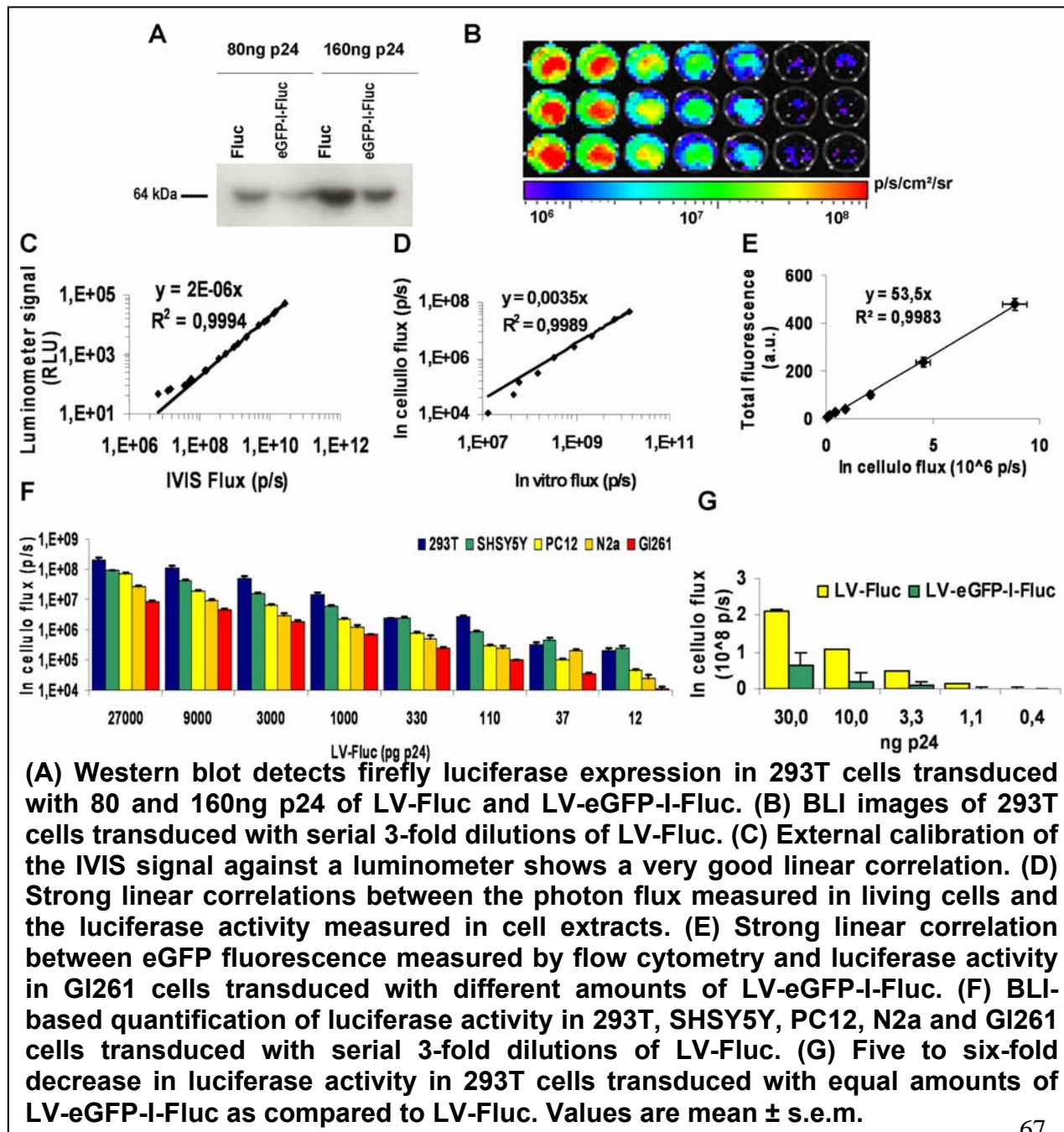
Figure 1



The expression of firefly luciferase in 293T cells transduced with LV-Fluc or LV-eGFP-I-Fluc was confirmed by Western blotting (Figure 2A). Luciferase activity in cell culture after lentiviral vector transduction was measured using BLI (Figure 2B) and luminometry. We first validated BLI by comparison with the luminometry results obtained from the same transduced cells. Although a nearly perfect correlation ($r^2=0.9994$) between both data sets was obtained, BLI displayed a higher dynamic range in the lower values (Figure 2C). Luciferase activity measured with BLI in intact cells was ~ 300 -fold lower than that in cell lysates with a nearly perfect correlation ($r^2=0.9989$) (Figure 2D). We then

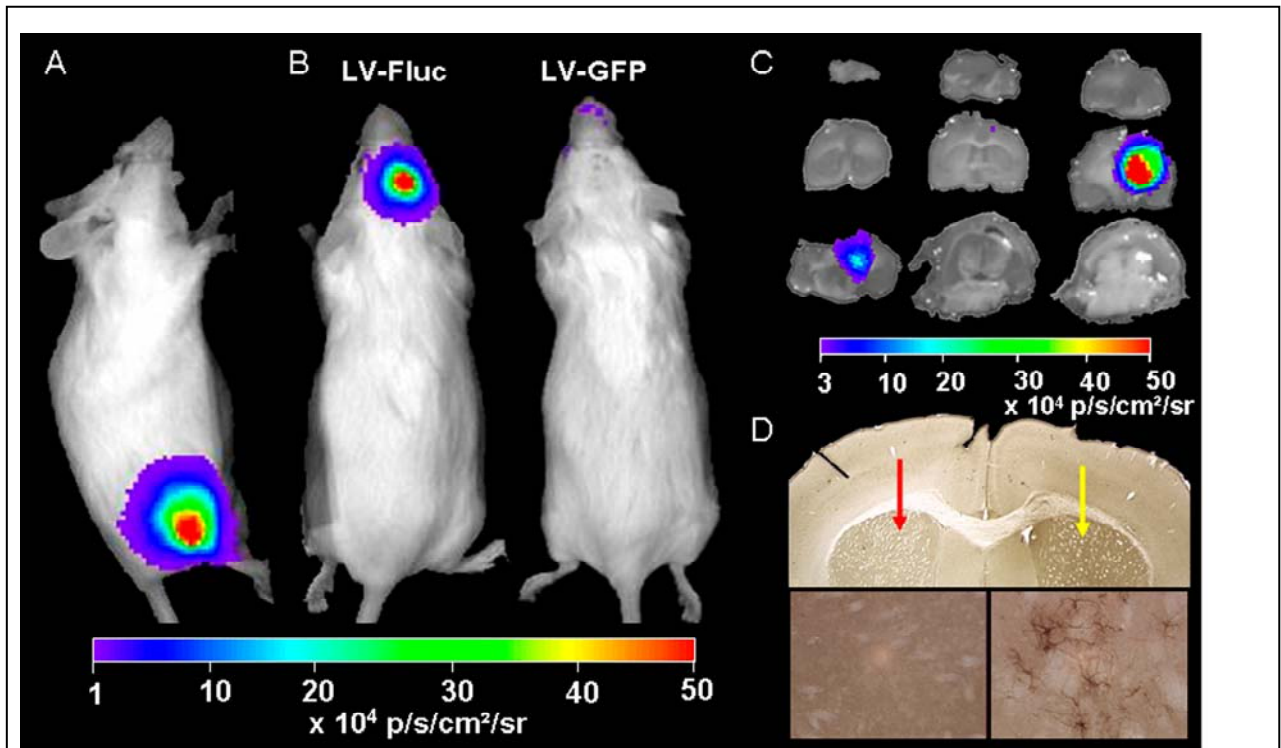
measured luciferase activity after transduction of SHSY5Y, PC12, N2a and GI261 cells with serial dilutions of LV-Fluc or LV-eGFP-I-Fluc and compared these to 293T cells. The following results were obtained: (i) mean luciferase activities were 48%, 20%, 11% and 5% of the activity in 293T cells respectively for LV-Fluc (Figure 2F) and similar values were obtained for LV-eGFP-I-Fluc (data not shown) (ii) in these cell lines, the mean luciferase activity of the LV-eGFP-I-Fluc vector was 5.2±2.0 fold lower than that of LV-Fluc (range 2.3-7.6) (Figure 2G and data not shown) and (iii) a very good correlation ($r^2=0.99\pm 0.02$) between luciferase activity (measured by BLI) and eGFP fluorescence (measured by flow cytometry) was obtained for 293T, N2a and GI261 cells transduced with LV-eGFP-I-Fluc (Figure 2E and data not shown).

Figure 2



Thus, our lentiviral vectors encoding firefly luciferase are able to transduce various cell types, including relevant neuroblastoma, pheochromocytoma and glioma cell lines. These *in vitro* data validate our lentiviral vectors and support the use of the IVIS system to detect and quantify luciferase activity.

Figure 3



BLI imaging of luciferase expression in LV transduced mouse muscle and brain

(A) An intense BLI signal was detected in the right leg of a mouse 21 days after intramuscular injection of 2 μ L LV-Fluc. (B) A BLI signal located on the right side of the skull was detected in a mouse that received a stereotactic injection of 2 μ L LV-Fluc into the right striatum. Note the absence of specific BLI signal in the mouse injected into the striatum with a control vector (LV-eGFP); only some faint signal comes from the nose. (C) BLI of coronal sections of a mouse brain 14 days after LV-Fluc vector injection into the right striatum. (D) Immunohistochemistry confirms the localized expression of firefly luciferase in the right striatum (yellow arrow) without expression on the contralateral side (red arrow) at low magnification (x1.6). The insets shows positively stained individual neurons in the right striatum at high magnification (x40) that are not found on the contralateral side.

1.2. BLI of Luciferase Expression in LV-Transduced Mouse Muscle and Brain

Next, we injected 2 μ L of LV-Fluc (17ng p24) in the gastrocnemius muscle of 3 NMRI mice. Seven days after injection the mice were imaged in lateral decubitus after IP injection of luciferin. The detected signal (photon flux: $3.6 \times 10^5 \pm 1.3 \times 10^5$ p/s) was significantly higher than in 4 non-injected control mice ($5.3 \times 10^4 \pm 3.4 \times 10^3$ p/s, $p < 0.05$). The signal measured 21 days after injection was higher ($2.3 \times 10^6 \pm 2.3 \times 10^6$ p/s), but this increase was not significant ($p > 0.05$) (Figure 3A). *In vivo* detection of luciferase activity in muscle is in accordance with Wu et al. [226] who imaged luciferase expression after transduction with adenoviral vectors.

When we injected 2 μ L of LV-Fluc (17ng p24) in the right striatum of 4 NMRI mice, a signal was detected projecting from the right side of the skull after IP injection of luciferin from day 5 onwards. The signal was significantly higher than observed in 4 control mice injected with LV-eGFP ($1.8 \times 10^6 \pm 7.2 \times 10^5$ vs. $1.4 \times 10^5 \pm 8.2 \times 10^4$ p/s, $p < 0.05$). In these control mice the signal was predominantly located in the snout (Figure 3B). Coronal sections of the brain of mice that were injected with D-luciferin and subsequently sacrificed, displayed a BLI signal in the right striatum as expected (Figure 3C), demonstrating that the photons are produced by endogenous cells within the brain. This conclusion was further corroborated by the detection of expression of luciferase protein by immunohistochemistry, revealing luciferase-positive cells in the right striatum (Figure 3D).

1.3. Characterization of the BLI Signal After Stereotactic Injection of LV-Fluc into the Mouse Striatum

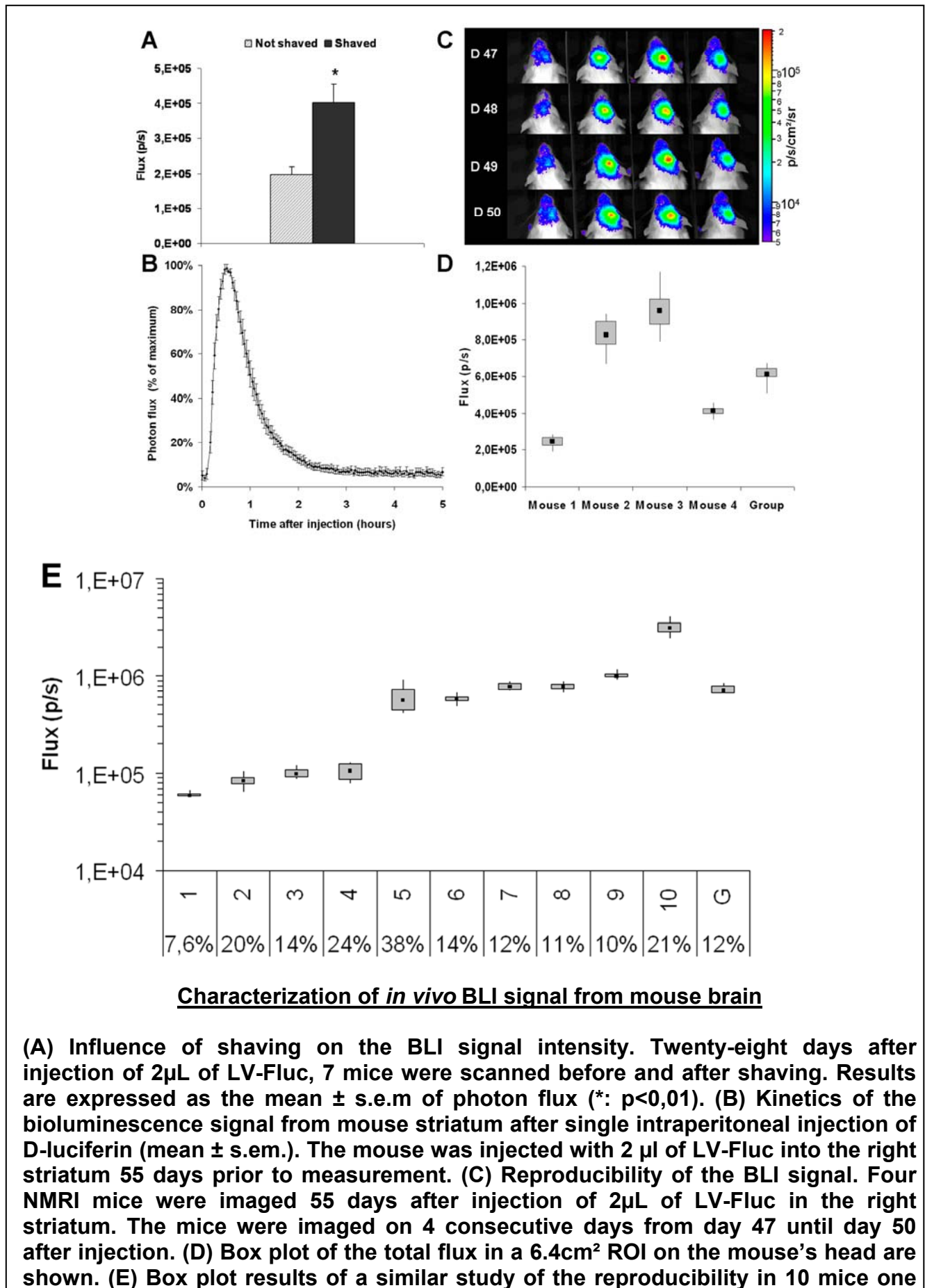
To study the influence of the fur on imaging, we imaged seven mice on day 28 post injection (LV-Fluc), before and after shaving the skull. The BLI signal in the shaved mice was 2-fold higher ($p < 0.01$) (Figure 4A), in concordance with previously published data [226]. Henceforth the skin covering the skull of all mice was shaved prior to imaging. The kinetics of the BLI signal were evaluated in 4 mice 55 days after LV injection. The mice were imaged immediately after IP injection of luciferin with successive 2-minute frames for more than 5 hours. The signal increased during the first 20 minutes following D-luciferin injection, reaching a peak at 31 ± 3 minutes and displayed an exponential drop afterwards. From 140 minutes after injection on, the signal decreased below 10% of its maximum (Figure 4B). This pharmacokinetic profile allows three measurements per day and the rapid testing of the influence of experimental variables on luciferase expression. To assess the reproducibility of imaging, 4 individual mice were scanned on 4 successive days (day

47 to 50 after LV injection) (Figure 4C). The coefficient of variation ranged from 9 to 17% for individual mice and was 12% for the group as a whole (Figure 4D). A similar experiment in 10 different mice 365 days after injection yielded a range from 8 to 38% in individual mice and again 12% for the group (Figure 4E). We consider this reproducibility sufficiently high and stable in time to address biological questions using BLI. Indeed, a prospective power calculation shows that with this coefficient of variation of 12%, differences between the means of two groups each containing 3 mice that are higher than 44% will be considered significant with a power of 0.9 at an alpha level of 0.05. To detect a 20% difference the number of mice per group will have to be increased to 9 keeping the same power and alpha level.

1.4. The Localisation of the BLI Signal Reflects the Anatomical Site of Injection

To determine whether the resolution of BLI would allow anatomical localization in the mouse brain, we analyzed the relation between the injection site and the localisation of the BLI signal on the skull. Mice were injected with LV-eGFP-I-Fluc into the left and right striatum (L and R Str), the right olfactory bulb (OB), the right substantia nigra (SN) and the right medial globus pallidus (GP) (n=3). On day 14 after injection, BLI scans were performed showing a focus on the left side of the head in the L Str mice, on the right side in the R Str mice (Figure 5A). In the OB mice, the focus was located more anterior and medial compared to the striatal injection site, whereas the focus was more posterior in the SN mice. The focus in the GP was located between the R Str and the SN foci. These sites correspond to the expected locations based on the injection coordinates. Using the BLI images, the mice could be unambiguously classified according to injection site, except for the GP mice that were hard to distinguish from the SN mice. The distance in the projection plane between OB and R Str is 4.3 mm, between L Str and R Str is 4 mm and between R Str and SN is 2.7 mm, and these sites could all be distinguished from each other. The distance between the SN and GP is 2.2 mm and these sites could not be distinguished from each other. We deduct that the minimal distance to distinguish two sites is between 2.2 and 2.7 mm, and as a corollary deduct that the localisation error will be within this same range.

Figure 4

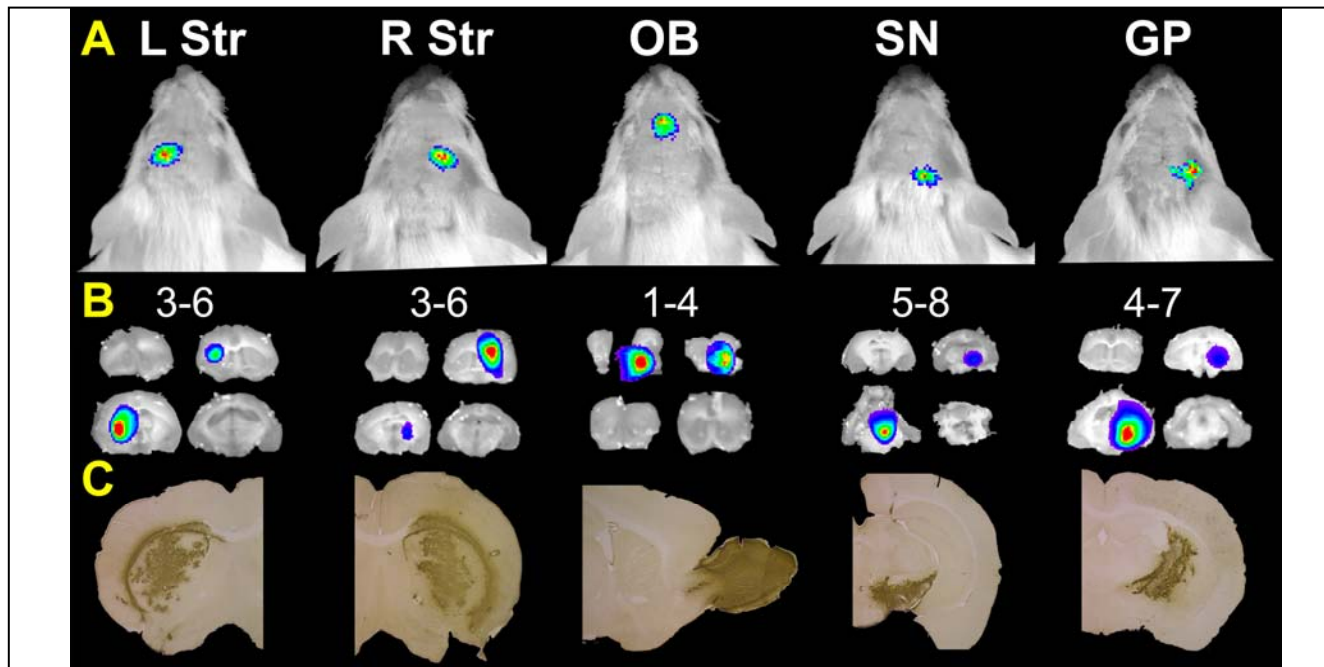


year after injection of LV-Fluc. The results of ten individual mice as well as the group (denoted by “G”) are shown, with the coefficient of variation displayed below each mouse.

The *in vivo* observations were validated by *ex vivo* BLI imaging of coronal slices (Figure 5B) and by immunohistochemistry for eGFP (Figure 5C), which demonstrated specific transduction of the injection site. There were no significant differences in photon flux between the different sites (all $p > 0.3$, multiple 2-sided t-tests on log normalised values) (data not shown).

We conclude that the spatial resolution of BLI in mouse brain is sufficient to localize the source of photon emission in the projection plane with an error lower than 3 mm. This will allow the use of BLI to study biological phenomena that involve migration of cells from one area of the brain to another, as has been done to study the migration of neuronal precursor cells [87, 88].

Figure 5



The Localisation of the BLI Signal Reflects the Anatomical Site of Injection

(A) The location of the BLI signal focus depends on the site of injection. BLI scans 14 days after injection of LV-eGFP-I-Fluc show a focus that is located above the injection site: caudal to the eyes and on the left side of the head for the left striatum (L Str), caudal to the eyes and on the right side for the right striatum (R Str), between the eyes for the olfactory bulb (OB), near the caudal edge of the skull for the substantia nigra (SN), and intermediate between R Str and SN for the globus pallidus (GP). These sites correspond to the expected locations based on the injection coordinates. (B) *Ex vivo* BLI of 1mm-thick coronal slices show the localisation of the signal at the site of injection. The slices are numbered in anteroposterior direction from bulbus olfactorius (1) to cerebellum (9). (C) Immunohistochemistry for eGFP confirms the site of injection.

1.5. BLI Allows Quantification of Luciferase Activity *In Vivo*

To confirm that the BLI signal is a good measure for luciferase activity *in vivo* we injected a dilution series of LV-Fluc (18, 6 and 2ng p24) into the striatum of NMRI mice (n=4 per titer). The signal was significantly higher than background in the groups injected with vector amounting to 18 or 6ng p24 ($p < 0.01$ and < 0.05 , respectively) and decreased upon vector dilution. At the highest dilution (2ng p24) the signal was not significantly higher than that from control mice injected with LV-eGFP corresponding with 6ng p24 (Figure 6A). We examined luciferase activity in individual mice that were injected with different titers (from 18 to 2ng p24). The *in vivo* BLI signal was compared with (i) *ex vivo* BLI images of one millimeter-thick brain slices and (ii) *in vitro* measurements of luciferase activity on tissue extracts from the striatum of the slice with the highest signal. There was a strong linear correlation between the *in vivo* BLI signal and the maximum pixel of the slices ($r^2 = 0.84$, $p < 0.001$) (Figure 6B), between the *ex vivo* BLI values and the *in vitro* luciferase activity ($r^2 = 0.89$, $p < 0.001$) (Figure 6C) and between the *in vivo* BLI signal and the *in vitro* luciferase activity ($r^2 = 0.76$, $p < 0.001$) (Figure 6D). The fact that the *in vivo* BLI values correlate better with the values from the brain slices than with those from the brain extracts is probably due to the experimental error associated with creating the brain extract. We conclude that the bioluminescence signal as measured in the living mice is a reliable measurement of luciferase gene expression in the brain, in groups as well as in individual mice.

1.6. Imaging of Long-Term Lentiviral Vector-Mediated Luciferase Expression in the Mouse Brain

A group of animals injected with LV-Fluc (n=10) and another group with LV-eGFP as control (n=4) were followed for more than one year with weekly to monthly BLI scans (Figure 7). After reaching a maximum at day 8 pi, the BLI signal decreased continuously during the first 37 days until the value reached about 16% of the peak value. From day 42 onwards the signal remained stable for more than 300 days. The signal remained significantly higher (by a factor of ~17) than in control mice that were followed during 150 days ($p < 0.01$ for all time points, unpaired t-test of log normalised values) and this during the entire experiment. Stable gene expression after lentiviral vector transduction is in accordance with the literature [176, 227]. However, most studies thus far relied on invasive methods to establish persistence of gene expression, requiring multiple cohorts of animals sacrificed at different time points. Yoshimitsu et al. [96] used BLI to evaluate luciferase

expression after intravenous injection of lentiviral vectors encoding luciferase in mouse neonates, transducing the brain amongst other organs. They also observed a signal that remained constant at 12 and 24 weeks after transduction but did not provide data for other time points. Shai et al. [228] observed a relatively stable luciferase expression in mouse salivary glands after LV transduction monitored on a weekly basis for three months.

Figure 6

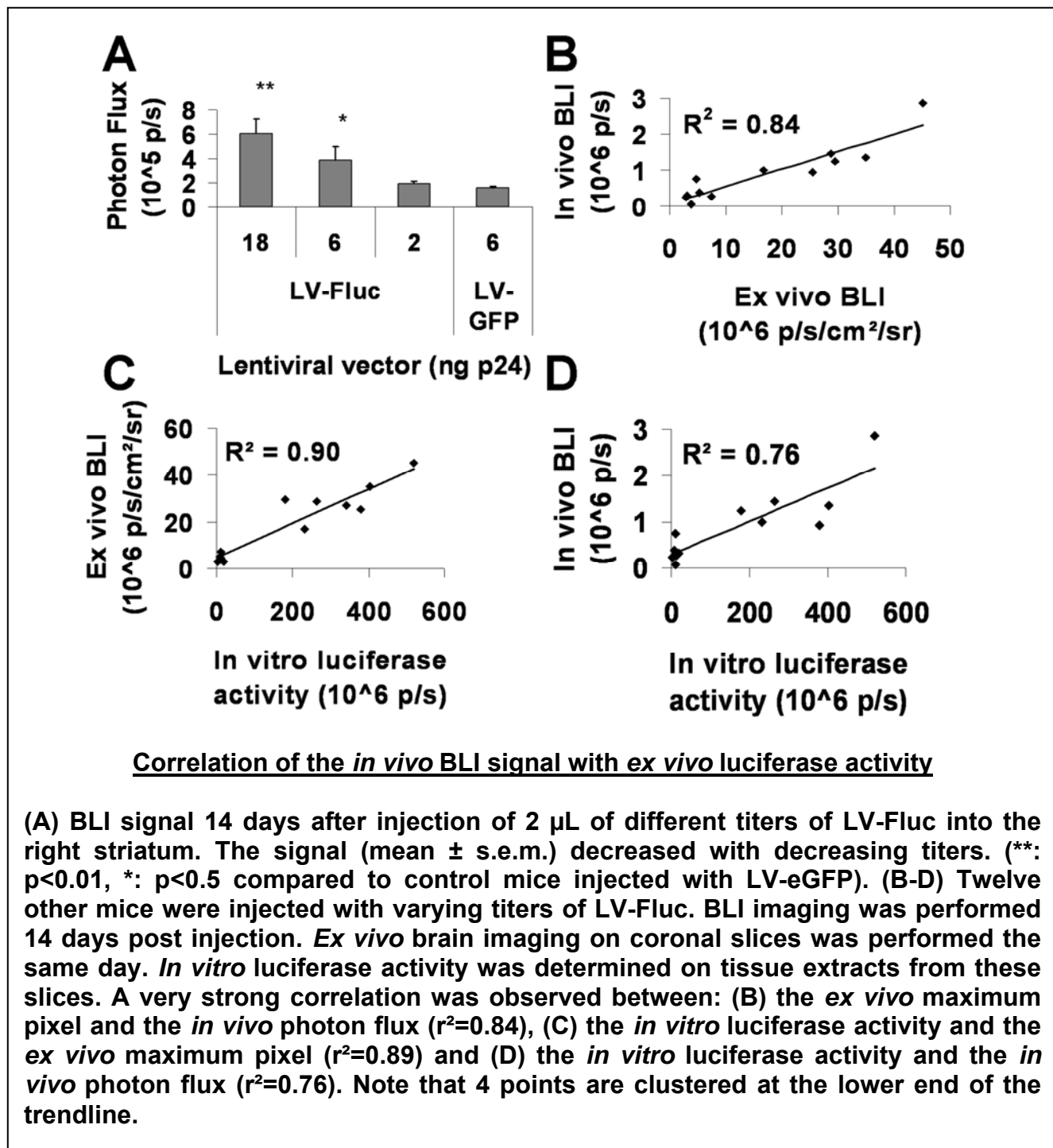
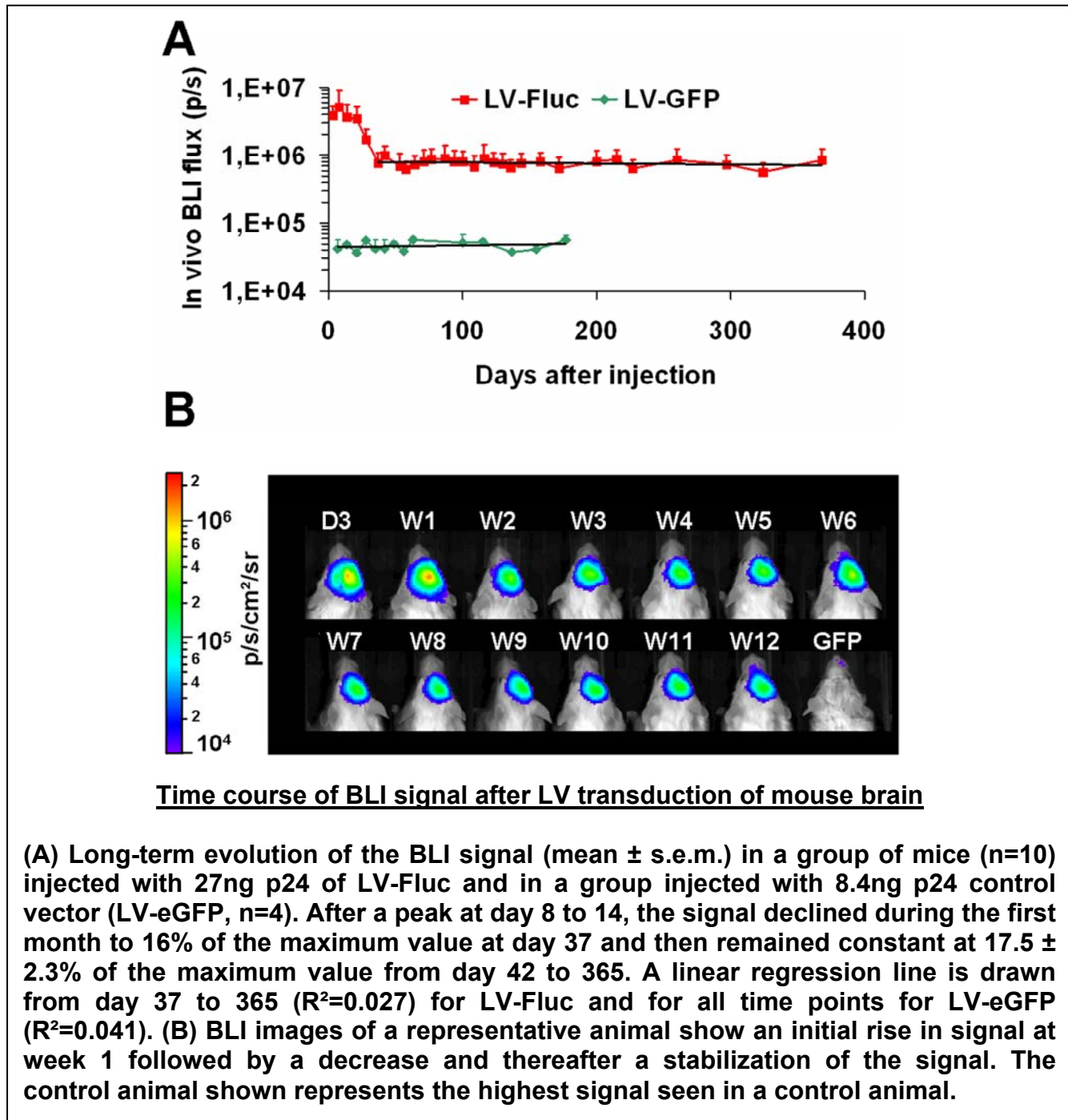


Figure 7



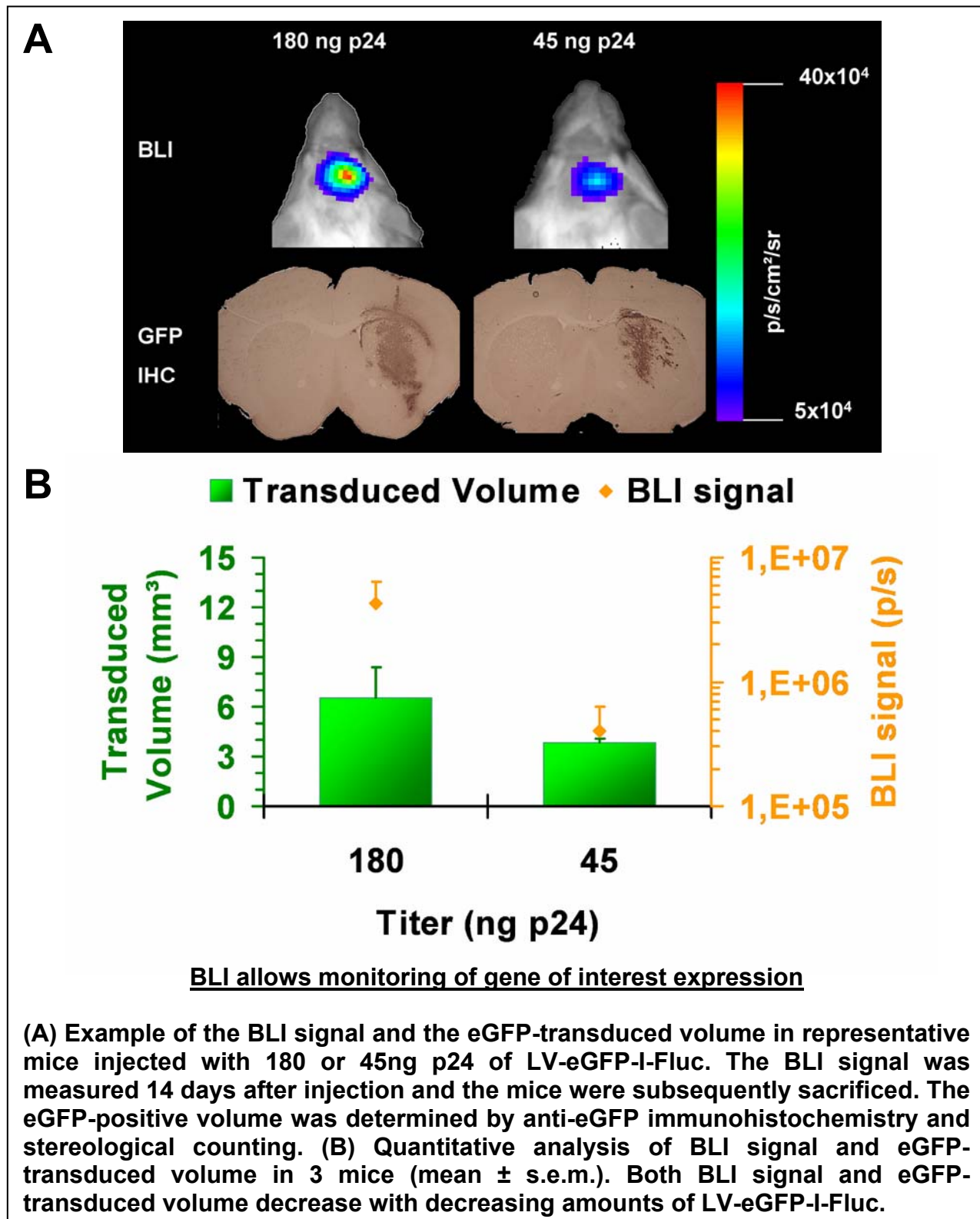
In many other studies, stable gene expression has been assessed by measuring secreted protein in plasma which cannot provide data about the local evolution of gene expression. The decrease in signal during the first month warrants further characterization. The decrease could be due to progressive transgene silencing or activation of gene expression driven from the hCMV-promoter in the early postoperative phase. Although no evidence for gene silencing or gene activation after LV transduction of brain has been reported before,

the sensitivity and reproducibility of BLI in individual mice may be required to detect these phenomena. BLI monitoring of kinetics of luciferase expression is therefore probably the method of choice to study transgene silencing in different neuronal cell types and to compare different promoters and insulators in the viral vector constructs. A transient increase in the passage of D-luciferin through an injured BBB after stereotactic injection, is unlikely since it has been demonstrated that D-luciferin does penetrate an intact blood-brain-barrier albeit at lower levels than in other tissues [73]. Since D-luciferin is administered at a high dose, its concentration in the brain will likely be saturating the limiting amount of luciferase enzyme present. Studies using luciferase transgenic animals [229] or after gene delivery without BBB disruption [96] have also demonstrated the feasibility of imaging luciferase expression with an intact BBB.

1.7. The BLI Signal Reports Expression of a Transgene of Interest

The usefulness of BLI monitoring of gene expression in brain would increase considerably if the signal can be used as an indirect measurement of expression of a transgene of interest. To verify whether BLI can report the expression of a gene of interest, we studied the relationship between the BLI signal and eGFP expression in mice injected with different amounts of LV-eGFP-I-Fluc (180ng p24 and 45ng p24, n=3). We compared the *in vivo* BLI signal with the eGFP-transduced volume as determined by immunohistochemistry and stereological counting (Figure 8A). The BLI signal was $4.3 \pm 2.1 \times 10^6$ p/s and $4.0 \pm 2.4 \times 10^5$ p/s in the high and low titer group, respectively. The corresponding transduced volume was $6.6 \pm 1.8 \text{mm}^3$ and $3.8 \pm 0.27 \text{mm}^3$ (Figure 8B). This represents a 91% decrease in BLI signal and a 42% decrease in transduced volume in the low titer group compared to the high titer one. In cell culture we observed a very strong correlation between BLI signal and fluorescence in cells transduced with different amounts of vector (Figure 2E). In mouse brain however, the decrease in BLI signal is more pronounced than the decrease in eGFP-transduced volume. This is likely due to the fact that stereological quantification of the transduced volume only measures the number of positive cells, not taking into account the level of eGFP expression in transduced cells, whereas the bioluminescent signal integrates the number of positive cells and the amount of luciferase expressed. Based on these data BLI results in a better quantification of gene expression than immunohistochemistry, providing data faster (as soon as four days after transduction) and more reproducibly, without invasive actions, which allows long-term follow-up.

Figure 8



1.8. BLI Detects Luciferase Expression in the Rat Substantia Nigra

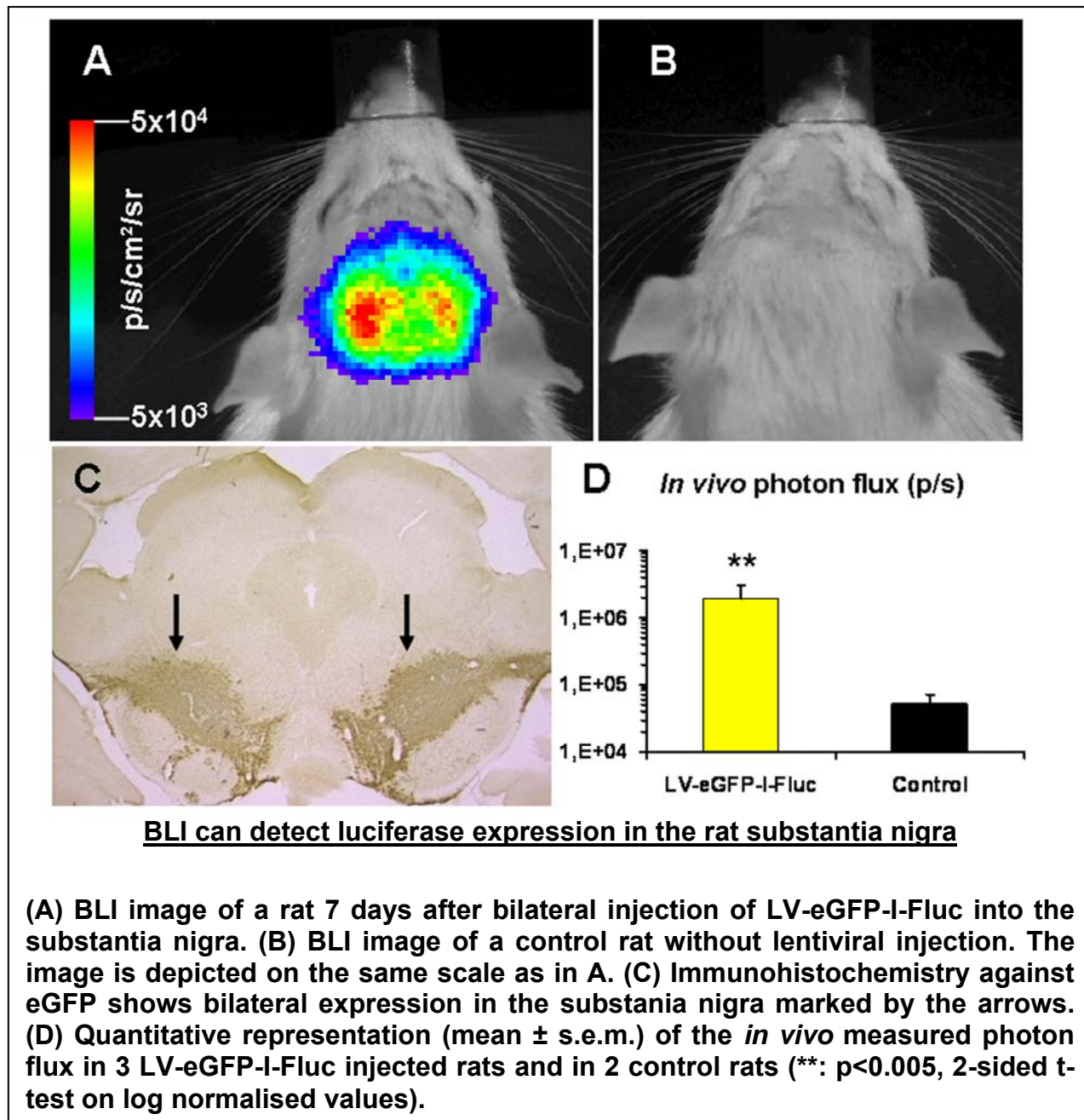
To evaluate if BLI monitoring of locoregional transgene expression would also be feasible in the rat brain, we performed a bilateral injection of LV-eGFP-I-Fluc targeting the substantia nigra in 3 rats. Seven days after injection, we could detect a signal projecting in 2 foci on the left and right caudal part of the skull, whereas there was no signal above background in control rats (Figure 9A-B). Quantitative analysis revealed a photon flux of $1.9 \pm 0.8 \times 10^6$ p/s and $5.2 \pm 1.8 \times 10^4$ p/s in the LV-eGFP-I-Fluc and control group respectively (37-fold increase, $p < 0.005$) (Figure 9D). Immunohistochemistry for eGFP showed that expression was localized in and above the pars compacta of the substantia nigra, where nearly all cells were positive (Figure 9C). We conclude that despite an increase in thickness of overlaying structures, the BLI signal is still sufficient to allow detection of firefly luciferase expression in deep structures of the rat brain, expanding the utility of this technique to this widespread model animal for neurological research. As signal can be detected from the substantia nigra, which is one of the deepest brain structures in the rat, it is likely that expression in any region of the rat brain can be detected.

1.9. BLI can Detect Migration of Endogenous Neural Stem Cells from the Subventricular zone to the Olfactory Bulb

The results of this paragraph are integrated in a manuscript by Reumers, Deroose et al., submitted for publication.

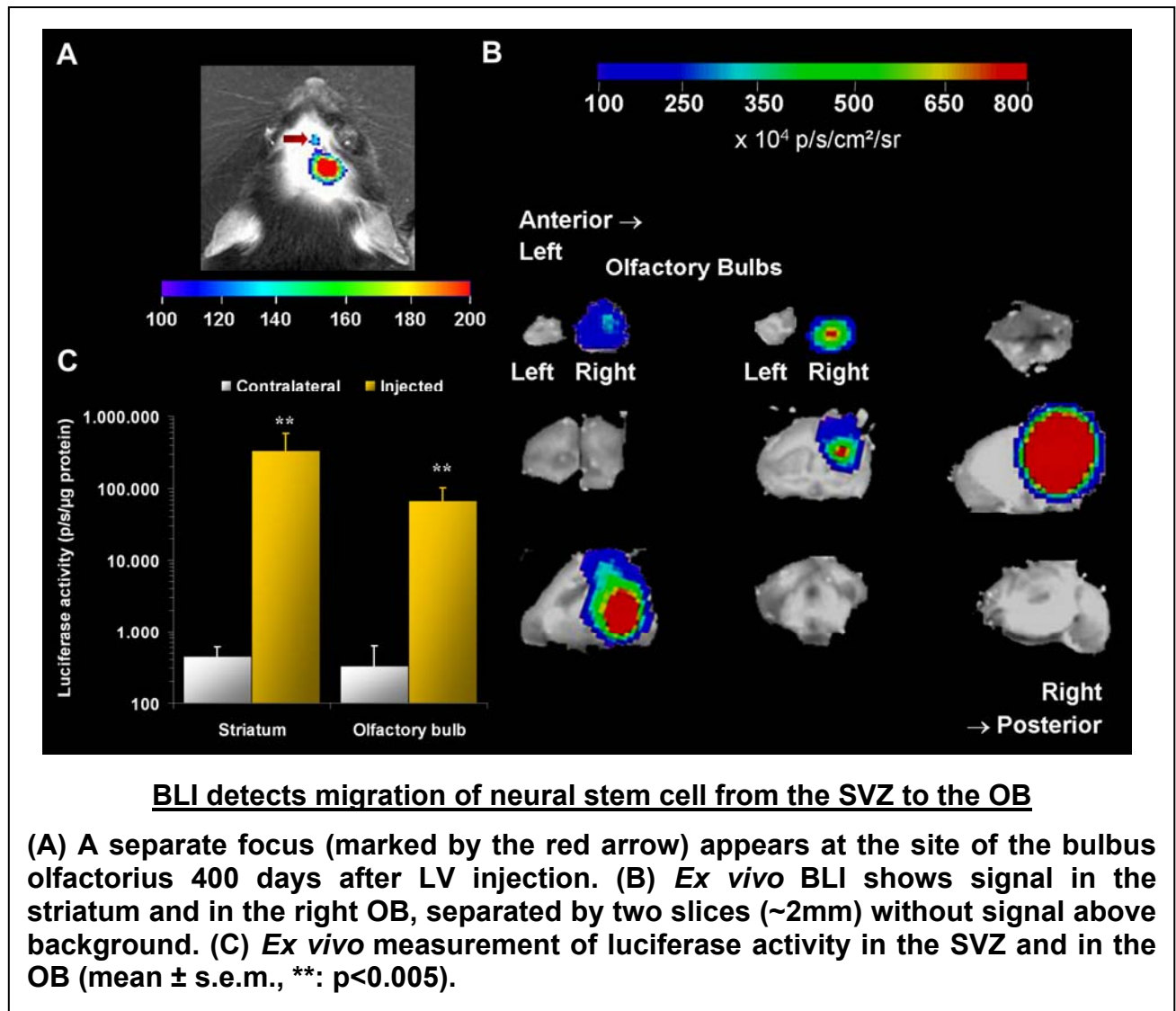
The site where Fluc activity in the OB projects on the skull was determined and the signal was localised paramedian between the eyes. We then injected 3 mice in the right subventricular zone (SVZ) with LV-eGFP-I-Fluc. BLI scans were performed on day 7, 14, 60, 120 and 400 after injection. At the time of the first three scans no focus was visible at the OB projection site. At day 120 a distinguishable focus at the OB became visible in one mouse. At day 400 it was present in two mice. At this time point the animals were sacrificed and *ex vivo* BLI showed a clear focus of photon emission in the right SVZ but also in the olfactory bulb. These 2 foci were separated by 2 slices (~2 mm) that showed no signal above background. *Ex vivo* luciferase activity determination showed activity in the

Figure 9



right SVZ (342 ± 233 p/s/mg protein) and also in the right OB (68.0 ± 35.6 p/s/mg protein). These values were respectively 765 and 208 times higher than in the contralateral brain region ($p < 0.005$). Taken together these data demonstrate that BLI can detect migration of offspring of stably marked endogenous stem cells.

Figure 10



BLI has a number of advantages compared to other molecular imaging techniques such as PET, SPECT, MRI and fluorescence tomography. The hardware is commercially available, is relatively inexpensive and the operating costs are low compared to radioisotope based techniques. The sensitivity is good as we were able to detect luciferase expression after injection of only 6ng p24 of LV-Fluc and the background signal is relatively low. Although the background signal derived from the snout is higher than that in oncology or cardiology studies, this is still many times lower than the typical fluorescent background encountered in fluorescent-based imaging strategies [230]. The major limitations of BLI (and fluorescence imaging) are the limited penetration through living tissue, restricting its use to mice and rats. SPECT, PET and MRI have low background and are tomographical in nature enabling three-dimensional localization of the signal. Although mathematical approaches have been worked out [231], there is currently only

limited data available regarding BLI tomography, limiting current BLI applications to planar imaging. Another limitation of BLI is the need to inject D-luciferin substrate, that has been overcome by genetically encoded fluorophores for fluorescence imaging and by magnetic proteins such as ferritin for MRI [123]. LV-mediated luciferase expression in the brain has up to now only been imaged by one other group [96]. There are a number of methodological and scientific differences between this work and ours that merit emphasising. First, Yoshimitsu *et al.* used neonatal animals that they injected intravenously through the superficial temporal vein, whereas we use (young) adult animals of 8 weeks old that are injected *in situ* in the brain. They do not provide data on efficient brain transduction in adult animals and they do not exclude that brain transduction is due to specific conditions in the neonatal stage, such as immaturity of the blood-brain-barrier. Indeed, in adult mice transduction of the brain after intravenous injection results in low transduction efficiencies of 0.01 to 1 genome copy per 100 genome equivalents [232]. In mucopolysaccharidose type I mice it has been shown that intravenous injection in the young adult stage (8 weeks) results in brain enzyme activities and genome copies that are almost 2 log orders lower than in neonates [233]. Furthermore, a systemic injection results in very high signal coming from other organs such as the liver, spleen and lungs which can interfere with brain assessment. It needs to be pointed out that there are no convincing images of brain signal presented by Yoshimitsu *et al.*, probably due to scaling constraints because of the very high signal in liver and spleen. They do present one convincing *ex vivo* image. One concern that is not addressed in their paper is the nature of the cells emitting the detected light. Indeed, the signal might come from endothelial cells that the lentiviral vectors can transduce without crossing the BBB. We have shown with immunohistochemistry that the cells display a typical neuron-like morphology, demonstrating that the signal is not coming from endothelial cells. No localisation within the brain is performed in their study contrary to ours where we demonstrate that the BLI images allow to discriminate expression in different parts of the brain. No relationship between BLI signal and gene expression is provided by Yoshimitsu *et al.* whereas we have thoroughly studied this relationship. Finally, no long-term quantitative data is presented by them, whereas we show a stable signal for more than one year of follow-up. The paper by Yoshimitsu *et al.* contains an extensive study of α -galactosidase expression in plasma and several organs and evaluates concentration of the toxic globotriaosylceramide that are beyond the scope of our study.

CONCLUSION

This is the first report on BLI monitoring of viral vector-mediated transduction of the adult brain in living mice. We were able to detect stable gene expression for more than one year. Our work opens perspectives for the use of BLI in the study of brain disease beyond malignancies and infectious diseases. BLI can be used for optimizing novel viral or non-viral vectors for gene transfer into the central nervous system, yielding data on the levels of gene expression as well as on the persistence of gene expression over time. Furthermore, by combining the luciferase reporter with a gene inducing neurodegenerative disease, neurodegeneration may be followed quantitatively over time and potential therapeutic strategies may be evaluated non-invasively. One disadvantage of this technique is that it is not applicable to humans due to increased photon attenuation.

2. *Multimodality Imaging of Tumor Xenografts and Metastasis in Mice with Combined Micro Positron Emission Tomography, Small Animal Computed Tomography and Bioluminescence Imaging*

The results of this section have been published in the article “*Multimodality imaging of tumor xenografts and metastasis in mice with combined microPET, microCT and bioluminescence imaging*” by Deroose CM, De A, Loening AM, Chow PL., Ray P, Chatziioannou AF and Gambhir SS in the Journal of Nuclear Medicine, 2007;48(2):295-303.

Systemic metastases are the primary cause of cancer mortality for most cancer types and represent a major therapeutic challenge in oncology. Determination of the presence and extent of metastases is a cornerstone of diagnosis in oncology. PET plays an increasingly important role in this staging process largely due to improved detection of lymph node and systemic metastases with [¹⁸F]-FDG [234] and the introduction of combined clinical PET-CT scanners has further strengthened this role.

Better understanding of the biological mechanism of metastasis has been achieved by studying migration and seeding of tumoral cells, tumor-stroma interactions, vascularization of tumors, genetic mouse models and gene expression and proteomic patterns that correlate with metastasis. These insights have highlighted the need for more realistic models than the currently used tumor xenografts models that suffer from altered vascularization, have no relevant tumor-stroma interactions and often rely on immunodeficient mice [179]. Recently progress has been made by our group and others to adapt whole body imaging techniques to small animals so that tumor burden can be visualized and quantified in one single animal over time. For this purpose we have developed reporter gene systems for PET [235] and for BLI [76]. We used these systems to study the role of specific genes in cancer progression [180], to study viral vector targeting of metastases [236] and for non-invasive monitoring of novel treatments for melanoma metastases [183, 237]. We have also developed a trimodality fusion reporter gene that allows detection of gene expression by fluorescence, BLI and PET [154]. For the latter, the reporter probe used is [¹⁸F]fluoromethylbutylhydroxyguanine ([¹⁸F]-FHBG) that will be phosphorylated by the reporter gene product, a mutant herpes simplex virus type 1 thymidine kinase (HSV1-tk) enzyme.

Small animal CT systems have recently been developed [238, 239] that allow imaging of the anatomy of living mice with a high spatial resolution of 50 to 200 micrometers based on differential X-ray absorption by different tissues. Tissue contrast mainly depends on differences in tissue density and on the presence of mass amounts of contrast agents providing limited if any molecular information. Hence most of the current applications of small animal CT have focused on specific tissues that can be well depicted because of their favourable contrast properties such as bone [239] or have required the use of specific contrast agents [240]. We have previously used small animal CT to study a localized model of prostate cancer bone metastasis in the tibia of mice [241].

The high specificity of PET tracers for their molecular target(s) provides little anatomical landmarks which is a disadvantage in studies where the origin of the signal is not known, such as in cell and metastases trafficking studies. To improve this weakness of PET, we investigated microPET and small animal CT imaging for a multimodality imaging method allowing visualization of molecular information within an adequate anatomical framework. We used BLI to validate our findings and to compare combined microPET-CT with BLI within the same animal.

Our study was a preliminary assessment of combined PET-CT with the following specific goals: (i) establishment of a methodology to obtain co-registered microPET and small animal CT images, (ii) validate these fused PET-CT images in tumor xenografts, (iii) evaluate fused PET-CT in the detection of pulmonary melanoma metastasis in a mouse model with [¹⁸F]-FDG and [¹⁸F]-FHBG (iv) evaluate fused PET-CT in the detection of systemic melanoma metastasis with [¹⁸F]-FDG and [¹⁸F]-FHBG and compare this to BLI metastasis detection.

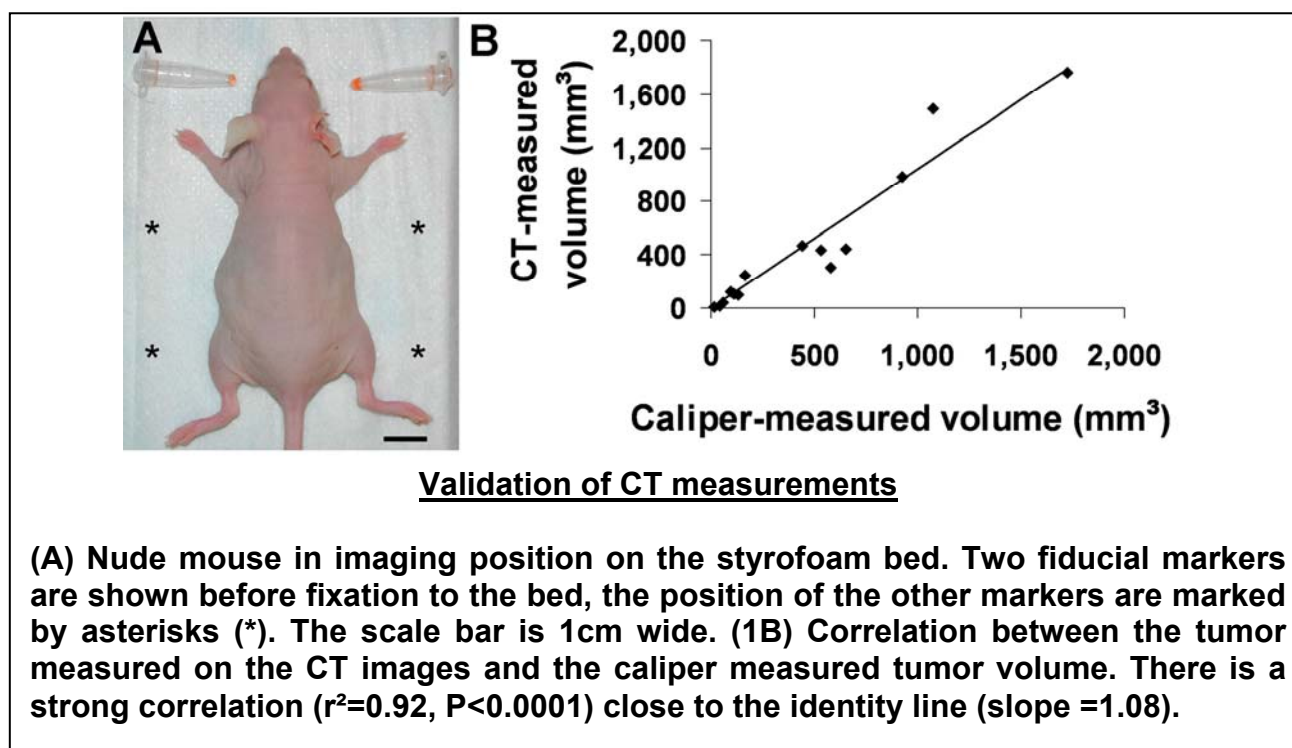
RESULTS

2.1. Establishment of a Fused MicroPET-CT Imaging Strategy

The mice were positioned in a reproducible manner on the styrofoam bed in the presence of 6 fiducial markers (Figure 11A). Due to the limited transaxial field of view of the small animal CT scanner, some fiducial markers were not visible in the CT dataset and on average only 4.5 ± 0.23 fiducial markers could be used for the alignment procedure. The required minimum of three fiducial markers was visible in all scans. The PET and CT images were aligned in AMIDE using the “alignment wizard”. After alignment, the mean fiducial reference error was 0.29 ± 0.072 mm per fiducial marker used. This error is well below the resolution of the microPET of ~ 1.85 mm and indicates that the alignment

procedure was adequately performed. The outlines of the body, the heart and the kidneys were systematically verified in 24 mice and showed a very good correspondence between the microPET and small animal CT images.

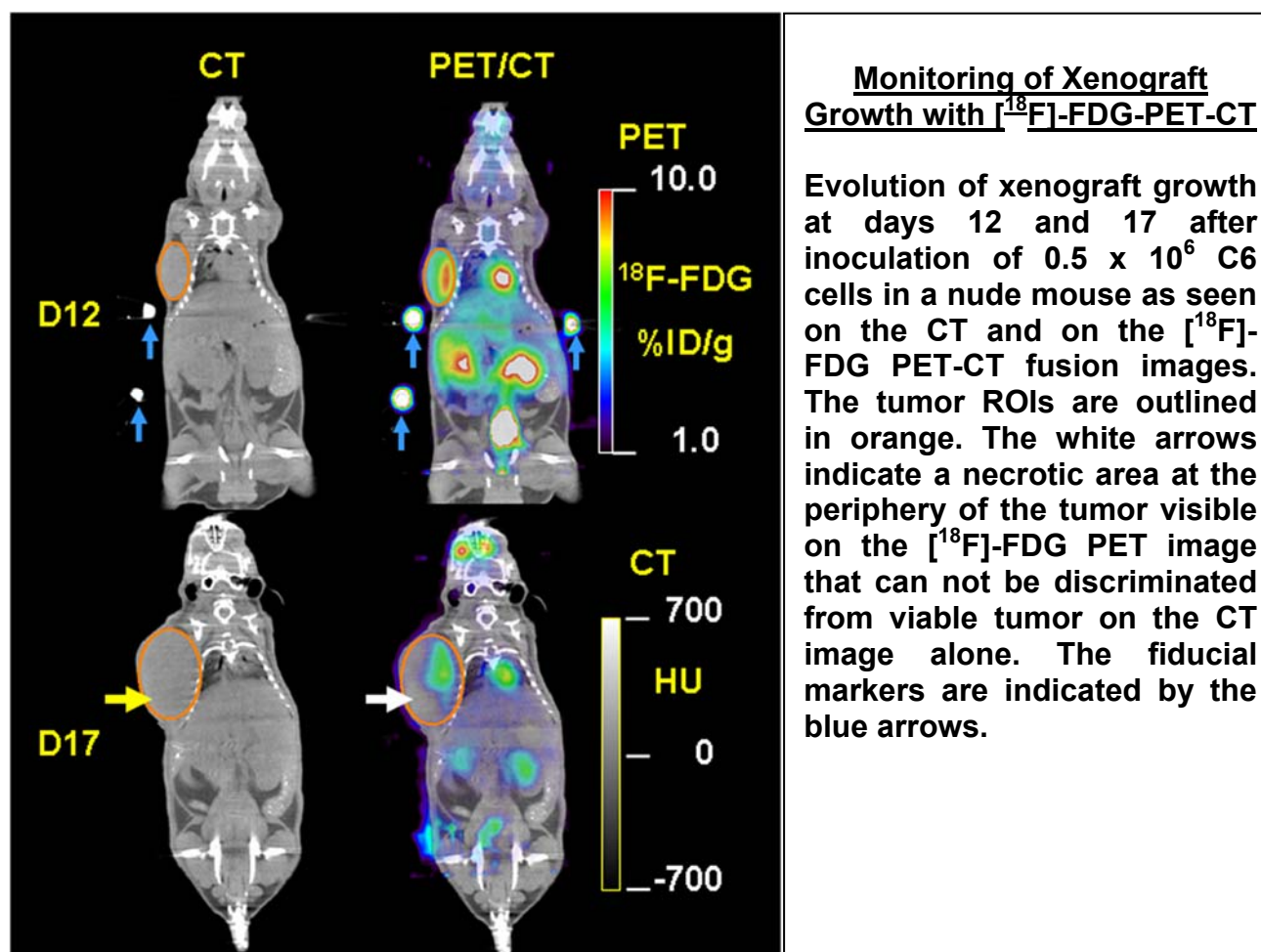
Figure 11



2.2. [¹⁸F]-FDG MicroPET-CT is Capable of Monitoring Growth of Tumor Xenografts

CT measurements using an ellipsoid ROI showed a good correlation with calliper measurements in the 13 scans performed on the xenograft models with a tumor size ranging from 15.6 to 1720 mm³ ($r^2=0.92$, $p<0.0001$) (Figure 11B). The microPET images showed a hypermetabolic signal in all the tumors that could be detected by external palpation. The microPET data showed increasing uptake of [¹⁸F]-FDG in the N2a xenografts from day 8 to 20 days after inoculation with a final maximum value of $4.52 \pm 0.69\%ID/g$. In the C6 xenograft model, [¹⁸F]-FDG uptake was not significantly different from day 12 to 17 after implantation as the mean [¹⁸F]-FDG uptake evolved from 4.54 ± 0.94 to $4.70 \pm 1.67\%ID/g$. and the maximum evolved from 7.07 ± 1.86 to $8.28 \pm 0.78\%ID/g$. Necrotic areas were visualized on the microPET images in all 4 C6 tumors but were not detected on the corresponding CT images, regardless of the settings of the Hounsfield thresholding windows (Figure 12).

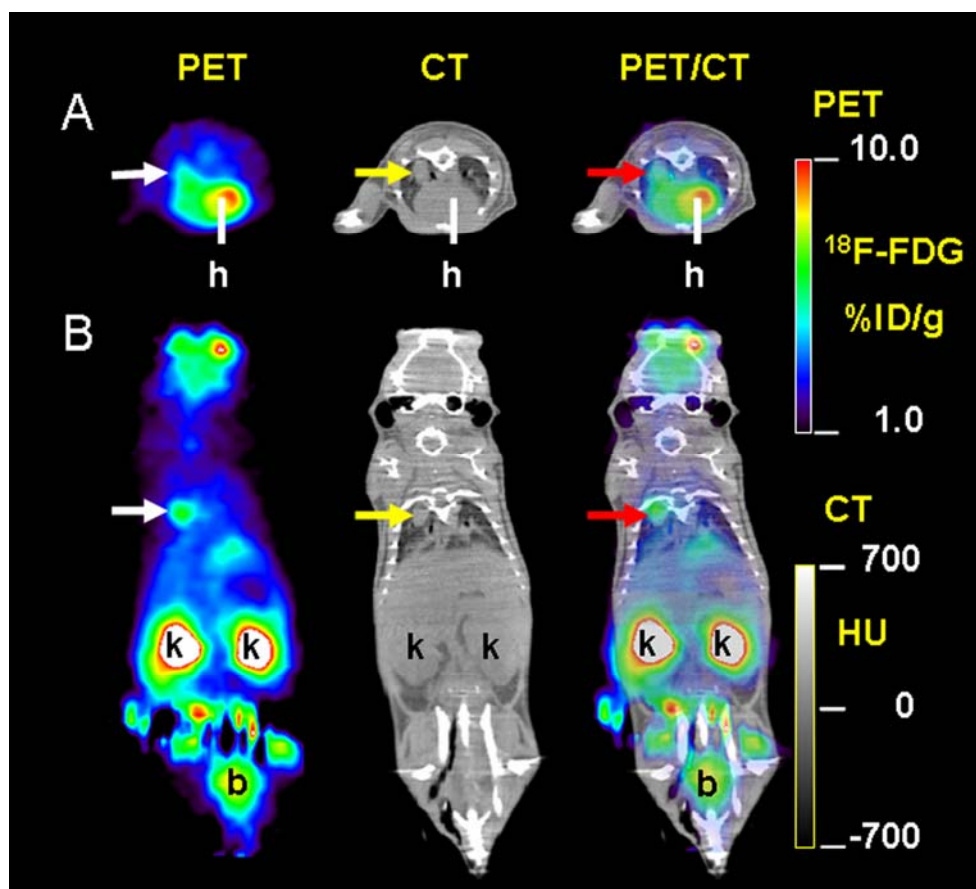
Figure 12



2.3. $[^{18}\text{F}]$ -FDG MicroPET-CT Detects Pulmonary Melanoma Metastases

$[^{18}\text{F}]$ -FDG PET-CT was capable of detecting pulmonary metastases in 4 out of 5 SCID mice 45 days after intravenous injection with A375M-Fluc cells. The CT images showed round nodular water-density lesions in the lung parenchyma and near the visceral pleura (Fig. 13). PET images showed high uptake of $[^{18}\text{F}]$ -FDG in the corresponding area. The $[^{18}\text{F}]$ -FDG uptake was $8.8 \pm 1.6\% \text{ID/g}$ (control: $1.1 \pm 0.2\% \text{ID/g}$, $p=0.0042$), the density was $98.3 \pm 38.8 \text{ HU}$ (control: -352 ± 21.5 , $p=3.8 \times 10^{-8}$) and the tumor volume was $24.4 \pm 12.0 \text{ mm}^3$ (range: 7.5 to 58 mm^3). High uptake in the heart, in the interscapular brown fat and in the bone marrow did interfere with detection and delineation of the lesions in two mice. $[^{18}\text{F}]$ -FDG PET-CT did not detect the numerous metastatic lesions in the mice injected with the B16F0 cells because of low $[^{18}\text{F}]$ -FDG uptake in this cell line (data not shown).

Figure 13



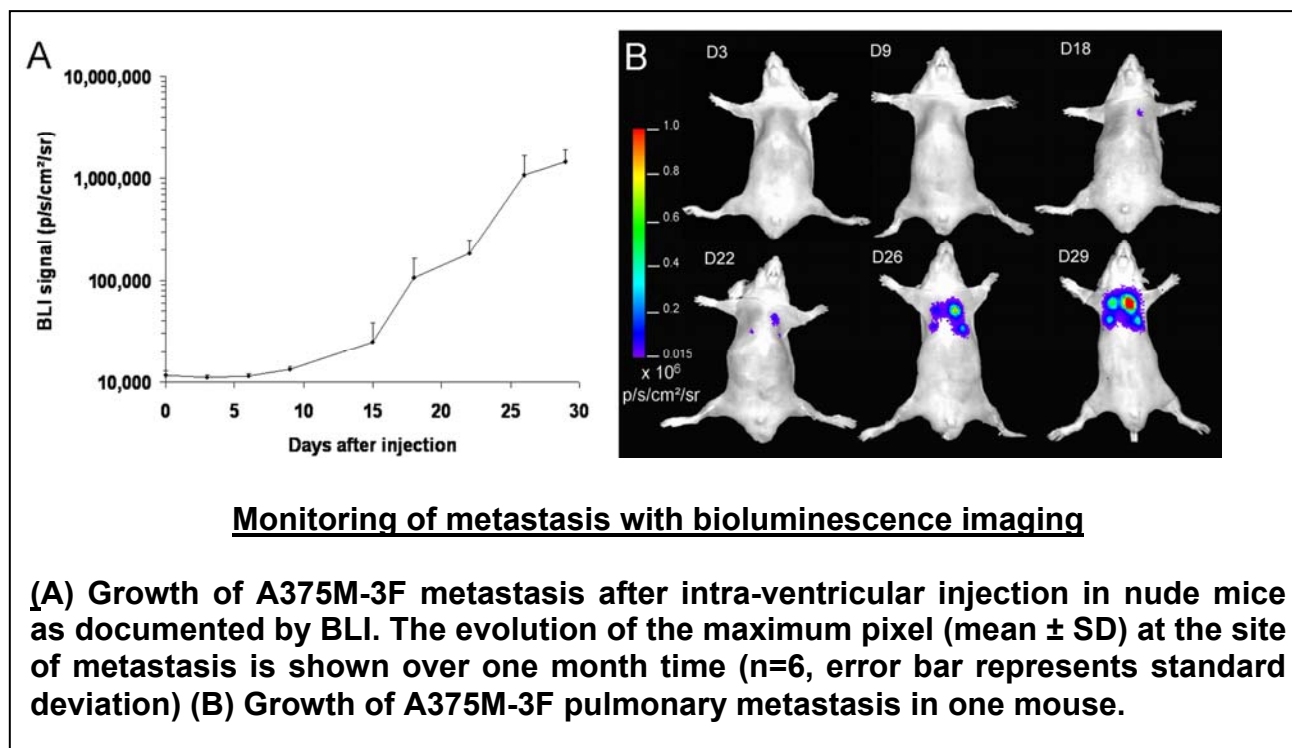
Detection of pulmonary metastasis with $[^{18}\text{F}]$ -FDG-PET-CT

Transverse (3A) and coronal (3B) sections of co-registered $[^{18}\text{F}]$ -FDG-PET and CT images of a SCID mouse 45 days after tail-vein injection with 0.7×10^6 A375M-Fluc melanoma cells. The white arrows indicate the hypermetabolic area seen on the $[^{18}\text{F}]$ -FDG PET image. The yellow arrows show a water density nodule located in the dorsal part of the apex of the right lung in the CT image. The PET-CT fusion image confirms the localization of the hypermetabolic image on the anatomical reference (red arrow). Physiological tracer uptake in the heart (h), kidney's (k) and bladder (b) is marked.

2.4. $[^{18}\text{F}]$ -FHBG MicroPET-CT and Bioluminescence Imaging of Systemic Melanoma Metastases

After twelve cell culture generations, the A375M-3F cell line showed a good activity for herpes simplex virus 1 thymidine kinase assay ($1.98 \pm 0.28\%$ penciclovir/minute/ μg protein) and good *Renilla* luciferase activity (5098 ± 791 RLU/min/ μg protein). The six mice that received an intra-ventricular injection of A375M-3F cells were monitored with BLI imaging every 3 to 4 days (Figure 14A and B).

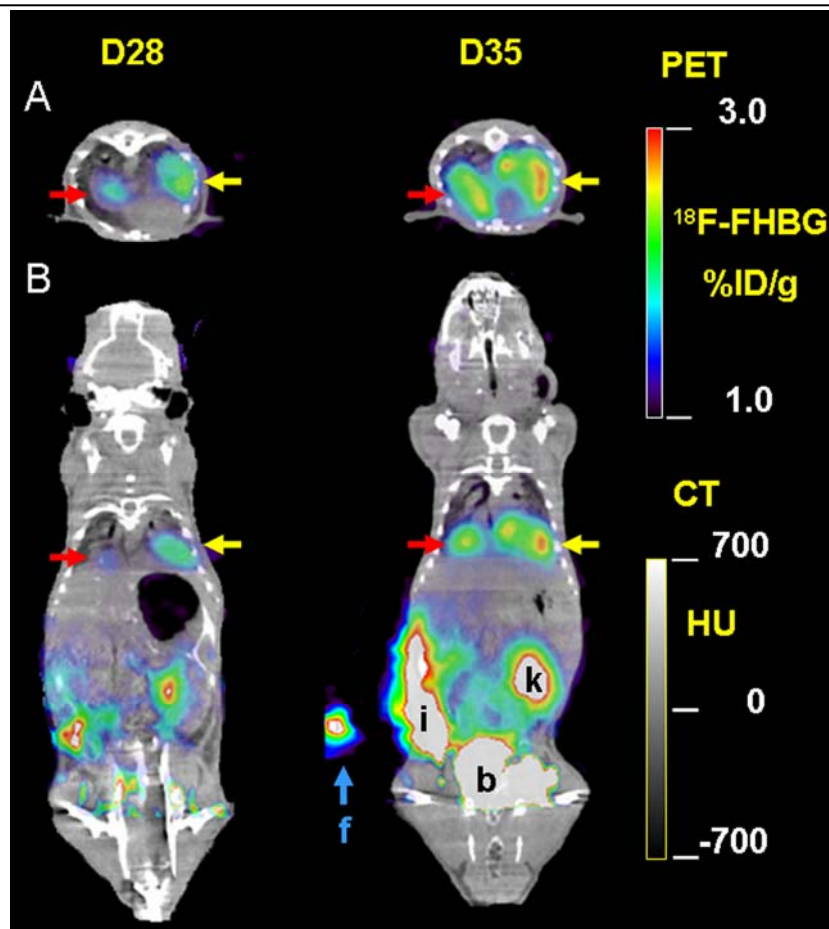
Figure 14



From day 15 on, metastatic sites could be detected with BLI and subsequent [^{18}F]-FHBG PET-CT scans on day 28 showed increased uptake at these sites. Metastases were detected in the following organs: bone (mandibula (n=3), long bones (n=2)), liver (n=2), lung (n=1), and eye (n=1). The mean uptake of [^{18}F]-FHBG on day 28 was $3.3 \pm 1.3\%$ ID/g. When the animals were scanned one week later on day 35, the uptake of [^{18}F]-FHBG in these lesions was increased (Figure 15). The CT images showed increased soft tissue in the pulmonary lesions (n=2), an enlargement of the liver (n=2) and spleen (n=1). No osteolytic lesions were documented in the bone lesions detected on PET.

The combination of the PET and CT images allowed a precise anatomical localization of the lesions (Figure 16 A and B) that could be captured in a single image using three dimensional rendering (Figure 18). The localization of the lesions as detected by microPET-CT was confirmed by necropsy and by *Renilla* luciferase and TK assay on tissue samples (Figure 16C).

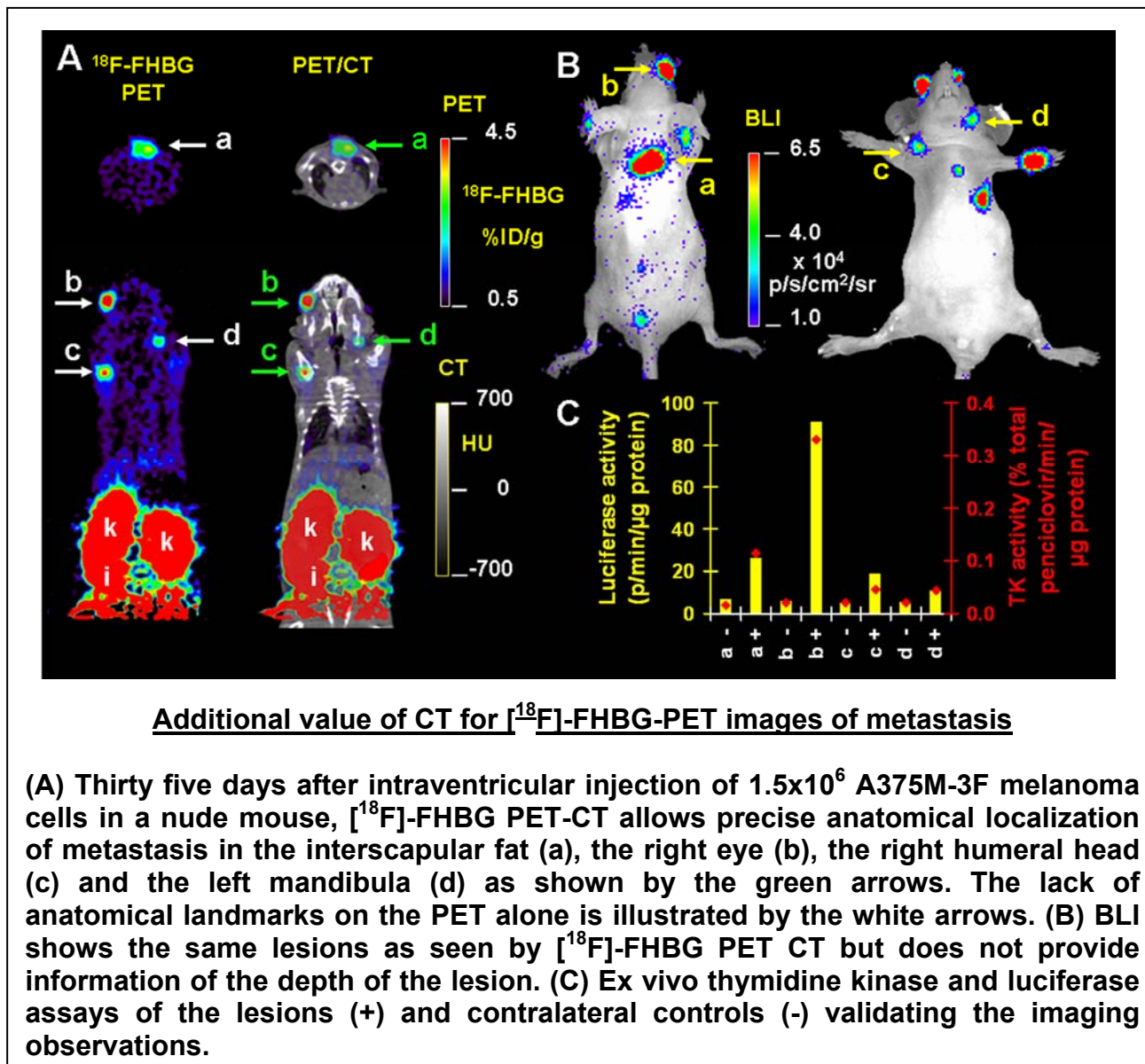
Figure 15



Evolution of metastasis with [^{18}F]-FHBG-PET-CT

(A) Transverse and (B) coronal sections of co-registered [^{18}F]-FHBG PET-CT images of a nude mouse injected with A375M-3F in the left ventricle. The left (yellow arrows) and right (red arrows) basal fields of the lung show a 39% increase in tracer uptake from 1.8 to 2.5%ID/g and from 1.4 to 2.1%ID/g (50% increase) from week 4 to week 5 indicating progressive growth of pulmonary metastasis. The blue arrows indicate fiducial markers. Physiological tracer uptake in the intestines (i), right kidney (k) and bladder (b) is marked.

Figure 16



2.5. $[^{18}\text{F}]$ -FHBG MicroPET-CT is More Sensitive than $[^{18}\text{F}]$ -FDG MicroPET-CT for Detection of Systemic Metastases

Two days after $[^{18}\text{F}]$ -FHBG scanning, an $[^{18}\text{F}]$ -FDG PET-CT was performed. These scans allowed detection of the metastasis in some of the lesions seen on the $[^{18}\text{F}]$ -FHBG scans but not in all of them. The mean uptake of $[^{18}\text{F}]$ -FDG ($8.7 \pm 4.4\%$ ID/g) was higher than the uptake of $[^{18}\text{F}]$ -FHBG ($3.3 \pm 1.3\%$ ID/g, $P < 0.01$) (Figure 17A). Delineation of the lesions that were detected was more difficult due to the increased background uptake of $[^{18}\text{F}]$ -FDG (Figure 17B). The tumor to background contrast for $[^{18}\text{F}]$ -FHBG for muscle, liver, heart, brown fat, and intestine was 0.88 ± 0.02 , 0.78 ± 0.04 , 0.83 ± 0.03 , 0.84 ± 0.03 and -0.77 ± 0.08 respectively whereas for $[^{18}\text{F}]$ -FDG they were 0.61 ± 0.07 , 0.46 ± 0.09 , -0.14 ± 0.31 ,

0.06±0.28 and 0.15±0.12 (Figure 17C). Despite the lower absolute uptake, there is a significant increase in [¹⁸F]-FHBG contrast for muscle, liver, heart, brown fat with 0.27, 0.32, 0.97 and 0.77 compared to [¹⁸F]-FDG (all P<0.001).

Figure 17

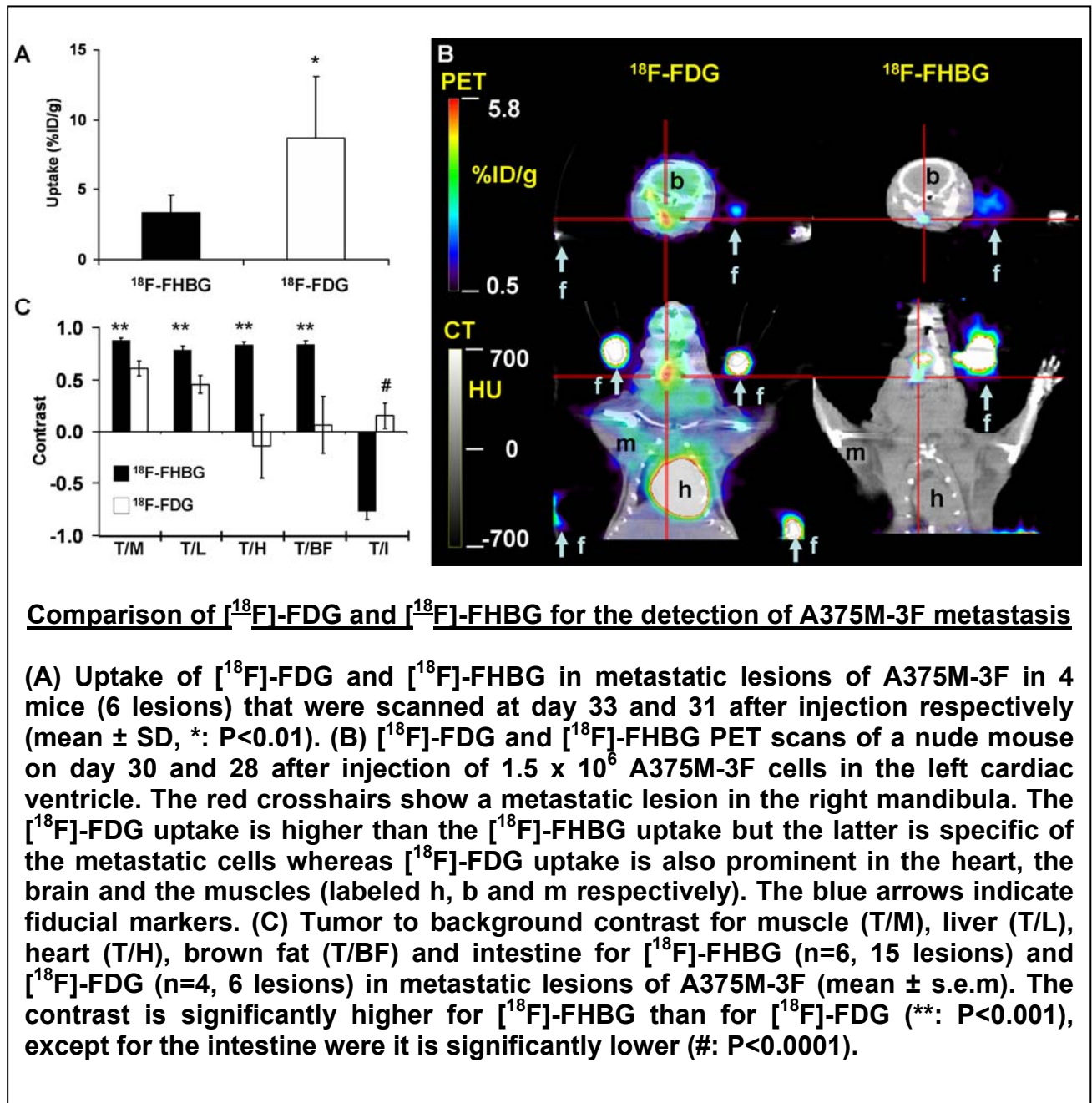


Figure 18



Three dimensional rendering of metastases detected by PET reporter gene imaging

Three dimensional rendering of a combined [^{18}F]-FHBG PET-CT image of a nude mouse 35 days after intracardiac injection of 1.5×10^6 A375M-3F cells. The [^{18}F]-FHBG-PET data is displayed in yellow-red, the CT data in grayscale. This representation allows assessment of the tumor burden in on single image with the presence of appropriate anatomical landmarks.

DISCUSSION

In this study we demonstrated noninvasive, quantitative and tomographic imaging of tumor xenografts and metastasis in mouse models using combined microPET and small animal CT studies. We determined the feasibility of co-registration of microPET and small animal CT in xenograft models, explored the possibility of [^{18}F]-FDG PET-CT to detect pulmonary melanoma metastasis, and explored detection of systemic metastasis of a reporter gene expressing melanoma cell line with [^{18}F]-FHBG PET-CT and BLI.

We used a method based on fiducial markers for the fusion of the microPET images with the small animal CT images. As the error on the alignment was ~ 5 times lower than the resolution of the microPET, we consider this method sufficiently accurate. We did not perform any partial volume nor attenuation correction as this is beyond the scope of this

project. The reported values are therefore underestimations for lesions smaller than ~4 mm diameter.

Visualization of the tumor xenografts was possible with [¹⁸F]-FDG PET and small animal CT. The N2a xenografts showed increasing uptake with time whereas the C6 xenografts showed no differences over time in mean or maximum uptake. This is due to partial volume effect in the N2a xenografts as the volume in the early scans was around 45 mm³ (diameter ~4.5 mm). In the C6 xenografts, the increase in mean uptake was less than the increase in the maximum pixel value due to necrosis in the peripheral parts of the tumor. This necrosis was not seen on the CT images in any of the tissue windows we examined and this is due to the poor soft tissue contrast of small animal CT. This finding highlights the need for contrast agents for appropriate tumor characterization with small animal CT. These can be classical iodine based contrast agents, be tissue specific [240], or can come from another imaging modality, as in our approach where we used [¹⁸F]-FDG PET.

To study metastases we first used an established model of lung metastases [183] to take advantage of the contrast between the tumoral soft tissue and the air that is present in the lungs. We were successful in detecting pulmonary metastasis with CT and [¹⁸F]-FDG PET in 4 out of five SCID mice 45 days after intravenous injection of A375M-Fluc melanoma cells. These mice did represent an advanced stage of disease with lesion ranging in size from 7.5 to 58 mm³. High background uptake of [¹⁸F]-FDG in heart, muscle and brown fat did interfere with lesion delineation in two mice and because pulmonary metastases of B16-F0 melanoma cells did not show increased [¹⁸F]-FDG uptake we further focused on reporter gene based metastasis detection.

We used melanoma cells expressing the tri-modality fusion reporter gene hRL_mRFP_HSV1-sr39ttk after lentiviral transduction (A375M-3F). We showed that reporter gene activity was still present after 12 cell culture generations, which indicates that there is no significant silencing of reporter gene expression that might influence cell detection. A total of 9 metastatic sites were detected by [¹⁸F]-FHBG PET with a mean uptake of $3.3 \pm 1.3\%$ ID/g. The CT images showed changes in the lung and liver but not in the bone lesions. Earlier reports have shown the presence of osteolytic lesions caused by A375 cells [242, 243] but this is not the case for the derived cell line A375M that has been selected for its capacity to form lung metastases [244, 245]. Despite a higher uptake of [¹⁸F]-FDG in the A375M-3F cells, [¹⁸F]-FHBG was superior to [¹⁸F]-FDG because of its much lower background uptake in the thorax and the head. There was a significant increase of tumor to background contrast of at least 0.27 for [¹⁸F]-FHBG in the most

relevant thoracic organs. This better performance of [^{18}F]-FHBG compared to [^{18}F]-FDG in the thorax was anticipated, as [^{18}F]-FHBG is specifically designed to be retained only in cells expressing HSV1-tk, a viral enzyme that in these mice is only present in the tumor cells. Furthermore, it has a very favourable pharmacokinetic profile with very rapid washout of normal tissues. In contrast, [^{18}F]-FDG uptake is related to glucose metabolism and is primarily determined by the amount of active GLUT-transporters on the cell membrane and by hexokinase activity, and these are not restricted to tumor cells but also occur in brain, heart, brown fat and liver. In intestines, the non-specific physiological hepatobiliary clearance of [^{18}F]-FHBG causes higher activity levels that are responsible for the limited detection of metastatic lesions in the peritoneal cavity, the lumbar spine or pelvic bones. Novel molecules with better imaging characteristics such as 2'-fluoro-2'-deoxyarabinofuranosyl-5-ethyluracil (FEAU) [246] are currently under investigation and they might improve the detection of metastasis because they show an increased absolute uptake and lower gastrointestinal activity compared to [^{18}F]-FHBG. Using a rabbit model of VX2-carcinoma pulmonary metastasis, Kondo et al. [247] showed that the performance of [^{18}F]-FDG PET increased significantly in lesions larger than 4mm compared to smaller ones. Recently, oncological imaging of mice has been reported in clinical combined PET/CT systems [248] but the low resolution of 6mm interferes with accurate quantification of metastatic lesions.

The BLI signal intensity is depth dependent resulting in a higher signal for superficial lesions than for deeper lesions that showed a comparable [^{18}F]-FHBG uptake, confirming our previous observations [154]. BLI has the advantage of a relatively low cost and high throughput capability, making the depth dependence of the signal the major disadvantage in small animals. The other major limitation of BLI is the planar nature of the images impeding accurate three-dimensional localization of the signal. Recent studies have used BLI for non-invasive evaluation of metastasis [249], for evaluation of lymphoma therapy [250], for studying the influence of differential gene expression on the pattern of metastasis formation [251], and for studying the importance of cellular receptors for metastasis development [252]. Progress is being made in the development of tomographic optical systems as reviewed in [253]. These systems are using novel hardware that allows acquisition of BLI images from multiple angles and reconstruction algorithms that use models of photon transport in tissue to localize and quantify photon sources, but they still need substantial validation regarding localization and quantification of the luminescent signal. The low cost, high sensitivity and high throughput of planar BLI also make it suited as a routine monitoring tool that, when metastases are detected, can be complemented by

[¹⁸F]-FHBG microPET-CT for anatomical localization and quantitation. A slightly different strategy was used by Kang *et al.* [254] where BLI was used to detect MDA-MB-231 breast cancer bone metastases followed by PET reporter gene imaging of HSV1-tk expression under control of a TGF- β response element. The latter image represented signal transduction through the TGF- β /Smad pathway and it allowed to show *in vivo* that these cells are engaged in Smad-dependent transcription while growing as bone metastases. Thus, PET and BLI can be used to detect two different molecular signals from the same metastasis.

We have demonstrated that multi-modality imaging with PET, CT and BLI is a powerful tool in the study of metastatic mouse models. Because of low contrast of [¹⁸F]-FDG, even in a cell line that has a high [¹⁸F]-FDG uptake, PET reporter gene strategies are superior to [¹⁸F]-FDG imaging except for abdominal metastases. Based upon our results, we suggest the following imaging strategy: initial frequent BLI scans allow monitoring of animals while the metastases are below the detection thresholds for PET and CT. When BLI shows lesions that have reached the detection thresholds for PET or CT, combined PET-CT scans can then be used for detection (PET and CT), quantitation (PET), anatomical localization (CT), density and volume measurement (CT).

One of the major limitations of the current study is the lack of a histological gold standard for the assessment of tumor metastasis. For the identification of lesions as metastases this is partially compensated by the double detection of the lesions on PET and BLI and by the *in vitro* analysis of tissue extracts. However, there might have been lesions that did not reach the threshold of detection by either imaging method and that resulted in false negatives. This study however was designed as a feasibility study to show the potential of multimodality PET-CT and BLI detection of metastasis. Future work will have to address the issue of sensitivity and determine the threshold of detection for the different modalities. For instance, longer scan times than 10 minutes for PET might increase sensitivity. Histological standards will be needed and the mRFP moiety of the multimodality reporter gene will be useful in the detection and identification of fluorescent metastatic cells in tissue specimens. The mRFP moiety is also important for fluorescence activated cell sorting rather than for *in vivo* fluorescent imaging, where the high background and the weak signal generate a signal to noise ratio that is much lower than for BLI [230]. Another limitation is the fact that this methodology is not directly translatable to human use. Indeed, the technique uses cells that have been transduced with the reporter gene *ex vivo* that are then injected into the mouse. There is currently no robust way to introduce the reporter gene into disseminated metastases in a human patient.

CONCLUSION

We combined non-invasive molecular and anatomical information in mice by fusing microPET and small animal CT images acquired from independent systems. We demonstrated that our multimodality reporter gene approach is capable of detecting metastatic lesions in an early stage by using BLI and in a later stage these lesions can be accurately localized on three-dimensional combined PET-CT images. Non-invasive detection of reporter gene expression combined with accurate anatomical information can have important applications in the study of the biology of metastasis formation and progression, in the monitoring of novel cancer treatments and in the establishment of new transgenic models that combine oncogenic mutations with reporter genes. Combined molecular and anatomical imaging can also be useful in other areas of biomedical research such as tracking of immune cells and monitoring of stem cell based therapies.

3. Validation of Varicella Zoster Virus Thymidine Kinase as a Novel Reporter Gene for PET

The results of this section have been submitted for publication in the article “*Validation of varicella zoster virus thymidine kinase as a novel reporter gene for positron emission tomography*” by Deroose CM[®], Chitneni SK[®], Gijssbers R, Vermaelen P, Ibrahim A , Verbruggen AV, Balzarini J, Baekelandt V, Nuyts J, Bormans GM, Debyser Z and Mortelmans L.

Christophe Deroose performed lentiviral vector cloning and validation, cell culture and LV-transduction, radiotracer uptake experiments, mouse model inoculation and imaging.

Satish Chitneni performed all radiotracer syntheses and purifications, HPLC analyses and some radiotracer uptake experiments.

Recent developments in the field of molecular imaging have led to the development of imaging reporter genes. These genes encode proteins of which the distribution and concentration can be detected by specific non-invasive imaging strategies. Imaging reporter genes have been developed for radionuclide imaging (positron emission tomography and single photon emission tomography), magnetic resonance imaging (transferrin receptor [117], ferritin [123] and polylysine protein [127], bioluminescence imaging (Firefly luciferase, Renilla luciferase [76], Gaussia luciferase [85]) and fluorescence imaging (for review, see [20]). For radionuclide imaging, three main types of reporter genes have been described: intracellular enzymes, receptors (either membrane bound or intracellular) and membrane bound transporters. The most intensively studied PET reporter gene (PRG) is herpes simplex virus type 1 thymidine kinase (HSV1-tk), for which more than 15 different PET reporter probes (PRP) have been reported [5, 31]. In a cell expressing this enzyme phosphorylation of a substrate PRP will result in a metabolite that will remain trapped intracellularly because it is negatively charged and hence loses its ability to cross the plasma membrane by passive diffusion. This enzyme-dependent PRP accumulation will result in an increased concentration of radioactivity that can be detected by a PET scanner, allowing characterization of the location, magnitude and persistence of gene expression. Applications of the HSV1-tk PRG in preclinical models include studies of gene therapy in rodents [5] and large animals [255], monitoring

the fate of cells [256] and tissues [257] in cell/tissue based therapies, monitoring models of metastatic cancer [180, 258] and follow-up of endogenous gene expression [259]. HSV1-tk expression in clinical trials of suicide gene therapy has been detected by PET and its expression pattern correlated with the outcome of the therapeutic intervention. Jacobs *et al.* [42] used liposome mediated DNA transfer to relapsed glioblastoma and detected expression with the PRP [¹²⁴I]-FIAU in one patient. The volume of HSV1-tk expression was predictive of the volume responding therapeutically after administration of ganciclovir, a prodrug that is converted into a toxic metabolite in HSV1-tk expressing cells. Penuelas *et al.* [26] detected adenoviral vector-mediated HSV1-tk expression after direct intratumoral injection in patients with hepatocellular carcinoma. The gene expression maps could predict the clinical outcome: in all patients where PET detected specific accumulation of the PRP [¹⁸F]-FHBG stabilization of disease was achieved, whereas in all patients without significant PRP accumulation disease progression was seen. It is important to note that [¹⁸F]-FHBG has received approval of the Food and Drug Administration for use in human volunteers (Investigational New Drug #61,880) [34].

Despite the widespread use of the HSV1-tk system, a large effort has been put into the development of other PRG/PRP systems. The properties of an ideal reporter system have been presented in the introduction. Despite having some of these characteristics, the HSV1-tk system has some well documented disadvantages: (i) lack of blood-brain-barrier (BBB) penetration of all PRPs evaluated until now, including [¹²⁴I]-FIAU [41] and [¹⁸F]-FHBG [33] (ii) lung tissue accumulation of the PRP [¹⁸F]-FHBG does not linearly correlate with the tissue expression of a mutant HSV1-tk over the full range of transgene expression obtained in rat lung tissue [260] (iii) clearance of [¹⁸F]-FHBG is both urinary and hepatobiliary [33], precluding its use in the urinary and gastro-intestinal tractus. These limitations have spurred development of other PRP/PRG systems, such as the dopamine type 2 receptor [49], the human type 2 somatostatin receptor [261, 262], the human estrogen receptor ligand binding domain [60], the dopamine transporter [66], the norepinephrine transporter (hNET) [67, 68] and the human sodium-iodide symporter (hNIS) [62, 263]. Although some of these PRGs were initially evaluated with SPECT tracers, validated PRP are available for these targets as well. Except for hNET and hNIS, these systems all have a one to one stoichiometry between expressed protein and specifically bound PRP, whereas the enzyme HSV1-tk and the transporters hNIS and hNET can each trap multitudes of PRP molecules per protein. None of these systems has all the requirements of the ideal PRG. Furthermore, multiple independent reporter genes

are useful for multiplexing and many studies have used 2 different PRGs for non-invasive assessment of 2 molecular events [50, 51].

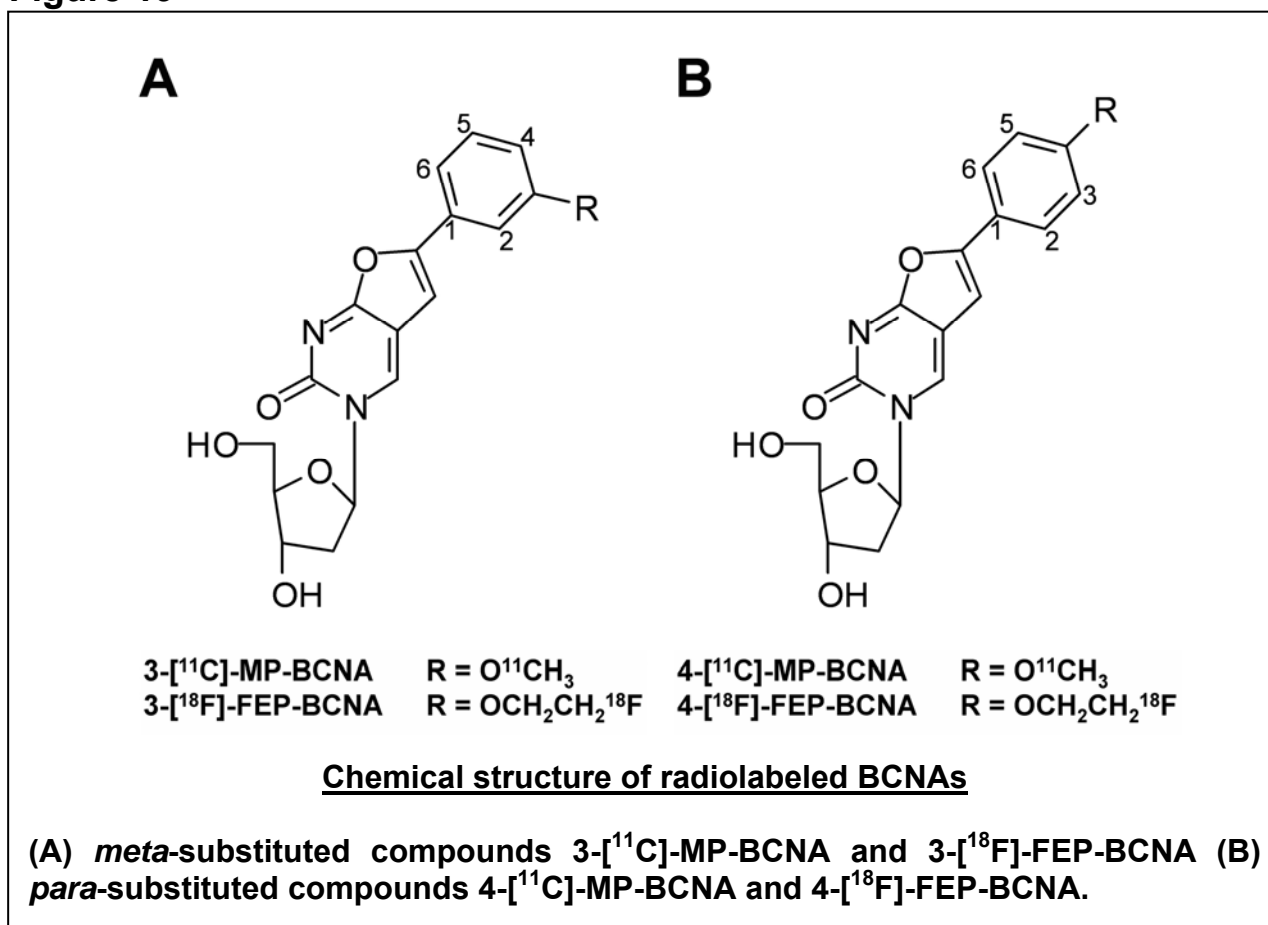
Because of the need for other PRG/PRP systems that allow imaging of gene expression behind the intact BBB, we decided to develop a new system based upon the thymidine kinase gene of the varicella zoster virus (VZV-tk) in combination with radiolabeled bicyclic nucleoside analogs. VZV or human herpes virus 3 is a member of the herpes virus family and is the cause of chicken pox and shingles in humans. Similar to HSV, VZV encodes a TK with loosened substrate specificity compared to the mammalian TK. This enzyme (VZV-TK) is a 341 amino acid protein that has an amino acid homology of only 29% with HSV1-TK. It catalyses the ATP-dependent phosphorylation of thymidine to thymidine phosphate. Note that the gene is referred to as VZV-tk, the enzyme as VZV-TK.

The bicyclic pyrimidine nucleoside analogues (BCNAs) are a novel class of nucleoside analogues [264, 265]. Several of these compounds are highly potent and specific inhibitors of VZV replication [264]. Since some of these molecules are highly lipophilic with calculated logP (ClogP) values ranging from 0.4 to 4.6, they have a good potential for BBB penetration. Finally, these molecules are stable and resistant against degradation by thymidine phosphorylase or dihydropyrimidine dehydrogenase [266]. BCNAs are phosphorylated by VZV-TK into mono- and diphosphates [184]. No triphosphates have been detected until now and it is not known if the phosphorylated BCNAs are substrates for DNA polymerases. In contrast, BCNAs are not phosphorylated, neither by HSV1 or HSV2 TKs nor by mammalian TKs. Monophosphate BCNA is not a substrate of HSV1-TK and the mammalian thymidilate kinase while the diphosphate BCNAs are not recognised by nucleoside diphosphate kinase.

We have previously synthesized 4 radiolabeled BCNA derivatives, the *meta*-substituted compounds 3-[¹¹C]-MP-BCNA and 3-[¹⁸F]-FEP-BCNA [181] and the *para*-substituted compounds 4-[¹¹C]-MP-BCNA and 4-[¹⁸F]-FEP-BCNA (Chitneni *et al.*, personal communication) (Figure 19). The affinity of these tracers for VZV-TK is 4.8 ± 1.7 , 53 ± 12 , 1.5 ± 0.2 and $4.2 \pm 0.6 \mu\text{M}$ respectively. Here we present the *in vitro* and *in vivo* evaluation of these tracers as potential PRPs with VZV-tk as PRG.

RESULTS

Figure 19



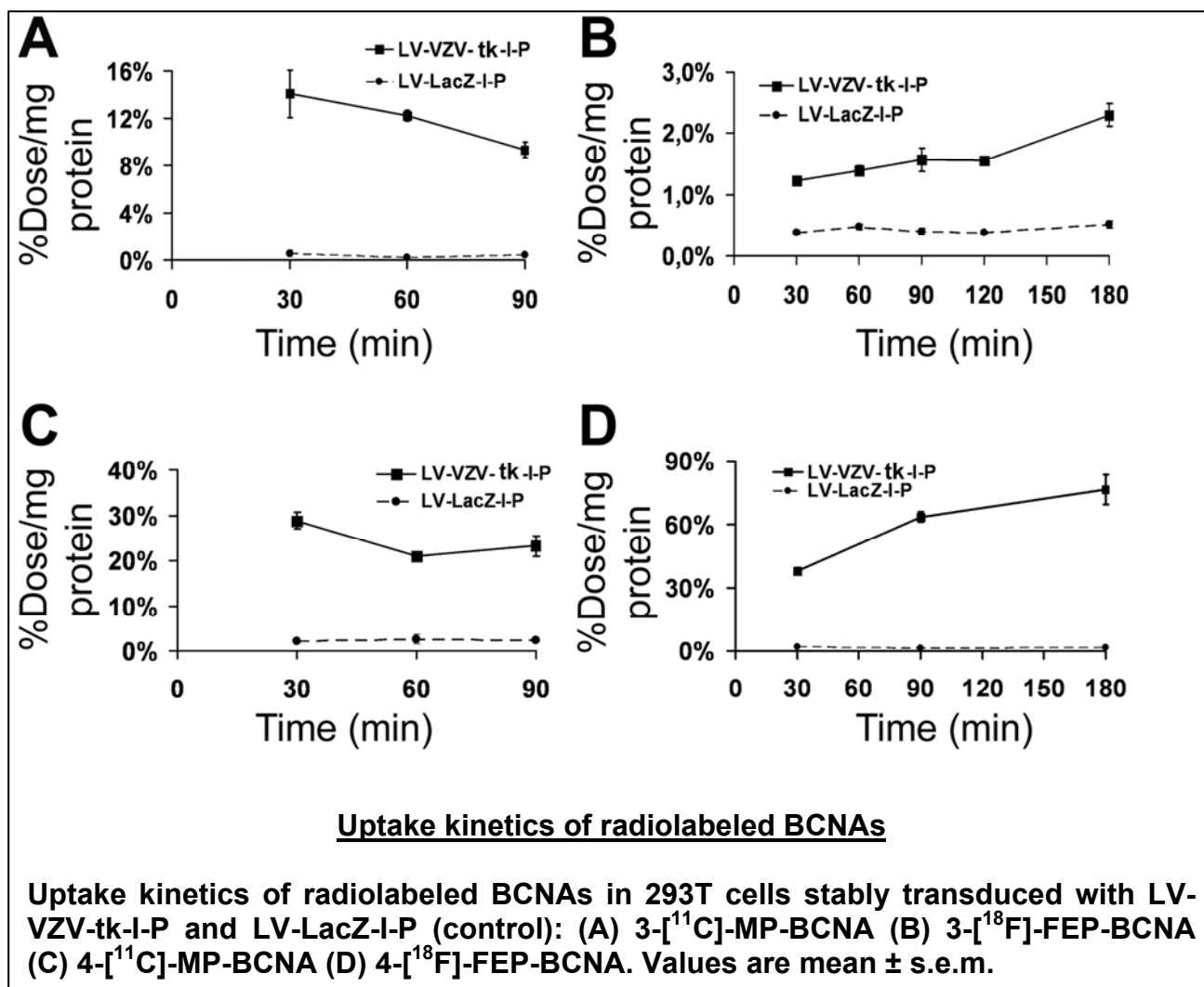
3.1. Uptake Kinetics of Radiolabeled BCNAs in Stably Transduced 293T

Cells

In 293T cells stably expressing VZV-tk the uptake of all four radiolabeled BCNAs after 30 min of incubation was significantly higher than in control cells (Figure 20). The uptake of 3-[¹⁸F]-FEP-BCNA however was low in absolute values (Figure 20B) and continued to increase until 180 min incubation. The uptake of the other 3 BCNAs was significantly higher ($p < 0.01$ for all comparisons) than the uptake of 3-[¹⁸F]-FEP-BCNA. For both 3-[¹¹C]-MP-BCNA (Figure 20A) and 4-[¹¹C]-MP-BCNA (Figure 20A) and 4-[¹¹C]-MP-BCNA (Figure 20C) values at later time points were significantly lower than at 30 min ($p < 0.005$ and $p < 0.05$ at 90 min respectively). The uptake of 4-[¹⁸F]-FEP-BCNA (Figure 20D) was characterized by significantly higher values at 90 and 180 min compared to 30 min ($p < 0.01$ for both). For all radiolabeled BCNAs the uptake in the control cells transduced with LV-LacZ-I-P was less than 1% of the total dose. The corresponding uptake ratios are shown in Figure 21. The uptake ratio of 3-[¹⁸F]-FEP-BCNA was

significantly lower than the uptake ratio of the other tracers at all time points ($p < 0.01$), except at the 90 min time point. The uptake ratio of the other tracers was similar at 30 min but at later time points the uptake ratio of 4- ^{18}F -FEP-BCNA was 2.5-fold higher than at the earlier time points ($p < 0.005$) where it remained stable for the two other tracers. In summary, BCNAs accumulate in VZV-tk expressing cells but only for 4- ^{18}F -FEP-BCNA there is a substantial accumulation that increases with time.

Figure 20

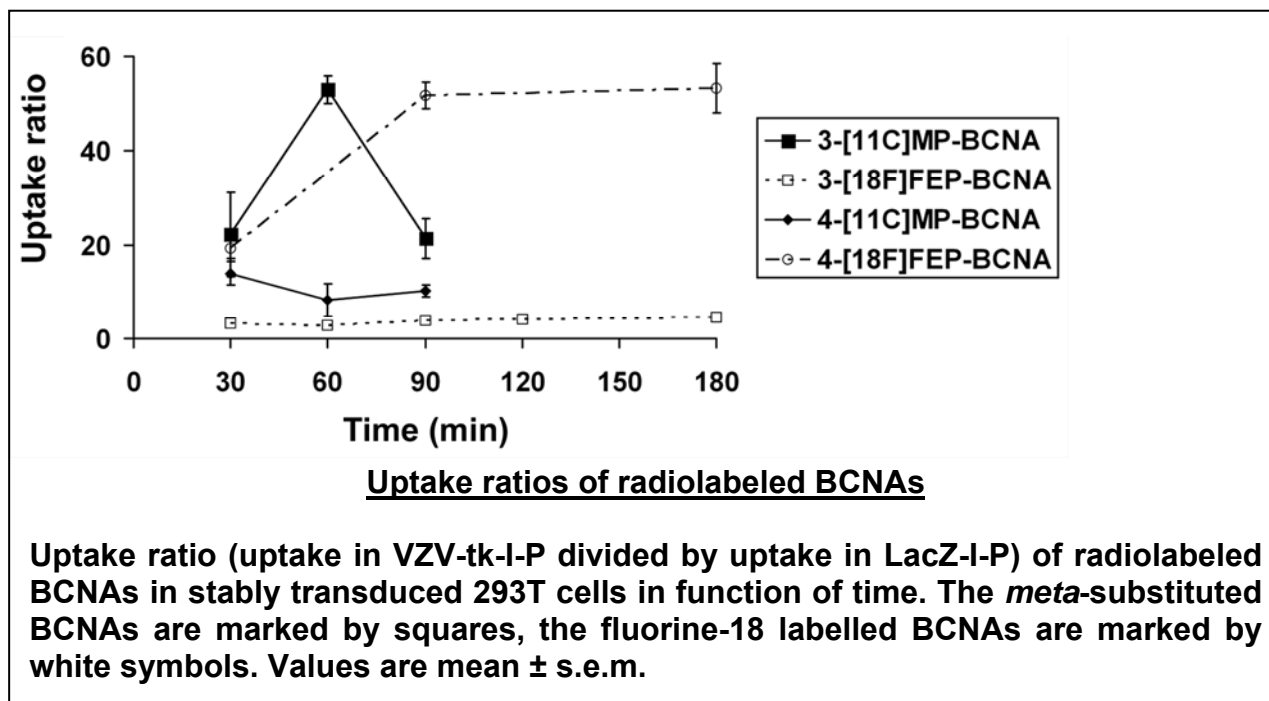


3.2. High Pressure Liquid Chromatography Shows Presence of Polar Metabolites in VZV-tk Expressing Cells

RP-HPLC of the lysate of VZV-tk expressing cells incubated with 3- ^{11}C -MP-BCNA shows the presence of 2 different polar metabolites in the cell lysate of VZV-tk expressing cells (Figure 22). These metabolites made up 80% of the resolved tracer in the VZV-tk

expressing cells but only 5.0% in the control cells. In the medium of VZV-tk and LacZ expressing cells the tracer was mainly present under its native form as the total amount of these metabolites was only 6.9% and 0.22% respectively.

Figure 21

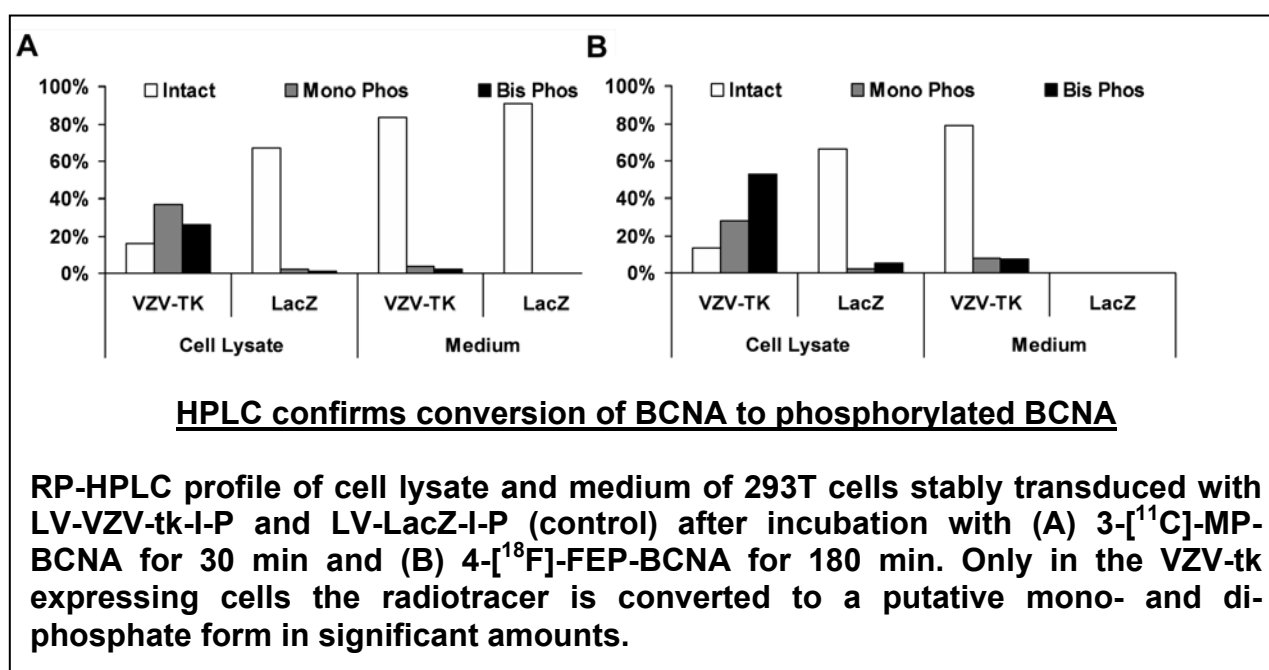


For cells incubated with 4-[¹⁸F]-FEP-BCNA similar results were obtained. The polar metabolites in the cell lysate amounted to 85% percent of the recovered tracer in the VZV-tk expressing cells but only 7% in the control cells. In the medium, the metabolites amounted to 16% in the VZV-tk expressing cells. This demonstrates that the radiolabeled BCNAs are specifically phosphorylated in VZV-tk expressing cells.

3.5. Thymidine Blocks Uptake of Radiolabeled BCNAs in Stably Transduced 293T Cells

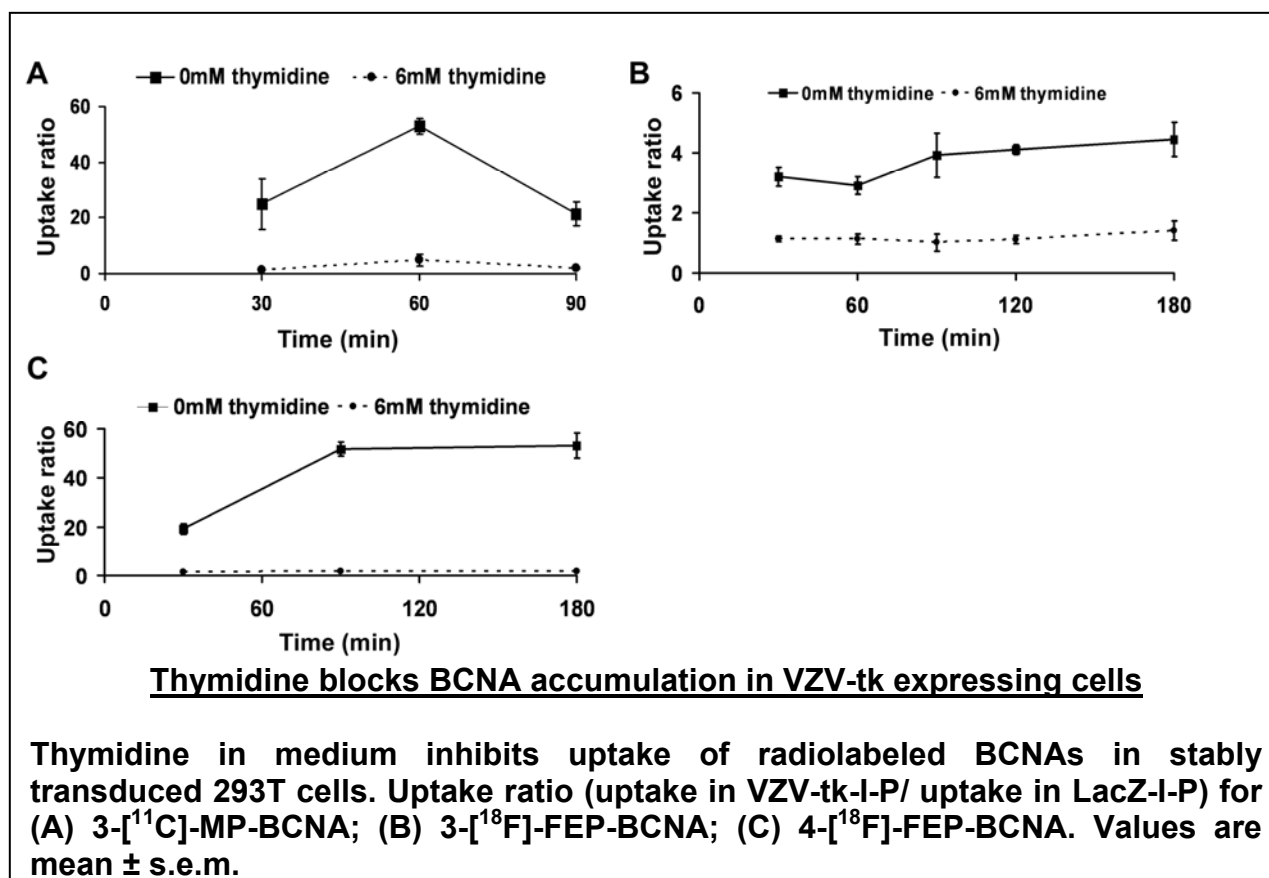
To show that the uptake mechanism of the radiolabeled BCNAs was dependent on the activity of VZV-TK, we performed uptake experiments with and without thymidine (6mM) in the medium during the uptake phase. For the tracers tested, 3-[¹¹C]-MP-BCNA (Figure 23A), 3-[¹⁸F]-FEP-BCNA (Figure 23B) and 4-[¹⁸F]-FEP-BCNA (Figure 23C), a significant reduction of the uptake ratio after addition of thymidine was observed at all time points ($p < 0.005$). The uptake ratio for 3-[¹¹C]-MP-BCNA and 4-[¹⁸F]-FEP-BCNA was reduced by 11 ± 0.9 and 14 ± 4.2 , respectively.

Figure 22



For 3-[¹⁸F]-FEP-BCNA the uptake in VZV-tk expressing cells in the presence of thymidine was not significantly different from the LacZ expressing control cells (p=0.09). Addition of thymidine to the medium thus drastically reduced BCNA uptake.

Figure 23



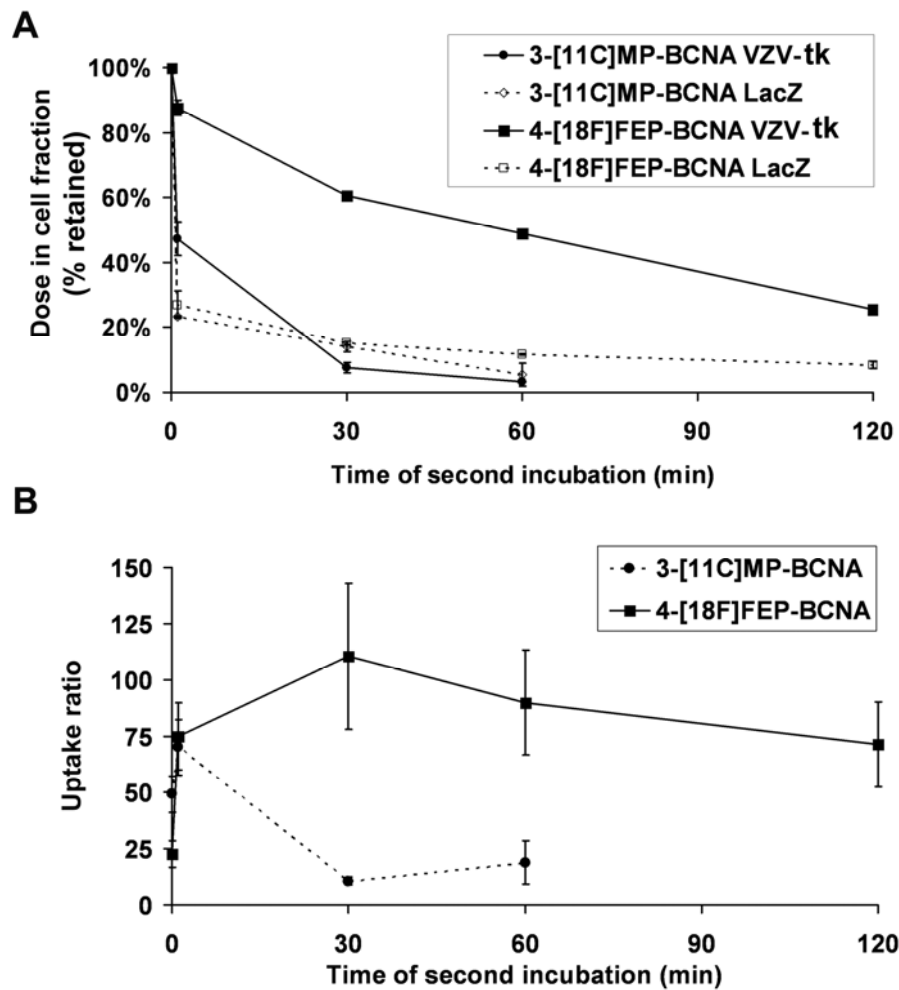
3.6. Variable Intracellular Retention of Radiolabeled BCNAs

We performed wash-out studies to verify that the tracer is retained intracellularly after metabolism by VZV-TK. For 3-[¹¹C]-MP-BCNA 1 min of reincubation already resulted in a significant loss of more than 50% of the accumulated tracer ($p < 0.0001$) (Figure 24A) and this efflux continued up to 60 min where only 3.3% of the initial tracer remained. For 4-[¹⁸F]-FEP-BCNA the situation was different with a low initial loss of 12% during the first minute and with still 49% of the initial tracer present at 60 min. This was 15 times higher than what was seen for 3-[¹¹C]-MP-BCNA ($p < 0.0001$). The resulting uptake ratios are shown in Figure 24B. Although the values at 1 min were similar for both tracers at ~70, there was a significant decline in uptake ratio for 3-[¹¹C]-MP-BCNA at the 30 and 60 min time point ($p < 0.0001$ for both). For 4-[¹⁸F]-FEP-BCNA the uptake ratio did not decrease during the entire 120 min period studied and remained at 71 ± 19 or higher. At the 30 and 60 min time points the uptake ratio for 4-[¹⁸F]-FEP-BCNA was at least 5-fold higher than for 3-[¹¹C]-MP-BCNA ($p < 0.001$ for both). The retention profile of 4-[¹⁸F]-FEP-BCNA is clearly more favourable than the profile of 3-[¹¹C]-MP-BCNA.

3.7. The Accumulation of Radiolabeled BCNA Reflects the LV Titer

To show that radiolabeled BCNA uptake reflects gene expression, we performed uptake studies with 293T cells transduced with serially diluted LV-VZV-tk. For 3-[¹⁸F]-FEP-BCNA there was a gradual decrease in uptake after 120 min with decreasing amounts of LV (Figure 25A). Uptake was significantly higher up to a 9-fold dilution ($p < 0.005$). A similar decrease of uptake with LV titer was seen for 3-[¹¹C]-MP-BCNA at 30 min, but because of the previously described higher uptake of this tracer, accumulation in cells exposed to up to 16-fold diluted LV was still significantly higher ($p < 0.05$) than in control cells (Figure 25B). Finally, in accordance with the higher accumulation and retention of 4-[¹⁸F]-FEP-BCNA observed previously, this tracer showed accumulation significantly higher than in control cells at dilutions up to 256 ($p < 0.05$) (Figure 25C). So radiolabeled BCNA uptake reflects VZV-tk gene expression levels with a dynamic range depending on the affinity and the retention of the specific tracer used.

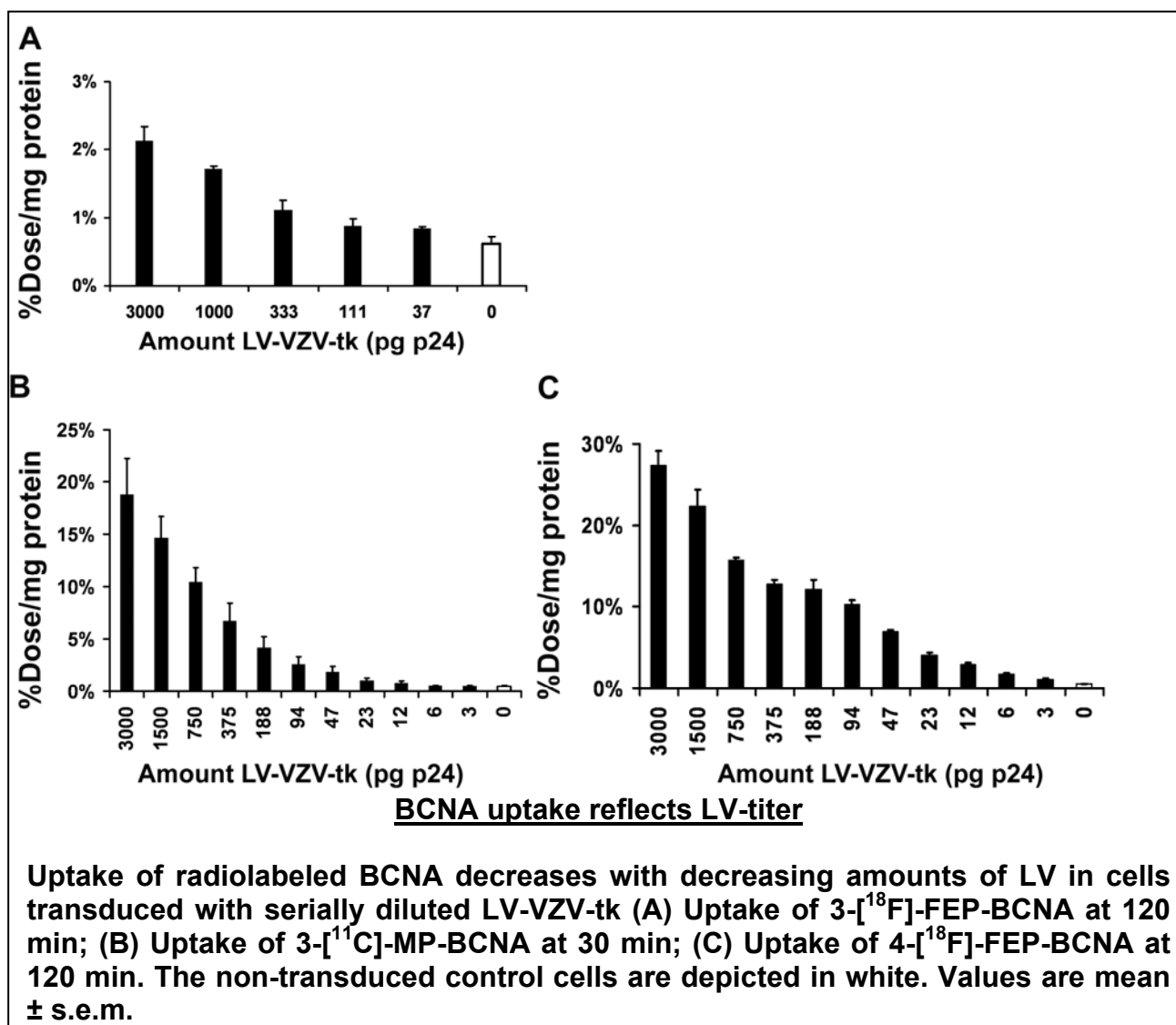
Figure 24



Retention of radiolabeled BCNAs in 293T cells

Retention of radiolabeled BCNAs in 293T cells stably transduced with LV-VZV-tk-I-P and LV-LacZ-I-P (control). After 30 min incubation with radiolabeled BCNA, medium was removed and cells were washed 3 times with PBS. Cells were incubated with cold medium for various time points. (A) Activity in cell fraction as percentage of retained dose (activity in cell fraction + activity in cold medium); (B) Corresponding uptake ratios. Values are mean \pm s.e.m.

Figure 25

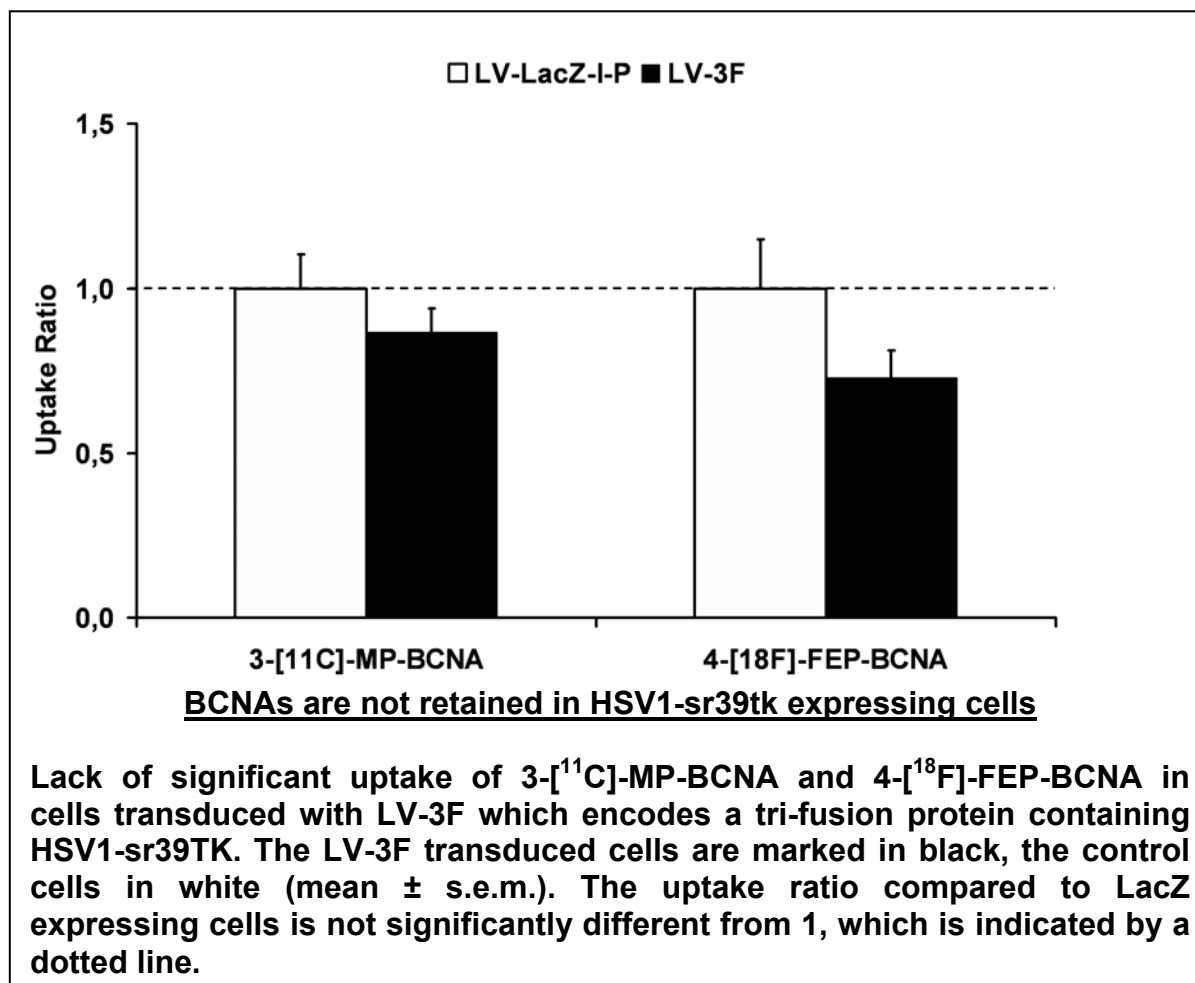


3.8. Radiolabeled BCNAs Do Not Accumulate in Cells Expressing an HSV1-sr39TK-Containing Fusion Protein

To determine if the radiolabeled BCNA would accumulate in cells expressing HSV1-TK, we transduced cells with a previously validated [267] LV (LV-3F) encoding a triple fusion protein containing a truncated and mutated HSV1-TK moiety [154]. We tested both 3-[¹¹C]-MP-BCNA and 4-[¹⁸F]-FEP-BCNA. For both tracers the uptake was not significantly higher in the LV-3F transduced cells than in control 293T cells stably expressing LacZ (Figure 26). The uptake ratios in the LV-3F transduced cells were 0.87 ± 0.07 for 3-[¹¹C]-MP-BCNA and 0.73 ± 0.08 for 4-[¹⁸F]-FEP-BCNA respectively. This demonstrates that

radiolabeled BCNAs are not retained in HSV1-tk expressing cells, in accordance with our previous results.

Figure 26

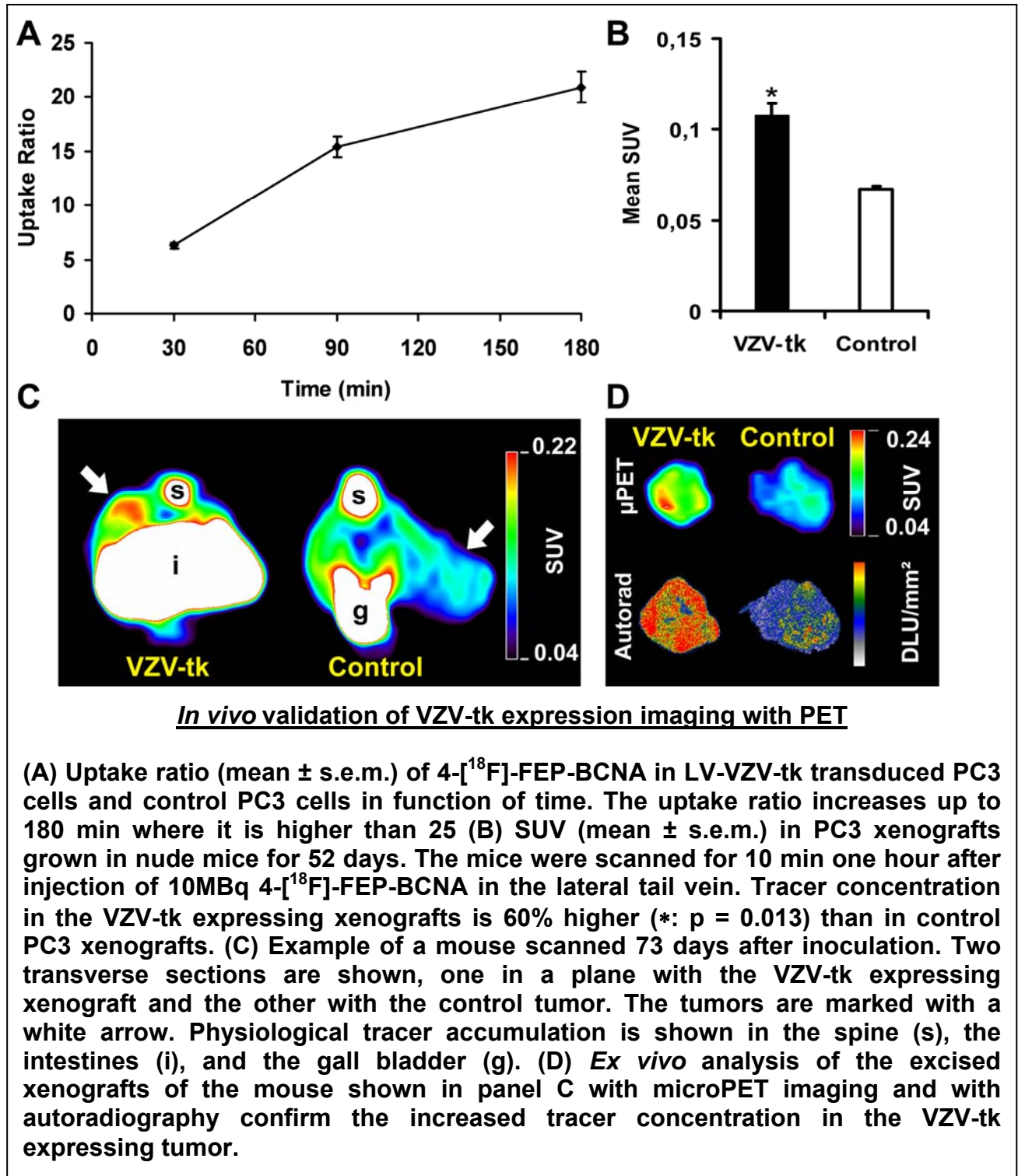


3.9. MicroPET Imaging of Accumulation of 4-[¹⁸F]-FEP-BCNA in VZV-tk Expressing Prostate Cancer Xenografts

Unfortunately, biodistribution analysis of radiolabelled BCNAs in mice showed no brain uptake at minutes 2 and 60 (data not shown). We therefore did not perform the initially planned experiments where mice injected with LV encoding VZV-tk would be imaged with PET studies. However, we still wanted to demonstrate that we could image VZV-tk expression outside of the brain. To demonstrate the feasibility of imaging VZV-tk expression *in vivo* we transduced PC3 cells, a well studied prostate cancer cell line, with LV-VZV-tk-I-P and LV-LacZ-I-P. Only 4-[¹⁸F]-FEP-BCNA was evaluated because of its favourable uptake and retention profile and relatively long half-life. After antibiotic selection

the cells were shown to accumulate 4-[¹⁸F]-FEP-BCNA with uptake ratios increasing over time up to 25 at 180 min incubation time (Figure 27A).

Figure 27



Two xenografts were inoculated in nude mice, each mouse bearing a VZV-tk expressing tumor and a control tumor (n=4). When tumor size was higher than 250mm³ the mice were scanned after injection of 4-[¹⁸F]-FEP-BCNA. The mice had 3 VZV-tk expressing tumors and 4 control tumors at the time of the scan as one VZV-tk tumor failed to establish. The average SUV_{mean} was 60% higher in the VZV-tk expressing xenografts than in the control tumors (p: 0.013) (Figure 27B). Only one mouse was available for *ex vivo* confirmation experiments. The mouse was scanned in the microPET (ratio VZV-tk/control: 1.68) (Figure 27C) and immediately afterwards the tumors were excised and scanned in the microPET. This also showed increased tracer concentration in the VZV-tk expressing tumor (ratio: 1.79) (Figure 27D). These findings were confirmed with *ex vivo* autoradiography (Figure 27D) of tumor sections (ratio: 1.80) and with scintillation counting of the tumor (ratio 2.04). Thus, *in vivo* expression of VZV-tk can be detected by PET in mice.

DISCUSSION

In this study we have tried to validate a new PET reporter gene for imaging in the brain, namely VZV-tk. We evaluated 4 different PET reporter probes for this reporter gene. The uptake kinetics of the 4 PRPs studied showed 3 notable trends. First, uptake in control cells was low. Second, there was a significant difference in maximum tracer uptake between 3-[¹⁸F]-FEP-BCNA and the other PRPs of roughly an order of magnitude. This is consistent with the fact that this PRP has an affinity of ~50μM for the VZV-TK enzyme, whereas the other PRPs affinity is ~5μM. Third, for the other PRPs, there is a significant decrease in tracer accumulation at time points later than 30 min except for 4-[¹⁸F]-FEP-BCNA. The latter is the only tracer showing high uptake ratios (>50) that increase or remain stable over time, consistent with metabolic trapping of the tracer. Based on these properties, the latter PRP seems the best agent.

To demonstrate that the accumulation of PRP in the VZV-tk expressing cells is mediated by VZV-TK, we performed competitive inhibition experiments where cells were incubated with the respective tracers and high concentrations of thymidine. These experiments showed an uptake ratio ~1 for 3-[¹¹C]-MP-BCNA and 3/4-[¹⁸F]-FEP-BCNA at all time points studied. This shows that uptake can be blocked by excess thymidine that acts as a competitive inhibitor for the VZV-TK enzyme. This experiment might be confounded by the fact that thymidine is also competing with the BCNAs for membrane nucleoside transporters that are responsible for cell entry of nucleosides and their analogs. Indeed, it is possible that the BCNAs enter the cell through either the concentrative or

equilibrate nucleoside transporter (CNT and ENT respectively), in which case the low accumulation caused by thymidine seen in our experiments might be due to blocking of cell entry rather than VZV-TK mediated phosphorylation. However, due to the pronounced lipophilicity of the radiolabeled BCNAs (log P range 1.2 – 1.3) [181], it is likely that at least part of the PRP fraction that enters the cell does so through passive diffusion. This fraction would then have been available for metabolism by VZV-TK if this enzyme wouldn't have been inhibited by the excess thymidine.

The next step we performed to demonstrate the metabolic trapping of the PRPs by VZV-TK were wash-out studies where, after initial incubation with PRP, the cells were incubated with cold medium to demonstrate the persistence of the PRP accumulation. To our surprise, the initial studies with 3-^[11C]-MP-BCNA showed a very rapid wash-out for the VZV-tk expressing cells, with a half life of less than 1 min and wash-out kinetics similar to untransduced cells. This resulted in low absolute and relative uptake at the late time points. The RP-HPLC data clearly show conversion to 2 different polar metabolites that are also detected in the medium, so it is likely that these polar metabolites are not trapped inside the cell. One possibility is that these metabolites are actively transported out of the cells by members of the ATP-binding cassette transporters, such as the multidrug resistance-associated proteins (MRPs) 4, 5 and 8, that are able to transport nucleoside mono-phosphate analogues (for review, see [268]), or by the human renal organic anion transporter 1 (hOAT1). Preliminary experiments have shown that co-incubation of 3-^[11C]-MP-BCNA with 100µM indomethacine (a substrate for MRP 4 and hOAT1) and 80µM cyclosporine (a substrate for MDR1) result in an increase in absolute tracer retention of respectively 4.6 ± 0.9 and 2.5 ± 0.5 (data not shown), confirming that active transport plays a role in the observed efflux. Further characterization of this effect is warranted but falls outside the scope of this thesis. The behaviour of intracellular 4-^[18F]-FEP-BCNA was strikingly different, with a half-life that is ~60 times longer and absolute retention that is more than an order of magnitude higher at the one hour time point. This resulted in uptake ratios of more than 70 at all time points studied for this tracer, warranting the further *in vivo* exploration of this PRP. Because of the unfavourable uptake kinetics (3-^[18F]-FEP-BCNA) and radionuclide half-life (4-^[11C]-MP-BCNA), we did not perform these wash-out studies with the other radiolabeled BCNAs.

The RP-HPLC data shows detection of high amounts of 2 metabolites of the radiolabeled BCNAs in the VZV-tk expressing cells that are almost not detected in control cells. This is consistent with the formation of monophosphorylated and diphosphorylated BCNAs. We did not formally identify the mono- and diphosphate compounds by an internal

HPLC standard. However, in previous work we have shown that 2 different prototypical BCNAs, after 10 and 40 min of incubation with recombinant VZV-TK, showed metabolites which on HPLC co-eluted with chemically synthesized and fully characterized 5'-monophosphate BCNA [184]. We also confirmed phosphorylation by liquid chromatography mass spectroscopy (LC-MS) analysis. With this technique the formation of monophosphate was detected after incubation of nonradioactive 4-FEP-BCNA with purified VZV-TK enzyme (Chitneni *et al.*, personal communication).

A small fraction of the BCNAs in the medium of the VZV-tk cells, but not of the LacZ cells, is under metabolised form. This is consistent with the rapid efflux kinetics observed in the wash-out experiments. We like to point out that the fraction of phosphorylated compounds in the medium is relatively similar for both 3-[¹¹C]-MP-BCNA and 4-[¹⁸F]-FEP-BCNA, despite an incubation period that is 6 times longer (30 vs. 180 min) for the latter, reflecting the improved retention of this PRP.

We then showed that the uptake of the PRP is a measure for the amount of PRG expression with uptake studies of cells transduced with different titers of LV-VZV-tk. Both the low affinity PRP 3-[¹⁸F]-FEP-BCNA and the high affinity PRPs 3-[¹¹C]-MP-BCNA and 4-[¹⁸F]-FEP-BCNA showed clear decrease in PRP uptake with decreasing amounts of LV. As expected, the high affinity tracer showed increased uptake in cells transduced with amounts of LV that didn't result in increased uptake of the low affinity PRP. The range of titers resulting in significant PRP accumulation is acceptable for 4-[¹⁸F]-FEP-BCNA as this range spans more than 2 orders of magnitude.

We also studied accumulation of the PRP in cells expressing a truncated HSV1-sr39TK containing fusion protein. The LV-3F construct was previously tested and mediated uptake of [¹⁸F]-FHBG, a substrate for HSV1-sr39TK, in 293T cells and in mice [269]. We used the mutant enzyme because it has been shown to have a higher affinity for [¹⁸F]-FHBG than the wild type enzyme. As can be expected from our previous studies [270], there is no significant uptake of radiolabeled BCNAs in these cells, because the BCNAs in general and the studied radiolabeled molecules in particular are not substrates for the thymidine and thymidilate kinase activities of HSV1-TK. We have shown that this is due to a steric clash between the substituant on position 6 of the base and amino acids 167 and 168 of HSV1-TK [271]. It was therefore expected that the sr39 mutant will also not metabolise the BCNAs as this mutant has conserved the alanine at position 167 and replaced the alanine at position 168 by the bulkier phenylalanine [272]. This shows that the PRPs for VZV-TK will not be metabolised and trapped by HSV1-TK, allowing the

development of the VZV-tk/BCNA system as an alternative system that can be used in conjunction with the widespread HSV1-tk system.

When we moved on to *in vivo* studies, we observed that none of the 4 radiolabeled BCNAs that we evaluated showed any significant BBB penetration. Further studies (Chitneni *et al*, personal communication) have shown that this is likely a class effect of the BCNAs and therefore it is unlikely that chemical modifications will result in robust brain uptake. The initially planned experiments where mice would be imaged after injection of LV encoding VZV-tk were not performed because of the absence of BBB penetration. To demonstrate that VZV-tk expression outside of the brain could be detected with this system, we used mouse xenografts for *in vivo* evaluation.

Based on the characteristics shown in the different experiments, 4-^[18F]-FEP-BCNA is clearly the PRP of choice because of (i) the favourable radionuclide half-life; (ii) the most rapid and highest uptake in VZV-tk expressing cells; (iii) a ~10 fold higher retention than the other radiolabeled BCNA studied. We thus only used this tracer for our *in vivo* experiments. Our initial *in vivo* evaluation shows an increase of at least 50% in 3 VZV-tk expressing tumors when compared to 4 control tumors. Three mice had to be sacrificed before the second scan because of cachexia. These results were confirmed in the surviving mouse by *ex vivo* imaging of the tumors, autoradiography and scintillation counting. All modalities showed ratios between 1.6 and 2.1, confirming the increased uptake in the VZV-tk expressing tumors. These *in vivo* ratios are more than one log order lower than those obtained with other PRG/PRP combinations such as. HSV1-tk, hNIS, and hNET. With the current results it is not advisable to use this system when probing gene expression *in vivo* in animal models nor is translation to human studies warranted. This system needs a gain in uptake ratio of around one order of magnitude. One strategy that might improve the uptake ratio is a characterisation of the efflux mechanism of the metabolised BCNAs that might lead to a pharmacological blocking of the efflux mediator that would increase uptake. It is not very likely that this will result in such a big gain in uptake ratio. Furthermore, adding a pharmacological intervention to the scanning procedure might result in side effects and the pharmacokinetics/dynamics of these compounds might result in confounding factors that might impede the interpretation of the images.

CONCLUSION

We have characterized the uptake kinetics, metabolism by VZV-TK and its inhibition by thymidine, intracellular retention, relationship with LV-VZV-tk titer, and finally accumulation in LV-3F transduced cells of radiolabeled BCNAs. These experiments point to 4-[¹⁸F]-FEP-BCNA as the most interesting PRP. Because this PRP does not cross the BBB, it was not evaluated in mouse models expressing VZV-tk in the brain. We showed that this tracer can be used to detect VZV-tk expression *in vivo* in xenografts. We propose VZV-tk as a new PET reporter gene in conjunction with 4-[¹⁸F]-FEP-BCNA as PET reporter probe that is not recognised by the prototypical reporter gene HSV1-tk. In its current form, this system needs further optimization before it can be used to address biological questions or before considering clinical translation.

Chapter 5: General Discussion & Perspectives

Molecular imaging has emerged as a powerful tool in fundamental, pre-clinical and clinical research. Molecular imaging may revolutionize fields that currently rely on tissue samples obtained after death of the subject or on biopsies from living animals. Although modern biomedical research has been able to generate a detailed mechanistic insight relying on these samples, non-invasive strategies complement these studies and allow the detection of gene expression in a single subject over time. In the present thesis, we sought to validate a new reporter gene for PET and applied existing reporter genes to two different biological fields.

The first field where we applied reporter gene imaging was lentiviral vector-mediated transgene expression in the mouse and rat brain. We developed LV encoding BLI reporter genes that allowed us to detect gene expression in mice and rats after intracerebral injection without having to sacrifice these mice. Expression could be detected from day 3 on after injection. The detected signal was ~2 orders of magnitude higher than in control mice and ~1 order of magnitude higher than in control rats. We optimized the technical parameters of the method and demonstrated good reproducibility. We showed that the *in vivo* signal correlated with *ex vivo* reference measures of gene expression. Despite the rather limited intrinsic resolution of BLI, we were able to show that expression in different areas of the mouse brain can be discriminated with the BLI images. Using BLI we were the first to show long-term persistence of LV-mediated gene expression in the adult brain within the same animal. Indeed, many groups including our own laboratory previously showed that LV-mediated expression into the mammalian brain results in stable gene expression [132, 142, 176], but this conclusion was based on groups of animals that were sacrificed at different time points. This precluded the study of the evolution of gene expression within a single animal. After our report was published, others have also reported non-invasive detection of transgene expression in the brain [47]. The latter authors used PET to detect AAV-mediated expression of hAADC in monkeys over a 6 year period. Finally, we were able to show that the BLI signal is a useful proxy biomarker for expression of a gene of interest.

There are three major reasons why the approach of locoregional gene transfer into the brain warrants further attention. First, by allowing the temporally controlled expression of specific transgenes in the rodent brain, we have a tool to study the function of particular genes and gene mutants within an intact animal. We can determine the relevance of the gene to normal physiology and the role in the pathogenesis of disease. This functional genomics method has been used in our laboratory to study the development of neurodegeneration after overexpression of α -synuclein [133] or to study the protective role of parkin [273]. The gene encoding α -synuclein was the first gene that was identified as a cause of autosomal dominant hereditary PD, a rare form of PD. Either gene mutations [274] or locus triplication [275] have been identified as the causative genetic feature. The gene encoding parkin is mutated in most patients with autosomal recessive juvenile PD [276] and it is thought that disease is caused by the loss of the protective function of the parkin protein. Both studies, although still based on the *post-mortem* histological assessment of rodent brain, resulted in important novel insights. In ongoing and future work, we plan to follow the temporal kinetics of LV-mediated α -synuclein overexpression in the mouse brain non-invasively using BLI. For this purpose, vectors encoding α -synuclein linked to Fluc have already been designed and optimised. The work in this thesis serves as a validation for this approach. In another application our lab has used BLI to optimize bicistronic lentiviral vectors using various genetic elements to direct co-expression of each cistron. Finally, we have used BLI to engineer conditional LV that transduce all brain cells but will not be expressed until a specific molecular switch activates the proviral DNA. These studies have been greatly expedited by the potential of BLI to assess gene expression rapidly in living mice.

A second reason why gene expression in rodents is of considerable interest lies in its translational potential for human gene therapy. This field is again yielding promising results after a troubled period where lack of clinical efficacy was a major problem and safety problems were raised. A number of recent landmark papers have demonstrated clinical efficacy of gene therapy. Children suffering from interleukin receptor- γ deficiency induced severe combined immunodeficiency (SCID-X1) have been cured after infusion of hematopoietic stem cells transduced with retroviral vectors encoding this receptor [277]. A number of these children suffered from a major side effect, T-cell leukemia (4 out of 20), which led to death in 1 of them [131]. The combination of overexpression of the interleukin receptor- γ together with insertional mutagenesis by the retrovirus resulted in overexpression of the LMO2 gene and caused this lymphoproliferative disease. An oncogenic contribution of the transgene might have contributed to lymphogenesis [278] but

this has been refuted by other authors. Despite this setback, this study still marks a significant progress as it was the first to demonstrate that real clinical benefit can be obtained with gene therapy. All cases of leukemia occurred within one trial, whereas no leukemia occurred in the 10 patients treated in a different trial, suggesting that some specific aspect of the protocol is contributing to leukemogenesis. Adenosine deaminase SCID was also corrected using retroviral vectors leading to partial or full correction in 9 patients. A similar approach was used in X-linked chronic granulomatous disease where the oxidative antimicrobial activity of phagocytes is impaired due to a mutation in the $gp91^{\text{phox}}$ gene [279]. Overexpression of a functional allele of this gene in autologous hematopoietic stem cells resulted in repopulation of the blood with functional myeloid cells. Similarly to the SCID-X1 trial, LTR-driven transactivation of endogenous genes was observed and this resulted in an oligoclonal expansion of functional myeloid cells. In contrast to the SCID-X1 study, the myeloid cell numbers did not rise above physiological levels. One patient died of infection more than 440 days after infusion of the modified cells but this was most likely due to a complication of the initial disease [280].

Gene therapy with genetically modified cells has recently been shown to deliver clinical benefit outside the realm of blood diseases. A patient with junctional epidermolysis bullosa, a severe and potentially lethal blistering skin disease caused by deficient function of the laminin 5 protein, was treated with skin grafts engineered from genetically modified autologous epidermal stem cells [281]. A retroviral vector encoding the cDNA of laminin 5 $\beta 3$ was used to transduce these epidermal stem cells. Nine grafts were transplanted onto surgically prepared regions of the patient's legs. A firmly adherent epidermis that remained stable for more than 1 year developed, without blisters, infections, inflammation or immune response. The latest major gene therapy achievement occurred in the field of PD. Kaplit *et al.* used AAV encoding the human glutamic acid decarboxylase and injected these AAV unilaterally in the subthalamic nucleus of PD patients [282]. By increasing the synaptic concentration of the inhibitory neurotransmitter gamma-aminobutyric acid (GABA), this enzyme strongly improved the motor function in the limbs contralateral to the site of injection during the year of follow-up. This is the first trial of *in situ* gene therapy showing a significant benefit throughout the entire patient group.

Although no imaging of gene expression was performed in any of the successful clinical trials, one can expect that future gene therapy trials will incorporate imaging of gene expression. Proof-of-principle studies were done with liposome-mediated gene transfer in patients suffering from relapsed glioblastoma multiforme, a brain tumor that has a very unfavourable prognosis after relapse [42]. Convection enhanced delivery of

liposomal vector encoding HSV1-tk was used in five patients. A dynamic [^{124}I]-FIAU PET was performed before gene therapy during 72 hours to determine the basal state of tracer accumulation and washout, and a similar scan was performed after gene delivery to detect areas of specific tracer retention. In one patient, there was a significant doubling of the accumulation rate of [^{124}I]-FIAU after gene delivery at the infusion site located within the center of the tumour. After ganciclovir treatment from day 4 to 18 post-transduction, necrosis could be documented by [^{18}F]-FDG PET and [^{11}C]-methionine PET in the volume where specific [^{124}I]-FIAU accumulation had been demonstrated prior to ganciclovir treatment. This study was the first to show non-invasive detection of transgene expression in patients and to demonstrate that the response to suicide gene therapy can be predicted by molecular imaging of gene expression. Similar results were obtained with HSV1-tk encoding adenoviral vectors that were locally injected in liver metastases from colorectal carcinoma imaged with [^{18}F]-FHBG PET [26]. In patients with specific accumulation of the tracer, stable disease was observed after ganciclovir treatment whereas in those patients without specific tracer accumulation on the PET images, disease progressed after ganciclovir treatment. In our own preclinical gene therapy research we have incorporated non-invasive reporter gene imaging with BLI and PET to detect long-term gene expression in a rodent model of fetal gene transfer to the lungs [267]. These imaging approaches will be incorporated in future pre-clinical gene therapy research efforts.

The third major reason why lentiviral vector-mediated gene transfer to the rodent brain is of interest, is the potential to transduce the adult neuronal stem cell, allowing stable genetic modification of these cells. This is a powerful tool for the study of the molecular processes regulating this stem cell niche and it might yield insights into the role of these cells in human disease. The turnover of neurons in the OB is believed to play a role in olfactory memory formation [206]. In human brain the analogous migration of neuroblasts to the olfactory bulb via a lateral ventricular extension was only recently demonstrated [193], albeit without clear functional role. It is well known that impaired odor discrimination is an early sign of PD and that the proliferation of progenitor cells in the SVZ and neuroblast migration is reduced in PD animal models and in PD patients [207, 208]. Altogether, the data suggest that endogenous neuronal stem cell proliferation and migration towards the OB play a physiological role in humans. It also follows that the rodent brain provides a relevant model to study migration, proliferation and differentiation of the neuronal stem cell population. Non-invasive imaging of stem cell migration in rodent brain would facilitate this research effort considerably. To the best of our knowledge, we are first to report whole body imaging of the migration of endogenous neural stem cells.

Pineda *et al.* have demonstrated the ability of BLI to track the migration of exogenous stem cells from the RMS to the OB [223]. These cells however were maintained in cell culture, were not exposed to the original stem cell niche and thus constitute a distinct cell population. Furthermore, these cells were derived from the external germinal layer of mouse cerebellum and immortalized with the v-myc gene [283], which will likely cause differences in gene expression patterns in comparison with true endogenous stem cells. Recently Shapiro *et al.* [284] reported on *in vivo* tracking of endogenous stem cells with MRI in rats. Although this technique has the advantage of a tomographical data set and detailed anatomical information, there were important limitations in this study. The animals were only followed for 5 weeks, no discrimination between live and dead cells was made, the labelling iron oxide particles could have been taken up by microglial cells after neuroblast cell death and the signal strength in the RMS and BO was quite variable between animals, probably reflecting the intrinsic variability of this method. There was no quantification of cells in the OB or RMS, neither for the *in vivo* nor for the *ex vivo* data, so this method is only qualitative.

The BLI technique developed in the scope of this thesis is currently used in our laboratory to investigate the influence of growth factors on the proliferation and migration of this stem cell population and will be used to study the behaviour of the endogenous neural stem cells in different brain disease models.

The second biomedical research field where we applied reporter gene imaging is oncology. Our work focused on detection and localisation of metastatic melanoma lesions, although it can be generalised to any solid tumor type. We first validated our combined PET-CT approach and we showed that we could detect tumor growth in tumor metastases. We then showed that we could detect pulmonary melanoma metastases with PET-CT. We applied this system to reporter gene expressing melanoma cells and were able to document growth of metastases as well as to accurately localise these lesions within the mouse. Finally, we showed that this reporter gene based approach resulted in much higher contrast than the gold standard PET tracer [¹⁸F]-FDG. Growing tumors as xenografts in syngeneic or immunocompromised rodents and measuring them with callipers has been a standard technique in oncological research for decades. These tumor xenograft models however suffer from altered vascularization, have no relevant tumor-stroma interactions and often rely on immunodeficient mice [179]. It is now recognised that these imperfections influence the result of pre-clinical studies since the behaviour of neoplastic cells is modulated to a large extent by the interaction with the surrounding

normal tissue [285, 286]. Furthermore, treatment response and toxicity of metastatic disease can vary from site to site and can be dependent on interactions with the immune system. Orthotopic and metastatic models are more appropriate to mimic human disease as they replicate some stroma-tumor interactions and some specificities of particular organs. In the brain, for example, the BBB, the immunoprivileged state and the lack of lymphatic system all influence tumor growth and treatment [287]. Traditionally, tumor growth and therapy induced changes could only be monitored through clinical signs and survival of the animal, by anatomical imaging (MRI) or by necropsy. The latter requires large series of animals to be sacrificed at different time points to overcome the intrinsic biological variability. Imaging strategies that measure the extent of the total tumor burden within an animal non-invasively meet a need of oncology researchers. Most studies have used BLI because of the high sensitivity and low cost associated with this technique. These techniques have been used to study xenografts, orthotopic mouse models as well as metastatic models. Another interesting approach at refining tumor models consists of using genetically engineered mouse models where deletion of tumor suppressor genes or overexpression of oncogenes can be achieved with spatiotemporal control, switching the gene on or off in a specific tissue at a particular time. These models replicate human cancer at the molecular and often at the histological level, but the time of tumour onset and growth rate can be variable making comparisons of therapeutic interventions difficult. Reporter gene imaging is ideally suited for these models as they are genetically engineered by definition and non-invasive determination of tumour burden allows randomization of different homogenous groups. This concept has been demonstrated in conditional knockout mice for the retinoblastoma gene (RB) [93]. The retinoblastoma gene is an important tumour suppressor gene controlling the passage of the cell cycle from the G₁ into the S phase. Inactivation of both alleles is lethal at the embryonic stage but inactivation limited to the pituitary results in pituitary tumours. Vooijs *et al.* developed a mouse in which expression of the DNA modifying enzyme Cre recombinase and of Fluc is regulated by the pro-opiomelanocortin (POMC) promoter which is exclusively active in the intermediate lobe of the pituitary gland. These mice were crossed with another transgenic strain where both the RB alleles are flanked by loxP sites that are recognised and excised by the Cre enzyme leading to loss of the RB gene. In the resulting mice, only pituitary cells express Fluc and Cre which leads to a RB^{-/-} genotype and tumorigenesis in the pituitary with Fluc expressing tumor cells that can be quantified with BLI. The effect of doxorubicin on tumour mass could be monitored on an individual basis and was predictive of a significant survival benefit. This mouse model represents the first model in which

spontaneous tumors can be non-invasively quantified and it is expected that reporter gene imaging will be applied to many other genetic tumor models. Other mice have been engineered with the Fluc gene driven by an ubiquitous promoter after Cre-mediated recombination, allowing cross-breeding with any Cre conditional mouse strain [288, 289]. It is expected that these techniques will be more and more adopted by the research community while continuous refinements are made to better study cancer in living mice. We currently have collaborations with three different labs at the KU Leuven where the technology developed in this thesis has been used to develop cancer cell lines that can be detected within living mice in xenografts, in orthotopic brain models and in a model of peritoneal carcinomatosis. Application of these techniques will be accelerated with the advent of the new Molecular Small Animal Imaging Center (MoSAIC) that will be functional in the first trimester of the academic year 2007/2008.

The last goal of this work was the development of a new PET reporter gene. The rationale for this work was the lack of a PET reporter gene system that can image gene expression behind an intact BBB with a good signal to noise ratio. We hypothesized that radiolabeled BCNAs might be used to image VZV-tk expression in the brain. We studied four different radiolabeled BCNAs in cell culture experiments. Three of these showed high retention in VZV-tk expressing cells. For one of these tracers retention increased over time. Conversion of the BCNAs to a metabolically trapped phosphorylated form was demonstrated by HPLC. Retention of radiolabeled BCNAs was acceptable for the tracer that showed the highest uptake; its retention half life was ~1 hour. We showed that the uptake of radiolabeled BCNA correlated with the titer of LV used to transduce cells and did not occur in HSV1-tk expressing cells. Finally, we detected *in vivo* VZV-tk expression in tumor xenografts in living mice by PET. These findings were corroborated by *ex vivo* PET measurements, autoradiography and scintillation counting.

We could unfortunately not use the radiolabeled BCNAs to study LV-mediated transgene expression in the brain because none of the four compounds efficiently crossed the BBB as shown by biodistribution studies [181]. This is certainly a limitation of this study. Developing a suitable PET reporter gene for the brain has remained challenging. The HSV1-tk system was developed more than 10 years ago and despite more than 15 tracers reported for this system, no single one crosses the BBB. Despite the fact that our primary objective was not reached, there are some considerable merits in this study. First, we validated reporter gene imaging of VZV-tk expression with 4-[¹⁸F]-FEP-BCNA PET and it is likely that this system will function in other tissues as well. This system represents a

new reporter gene in the toolbox of biomedical research and it might be used in parallel with other reporter genes to investigate multiple molecular events within the same subject. Second, the expertise acquired for the development and validation of PET imaging reporter genes has been used in other projects aimed at developing novel PET tracers for existing reporter genes (such as β -galactosidase) and at developing new PET reporter genes for brain applications. Finally, the use of LV-mediated overexpression in cell systems and xenografts has been widely recognised as a powerful tool for PET tracer development and validation and will be used in the future to optimize tracer development.

Summary

Molecular imaging has emerged as a powerful tool in fundamental, pre-clinical and clinical research. One of its most versatile applications is the imaging of gene expression. During the past decade, a number of reporter genes have been developed that allow non-invasive detection of gene expression.

In this thesis, we applied existing reporter gene technologies to study lentiviral-vector mediated gene transfer into the rodent brain. Bioluminescence imaging allows detection of *in vivo* expression of a luciferase enzyme by collecting the visible light that is produced when this enzyme oxidizes its substrate. Lentiviral vectors (LV) are viral vectors derived from the human immunodeficiency virus that can transduce dividing and non-dividing cells and that will integrate their genetic material into the host cell's genome. We used LV encoding firefly luciferase (Fluc) to transduce mouse and rat brain. We could detect Fluc expression from day 3 on after injection, with a signal more than an order of magnitude higher than background signal. The technical parameters of the method were optimized and the reproducibility of the method was demonstrated. The *in vivo* signal correlated with *ex vivo* reference measures of gene expression. We showed that expression in different brain areas can be resolved. We showed long-term persistence of LV-mediated gene expression in the adult mouse brain within the same animal. Subsequently, this method was applied to detect and follow migration of endogenous neural stem cells within the brain of living mice. We transduced these cells with LV encoding Fluc and were able to detect a specific signal from the olfactory bulb, the site where the offspring of these cells migrates to.

Secondly, we developed an integrated reporter gene imaging strategy to detect the development of metastases in mice. We used a multimodality imaging gene containing the paradigm positron emission tomography reporter gene HSV1-tk fused to RLuc and mRFP. Our PET-CT approach combining molecular and anatomical images was validated with xenograft bearing mice and then applied to detect and monitor the growth of melanoma metastases. By combining these images with BLI we obtained a highly sensitive technique allowing accurate localisation of the lesions. Finally, our reporter gene based approach resulted in much higher contrast than the gold standard PET tracer [¹⁸F]-FDG. This technique has great potential to monitor the spread of tumor cells in mice models.

Finally we validated a new PET reporter gene, VZV-tk. One newly developed tracer for this enzyme showed high accumulation in cells expressing this gene, based on metabolic trapping of this tracer by VZV-TK. The formation of trapped species was documented by HPLC. Retention of this tracer was acceptable with a half-life of ~1 hour. Tracer uptake correlated with LV-titers in cells transduced with serially diluted vector. Finally, *in vivo* detection of VZV-tk with PET was performed in xenograft bearing mice and this was validated by autoradiography and scintillation counting.

This work lays the basis for further applications and developments of reporter gene imaging. Our validated BLI method in the mouse brain is currently been used for neurobiological studies, for vector optimization and for studying of neuronal stem cells. PET reporter gene imaging and BLI are used for preclinical optimization of gene therapy strategies and for tumor cell quantification in mouse models.

Samenvatting

Moleculaire beeldvorming heeft zich ontpopt tot een buitengewoon nuttig instrument in fundamenteel, preklinisch en klinisch onderzoek. Eén bijzonder veelzijdige toepassing is beeldvorming van genexpressie. Het voorbije decennium werden er een aantal reporter genen ontwikkeld die niet-invasieve beeldvorming van genexpressie toelaten.

In deze thesis werd bestaande reporter gen-technologie toegepast om gentransfer naar de hersenen van knaagdieren door middel van lentivirale vectoren te bestuderen. Bioluminescentie beeldvorming (BLI) laat toe om *in vivo* expressie van een luciferase enzym te detecteren door het collecteren van het zichtbaar licht dat vrijkomt wanneer dit enzym zijn substraat oxideert. Lentivirale vectoren (LV) zijn virale vectoren die afgeleid zijn van het humaan immunodeficiëntie virus, die zowel delende als niet-delende cellen kunnen transduceren en die hun genetisch materiaal in het genoom van de gastcel integreren. We hebben een LV die codeert voor vuurvlieg luciferase (Fluc) gebruikt om muizen- en rattenhersenen te transduceren. We konden Fluc expressie detecteren vanaf dag 3 na injectie met een signaalintensiteit die meer dan één orde van grootte hoger is dan achtergrondsignaal. De parameters van deze techniek werden geoptimaliseerd en de reproduceerbaarheid van de methode werd aangetoond. Het *in vivo* signaal correleerde sterk met de *ex vivo* metingen van genexpressie. We hebben aangetoond dat genexpressie in verschillende hersenregio's kan worden onderscheiden. We hebben aangetoond dat LV-gemedieerde genexpressie in hetzelfde dier persisteert gedurende meer dan één jaar. Vervolgens werd deze methode toegepast om volwassen endogene neurale stamcellen in de hersenen van muizen te detecteren en op te volgen. Deze cellen werden getransduceerd met LV coderend voor Fluc en we detecteerden een specifiek signaal afkomstig van de bulbus olfactorius, de regio waar de dochtercellen van deze stamcellen naar toe migreren.

Vervolgens hebben we een strategie ontwikkeld om de groei van metastasen in muizen te detecteren via beeldvorming van reporter genen. We maakten gebruik van een fusiegen dat een reporter gen voor positron emissie tomografie (PET), een reporter gen voor BLI en een fluorescerend eiwit bevat. Onze PET-CT aanpak die moleculaire en anatomische beelden combineert werd eerst gevalideerd in muizen geïnoculeerd met

xenogreffes en werd dan toegepast om metastasen van melanomacellen te detecteren in muizen en deze op te volgen in de tijd. Door deze beelden te combineren met BLI bekwamen we een zeer gevoelige techniek die accurate driedimensionale lokalisatie van de letsels toelaat. Onze reportergeren techniek had een duidelijk hoger contrast dan beeldvorming met [¹⁸F]-FDG, de huidige gouden standaard PET tracer. Deze techniek is veelbelovend voor de opvolging van de verspreiding en groei van tumoren in muismodellen.

Als laatste hebben we een nieuw reportergeren voor PET gevalideerd, VZV-tk. Eén van de tracers, die specifiek voor dit enzym ontwikkeld werden, vertoonde hoge accumulatie in cellen die dit gen tot expressie brengen. Deze opstapeling werd veroorzaakt door metabolisatie van de tracer door het VZV-TK enzym, welke werd aangetoond door hoge druk vloeistofchromatografie. De cellulaire retentie van deze tracer was aanvaardbaar met een halfwaardetijd van ongeveer één uur. Tracer opname correleerde met LV-titers in cellen getransduceerd met serieel verdunde vector. Deze tracer ging echter niet door de bloed-hersens barrière en kon niet gebruikt worden voor de vooropgestelde PET beeldvorming van VZV-tk expressie in de hersenen. Voor *in vivo* detectie van VZV-tk met PET werd gebruik gemaakt van muizen geïnoculeerd met xenogreffes en deze bevindingen werden gevalideerd door middel van autoradiografie en scintillatietelling.

Dit werk legt de basis voor verdere toepassingen en ontwikkeling van reportergeren beeldvorming. Onze gevalideerde methode voor hersenbeeldvorming via BLI wordt momenteel gebruikt voor neurobiologische studies, voor vector optimalisatie en ter bestudering van volwassen neuronale stamcellen. PET reportergeren beeldvorming en BLI worden gebruikt ter optimalisatie van vectoren voor gentherapie en ter detectie en quantificatie van kankercellen in muismodellen.

Curriculum Vitae

Christophe Deroose was born in Ghent on August 6th 1976. He attended secondary school (Latin-Mathematics) at the Collège Saint-Vincent in Soignies. He started a candidacy in Medical Sciences at the Facultés Universitaires Notre-Dame de la Paix in Namur in 1994 and graduated with *summa cum laude*. He then continued Medical Sciences at the Katholieke Universiteit Leuven. In 1999-2000 he went to South Africa for a 4 month internship. He obtained his M.D. in 2001 with *summa cum laude* and started a residency in nuclear medicine under the supervision of Prof. Dr Luc Mortelmans. In the framework of this residency, he fulfilled one year of clinical training in internal medicine from 2001 to 2002 under the supervision of Prof. Dr Johan Fevery in the University Hospital Leuven. From 2002 on he fulfilled a PhD training in Medical Sciences for which he obtained a fellowship from the Fund for Scientific Research Flanders (FWO). The first 2 years were spent in the Multimodality Gene Imaging Laboratory of Prof. Dr Sanjiv Sam Gambhir, at the University of California, Los Angeles and at Stanford University. For this stay, he obtained a Henri Benedictus fellowship from the Belgian American Educational Foundation (BAEF) together with the King Baudouin Foundation. From 2004, he performed research in the Division of Nuclear Medicine and the Division of Molecular Medicine under the supervision of Prof. Dr Luc Mortelmans, Prof. Dr Zeger Debyser and Prof. Dr Veerle Baekelandt. From 2006 on he resumed his residency in nuclear medicine in the University Hospital Leuven which he will complete in 2008. He received the award for Top Basic Science Young Investigator from the Academy of Molecular Imaging in 2003 and the First Place Neuroscience Young Investigator Award from the Society of Nuclear Medicine in 2005. In 2004 he married Isabelle Lousse. They have one daughter, Emilie, who was born in 2005.

Publication List

1a. Articles in international peer-reviewed journals

- Deroose CM, Reumers V, Debyser Z, Baekelandt V, *Seeing genes at work in the living brain with non-invasive molecular imaging*, Current Gene Therapy, in press.
- Chitneni SK, Deroose CM, Fonge H, Gijsbers R, Balzarini J, Debyser Z, Mortelmans L, Verbruggen AV, Bormans GM: *Synthesis and biological evaluation of a ¹²³I-labeled bicyclic nucleoside analogue (BCNA) as potential SPECT tracer for VZV-tk reporter gene imaging*, Bioorganic & Medicinal Chemistry Letters, 2007, 17:3458-3462
- Taymans JM, Vandenberghe LH, Van Den Haute C, Thiry I, Deroose CM, Mortelmans L, Wilson JM, Debyser Z, Baekelandt V: *Comparative analysis of adeno-associated viral vector serotypes 1, 2, 5, 7, and 8 in mouse brain*, Human Gene Therapy, 2007, 18:195-206
- Toelen J, Deroose CM, Gijsbers R, Reumers V, Sbragia LN, Vets S, Chitneni S, Bormans G, Mortelmans L, Deprest JA, Debyser Z: *Fetal gene transfer using lentiviral vectors: long-term in vivo follow-up in a rat model*, American Journal of Obstetrics and Gynaecology, 2007, 196:352 e351-356
- Chitneni S, Deroose CM, Balzarini J, Gijsbers R, Bex M, Terwinghe C, Celen S, de Groot T, Debyser Z, Mortelmans L, Verbruggen A, Bormans G: *Synthesis, preliminary evaluation of 18F and 11C-labeled bicyclic nucleoside analogues (BCNAs) as potential PET reporter probes for imaging varicella-zoster virus thymidine kinase gene expression*, Journal of Medicinal Chemistry, 2007 150:1041-1049
- Deroose CM, De A, Loening AM, Chow PL, Ray P, Chatziioannou AF, Gambhir SS: *Multimodality imaging of tumor xenografts and metastasis in mice with combined microPET, microCT and bioluminescence imaging*, Journal of Nuclear Medicine, 2007;48(2):295-303
- Deroose CM[Ⓢ], Reumers V[Ⓢ], Gijsbers R, Bormans G, Debyser Z, Mortelmans L, Baekelandt V: *Non-invasive detection of locoregional transgenesis of mouse brain with bioluminescence imaging*, Molecular Therapy, 2006; 14(3):423-31
- Prenen H, Deroose C, Vermaelen P, Sciot R, Debiec-Rychter M, Stroobants S, Mortelmans L, Schoffski P, Van Oosterom A.: *Establishment of a Mouse Gastrointestinal Stromal Tumour Model and Evaluation of Response to Imatinib by Small Animal Positron Emission Tomography*, Anticancer Research, 2006; 26(2A):1247-52.
- Janssens S, Dubois C, Bogaert J, Theunissen K, Deroose C, Desmet W, Kalantzis M, Herbots L, Sinnaeve P, Dens J, Maertens J, Rademakers F, Dymarkowski S, Gheysens O, Van Cleemput J, Bormans G, Nuyts J, Belmans A, Mortelmans L, Boogaerts M, and Van de Werf F: *Autologous Bone Marrow-Derived Stem Cell Transfer In Patients With ST-Segment Elevation Myocardial Infarction*, The Lancet, 2006; 367(9505):113-21
- Min JJ, Biswal S, Deroose C, Gambhir SS: *Tetraphenylphosphonium as a novel molecular probe for imaging tumors*, Journal of Nuclear Medicine, 2004; 45(4):636-43.

Ⓢ: Shared first author.

Ib. Articles for international peer-reviewed journals: submitted or in preparation.

- Chitneni SK, Deroose CM, Balzarini J, Gijsbers R, Celen SJL, Debyser Z, Mortelmans L, Verbruggen AM, Bormans GM: *para-[¹⁸F]Fluoroethoxyphenyl Bicyclic Nucleoside Analogue as Potential Positron Emission Tomography Imaging Agent for Varicella-Zoster Virus Thymidine Kinase Gene Expression*, Journal of Medicinal Chemistry, revisions submitted.
- Deroose CM[®], Chitneni SK[®], Gijsbers R, Vermaelen P, Ibrahim A, Verbruggen AV, Balzarini J, Baekelandt V, Nuyts J, Bormans GM, Debyser Z, Mortelmans L: *Validation of varicella zoster virus thymidine kinase as a novel reporter gene for positron emission tomography*, submitted.
- Celen S, Deroose CM, de Groot T, Chitneni S, Gijsbers R, Debyser Z, Mortelmans L, Verbruggen A and Bormans G: *Synthesis and Evaluation of ¹⁸F- and ¹¹C-labelled β -Galactosidase Substrates as Potential Probes for in vivo Visualization of LacZ Gene Expression using Positron Emission Tomography*, submitted
- Deroose CM[®], Reumers V[®], Gijsbers R, Krylychkina O, Geraerts M, Mortelmans L, Debyser Z, Baekelandt V: *Quantitative bioluminescence imaging of the migration of endogenous neural stem cells in mouse brain*, in preparation.
- Vande Velde G, Deroose CM, Gijsbers R, Vandeputte C, Reumers V, Thiry I, Baekelandt V, Mortelmans L, Debyser Z: *Systematic evaluation of bicistronic lentiviral vector constructs for reporter gene imaging*: in preparation.

II. Articles in other scientific journals.

III. Announcements on international congresses and symposia.

a) entirely published as proceedings

b) not published or only available as abstracts

- Reumers V, Deroose CM, Gijsbers R, Krylychkina O, Geraerts M, Mortelmans L, Debyser Z, Baekelandt V: *Detection and quantification of the migration of lentiviral vector-labelled endogenous neural stem cells in mouse brain with bioluminescence imaging*, Academy of Molecular Imaging and Society of Molecular Imaging Joint Annual Meeting, September 8-12, Providence, RI, USA.
- Deroose CM, Chitneni S, Gijsbers R, Baekelandt V, Verbruggen A, Balzarini J, Debyser Z, Bormans, G, Mortelmans, L: *In vitro evaluation of a novel radiolabeled bi-cyclic nucleoside analog as PET reporter probe for Varicella zoster virus thymidine kinase gene expression*, Society of Nuclear Medicine, Annual International Congress, 2-6 June 2007, Washington, USA.
- Deroose CM, Reumers V, Gijsbers R, Krylychkina O, Geraerts M, Debyser Z, Baekelandt V, Mortelmans L: *Quantitative bioluminescence imaging of the migration of endogenous neural stem cells in mouse brain*, Society of Nuclear Medicine, Annual International Congress, 2-6 June 2007, Washington, USA.
- Deroose CM, Gijsbers R, Vande Velde G, Vandeputte C, Reumers V, Thiry I, Baekelandt V, Mortelmans L, Debyser Z: *Systematic evaluation of bicistronic lentiviral vector constructs for reporter gene imaging*, Society of Nuclear Medicine, Annual International Congress, 2-6 June 2007, Washington, USA.
- Chitneni S, Deroose CM, Debyser Z, Mortelmans L, Verbruggen AM, Bormans GM: *Application of Waters Oasis® column in the purification and metabolite analysis of radiotracers*, International Symposium on High Performance Liquid Phase Separations and Related Techniques, 17-21 June 2007, Ghent.

- Chitneni SK, Deroose CM, Fonge H, Gijsbers R, Balzarini J, Debyser Z, Mortelmans L, Verbruggen AV, Bormans GM: *Synthesis and preliminary biological evaluation of Iodine-123labeled bicyclic nucleoside analogue (BCNA) as potential SPECT probe for varicella zoster thymidine kinase (VZV-tk) reporter gene imaging*, 17th International Symposium on Radiopharmaceutical Sciences, 30 April – 4 May, Aachen, Germany.
- Toelen J, Gijsbers R, Sbragia L, Deroose C, Debyser Z, Deprest J: *Long term pulmonary gene therapy with a lentiviral vector in a fetal rat model*, Society for Maternal-Fetal Medicine, Annual International Meeting, 5-10 February 2007, San Francisco, USA.
- Lories R, Derese I, Peeters J, Deroose C, Mortelmans L, Luyten F: *Uncoupling of inflammation and new tissue formation in a mouse model of ankylosing enthesitis*, American College of Rheumatology, Annual International Meeting, 10-15 November 2006, Washington D.C., USA.
- Chitneni S, Deroose C, Balzarini J, Verbruggen A, Bormans G: *Synthesis and preliminary evaluation of F-18 and C-11 labelled bi-cyclic nucleoside analogues (BCNAs) as potential PET reporter probes for imaging varicella-zoster virus thymidine kinase (VZV-tk) gene expression*, European Association of Nuclear Medicine, Annual International Congress, 30 September – 4 October 2006, Athens, Greece.
- Lories R, Derese I, Deroose C, De Bari C, Mortelmans L, Luyten F: *Joint ankylosis in remodelling arthritis is independent of Tumor Necrosis Factor*, European League Against Rheumatism, Annual International Congress, 21-24 June 2006, Amsterdam, The Netherlands.
- Deroose C, Chitneni S, Gijsbers R, Baekelandt V, Verbruggen A, Balzarini J, Debyser Z, Bormans G, Mortelmans L: *In Vitro Evaluation of Varicella Zoster Virus (VZV) Thymidine Kinase as a PET Reporter Gene with Radiolabeled Bi-Cyclic Nucleoside Analogs*, Society of Nuclear Medicine, Annual International Congress, 3-7 June 2006, San Diego, USA.
- Deroose C, Chitneni S, Gijsbers R, Reumers V, Baekelandt V, Verbruggen A, Bormans G, Debyser Z, Mortelmans L: *Multimodality Imaging of Lentiviral Vector-Mediated Gene Transfer to Mouse Muscle with micro Positron Emission Tomography (PET) and Bioluminescence Imaging (BLI)*, Society of Nuclear Medicine, Annual International Congress, 3-7 June 2006, San Diego, USA.
- Reumers V, Deroose C, Gijsbers R, Debyser Z, Mortelmans L, Baekelandt V: *Long-Term Bioluminescence Imaging of Lentiviral Vector-Mediated Gene Expression in Mouse Brain*, Society of Gene Therapy, Annual Congress, 29 October- 1 November, 2005, Prague, Tjech Republic.
- Reumers V, Deroose C, Gijsbers R, Debyser Z, Mortelmans L, Baekelandt V: *Long-Term Bioluminescence Imaging of Lentiviral Vector-Mediated Gene Expression in Mouse Brain*, The Society for Molecular Imaging, Annual Meeting, 7-10 September 2005, Cologne, Germany.
- Deroose C, Reumers R, Gijsbers R, Bormans G, Baekelandt V, Debyser Z, Mortelmans L: *Bioluminescence imaging of lentiviral vector mediated locoregional gene transfer into adult mouse brain*, The Society of Nuclear Medicine, Annual International Congress, 18-22 June 2005, Toronto, Canada.
- Chen IY, Ray S, Padmanabhan P, Gheysens O, Deroose C, Caffarelli A, Biswall S, Wu JC, Gambhir SS: *A generalizable bi-directional vector for non-invasive imaging and amplification of transgene expression mediated by a weak cardiac-specific promoter*, Academy of Molecular Imaging, Annual Meeting, 18-23 March, Orlando, USA.

- Janssens S, Dubois C, Bogaert J, Theunissen K, Deroose C, Desmet W, Kalantzis M, Herbots L, Sinnaeve P, Dens J, Maertens J, Rademakers F, Dymarkowski S, Gheysens O, Van Cleemput J, Bormans G, Nuyts J, Belmans A, Mortelmans L, Boogaerts M, and Van de Werf F: *Intracoronary autologous bone-marrow cell transfer after myocardial infarction: a double blind, randomized and placebo-controlled clinical trial*, American College of Cardiology, Annual Meeting, 6-9 March, Orlando, USA.
- Deroose C, De A, Loening AM, Collisson EA, Kolodney MS, Chow PL, Chatziioannou AF, Gambhir SS: *Small animal microPET/microCT imaging studies of a tumor metastatic model*, Academy of Molecular Imaging 2003, Madrid, Spain.

IV. Announcements on international congresses and symposia.

a) entirely published as proceedings

b) not published or only available as abstracts

- Deroose CM, Chitneni S, Gijsbers R, Baekelandt V, Verbruggen A, Balzarini J, Debyser Z, Bormans G, Mortelmans L: *Validation of Varicella Zoster Virus Thymidine Kinase Gene as Novel PET Reporter Gene*, Belgisch Genootschap voor Nucleaire Geneeskunde, Spa 2007, Belgium.
- Deroose CM, Reumers V, Gijsbers R, Krylychkina O, Geraerts M, Debyser Z, Baekelandt V, Mortelmans L: *Bioluminescence Imaging of Endogenous Neural Stem Cell Migration in Mouse Brain*, Belgisch Genootschap voor Nucleaire Geneeskunde, Spa 2007, Belgium.
- Deroose CM, Reumers V, Gijsbers R, Krylychkina O, Geraerts M, Debyser Z, Baekelandt V, Mortelmans L
- Toelen J, Sbragia L, Gijsbers R, Deroose C, Deprest JA, Debyser Z: *Long term transgene expression after fetal injection using a lentiviral vector in a rat model*. Belgische Vereniging Kindergeneeskunde, National Congress 2007.
- Deroose C, Reumers R, Gijsbers R, Bormans G, Baekelandt V, Debyser Z, Mortelmans L: *Non-invasive measurement of lentiviral vector mediated locoregional gene transfer into adult mouse brain with bioluminescence imaging*, Belgisch Genootschap voor Nucleaire Geneeskunde, Société Française de Biophysique & Médecine Nucléaire en Nederlandse Vereniging voor Nucleaire Geneeskunde, National Congress, 20-22 Mei 2005, Knokke, Belgium.
- Prenen H, Deroose C, Vermaelen P, Sciot P, Debiec-Rychter M, Stroobants S, de Bruijn E, Mortelmans L, van Oosterom A: *Evaluation of imatinib therapy in a mouse model of gastrointestinal tumor by micro positron emission tomography*, Belgisch Genootschap voor Nucleaire Geneeskunde, Société Française de Biophysique & Médecine Nucléaire en Nederlandse Vereniging voor Nucleaire Geneeskunde, National Congress, 20-22 Mei 2005, Knokke, Belgium.
- Deroose C: *FDG-PET in cutaneous sarcoidosis*: Belgisch Genootschap voor Nucleaire Geneeskunde, National Congress, Mei 2001, Knokke, Belgium.

V. Internal reports / VI. Thesis / VII. Books

VIII. Articles in or part of books

1. Gambhir SS, Deroose C, Walls Z: *Cell biology fundamentals*, Nuclear Medicine in Clinical Diagnosis & Treatment, P. Ell & S.S. Gambhir (Eds.), Churchill Livingstone Publishers, Third Edition, 2004, p. 1687-712.

References

1. Pauling, L., Itano, H. A., and et al. (1949). Sickle cell anemia, a molecular disease. *Science* 110: 543-548.
2. Massoud, T. F., and Gambhir, S. S. (2007). Integrating noninvasive molecular imaging into molecular medicine: an evolving paradigm. *Trends Mol Med* 13: 183-191.
3. Massoud, T. F., and Gambhir, S. S. (2003). Molecular imaging in living subjects: seeing fundamental biological processes in a new light. *Genes Dev* 17: 545-580.
4. Burns, H. D., et al. (2007). [18F]MK-9470, a positron emission tomography (PET) tracer for in vivo human PET brain imaging of the cannabinoid-1 receptor. *PNAS* 104: 9800-9805.
5. Gambhir, S. S., et al. (1998). Imaging of adenoviral-directed herpes simplex virus type 1 thymidine kinase reporter gene expression in mice with radiolabeled ganciclovir. *J Nucl Med* 39: 2003-2011.
6. Paulmurugan, R., Umezawa, Y., and Gambhir, S. S. (2002). Noninvasive imaging of protein-protein interactions in living subjects by using reporter protein complementation and reconstitution strategies. *Proc Natl Acad Sci U S A* 99: 15608-15613.
7. Ciana, P., et al. (2003). In vivo imaging of transcriptionally active estrogen receptors. *Nat Med* 9: 82-86.
8. Luo, J., Lin, A. H., Masliah, E., and Wyss-Coray, T. (2006). Bioluminescence imaging of Smad signaling in living mice shows correlation with excitotoxic neurodegeneration. *Proc Natl Acad Sci U S A* 103: 18326-18331.
9. Laxman, B., et al. (2002). Noninvasive real-time imaging of apoptosis. *PNAS* 99: 16551-16555.
10. Narula, J., et al. (2001). Annexin-V imaging for noninvasive detection of cardiac allograft rejection. *Nat Med* 7: 1347-1352.
11. Vastenhouw, B., and Beekman, F. (2007). Submillimeter Total-Body Murine Imaging with U-SPECT-I. *J Nucl Med* 48: 487-493.
12. Mullins (2006). MR Spectroscopy: Truly Molecular Imaging; Past, Present and Future. *Neuroimaging Clinics of North America* 16: 605-618.
13. Nighswander-Rempel, S. P., Kupriyanov, V. V., and Shaw, R. A. (2005). Relative contributions of hemoglobin and myoglobin to near-infrared spectroscopic images of cardiac tissue. *Applied Spectroscopy* 59: 190-193.
14. Zacharakis, G., et al. (2005). Volumetric tomography of fluorescent proteins through small animals in vivo. *Proc Natl Acad Sci U S A* 102: 18252-18257.
15. Contag, C. H. (2006). Molecular imaging using visible light to reveal biological changes in the brain. *Neuroimaging Clin N Am* 16: 633-654, ix.
16. Venisnik, K. M., Olafsen, T., Loening, A. M., Iyer, M., Gambhir, S. S., and Wu, A. M. (2006). Bifunctional antibody-Renilla luciferase fusion protein for in vivo optical detection of tumors. *Protein Eng Des Sel* 19: 453-460.
17. So, M. K., Xu, C., Loening, A. M., Gambhir, S. S., and Rao, J. (2006). Self-illuminating quantum dot conjugates for in vivo imaging. *Nat Biotechnol* 24: 339-343.
18. Chalfie, M., Tu, Y., Euskirchen, G., Ward, W. W., and Prasher, D. C. (1994). Green Fluorescent Protein as a Marker for Gene-Expression. *Science* 263: 802-805.
19. Matz, M. V., et al. (1999). Fluorescent proteins from nonbioluminescent Anthozoa species. *Nature Biotechnology* 17: 969-973.
20. Shaner, N. C., Steinbach, P. A., and Tsien, R. Y. (2005). A guide to choosing fluorescent proteins. *Nat Methods* 2: 905-909.
21. Yaghoubi, S. S., et al. (2001). Direct correlation between positron emission tomographic images of two reporter genes delivered by two distinct adenoviral vectors. *Gene Ther* 8: 1072-1080.

22. Liang, Q., et al. (2002). Monitoring adenoviral DNA delivery, using a mutant herpes simplex virus type 1 thymidine kinase gene as a PET reporter gene. *Gene Therapy* 9: 1659-1666.
23. Wang, Y., Iyer, M., Annala, A. J., Chappell, S., Mauro, V., and Gambhir, S. S. (2005). Noninvasive monitoring of target gene expression by imaging reporter gene expression in living animals using improved bicistronic vectors. *J Nucl Med* 46: 667-674.
24. Ray, S., et al. (2004). Novel bidirectional vector strategy for amplification of therapeutic and reporter gene expression. *Hum Gene Ther* 15: 681-690.
25. Szymczak, A. L., et al. (2004). Correction of multi-gene deficiency in vivo using a single 'self-cleaving' 2A peptide-based retroviral vector. *Nat Biotechnol* 22: 589-594.
26. Penuelas, I., et al. (2005). Positron emission tomography imaging of adenoviral-mediated transgene expression in liver cancer patients. *Gastroenterology* 128: 1787-1795.
27. Valery, C. A., et al. (2002). Long-term survival after gene therapy for a recurrent glioblastoma. *Neurology* 58: 1109-1112.
28. Immonen, A., et al. (2004). AdvHSV-tk gene therapy with intravenous ganciclovir improves survival in human malignant glioma: a randomised, controlled study. *Mol Ther* 10: 967-972.
29. Tjuvajev, J. G., et al. (1995). Imaging the expression of transfected genes in vivo. *Cancer Res* 55: 6126-6132.
30. Tjuvajev, J. G., et al. (1996). Noninvasive imaging of herpes virus thymidine kinase gene transfer and expression: a potential method for monitoring clinical gene therapy. *Cancer Res* 56: 4087-4095.
31. Tjuvajev, J. G., et al. (1998). Imaging herpes virus thymidine kinase gene transfer and expression by positron emission tomography. *Cancer Res* 58: 4333-4341.
32. Alauddin, M. M., Shahinian, A., Gordon, E. M., Bading, J. R., and Conti, P. S. (2001). Preclinical evaluation of the penciclovir analog 9-(4-[(18F]fluoro-3-hydroxymethylbutyl)guanine for in vivo measurement of suicide gene expression with PET. *J Nucl Med* 42: 1682-1690.
33. Yaghoubi, S., et al. (2001). Human pharmacokinetic and dosimetry studies of [(18F]FHBG: a reporter probe for imaging herpes simplex virus type-1 thymidine kinase reporter gene expression. *J Nucl Med* 42: 1225-1234.
34. Yaghoubi, S. S., et al. (2006). Preclinical safety evaluation of 18F-FHBG: a PET reporter probe for imaging herpes simplex virus type 1 thymidine kinase (HSV1-tk) or mutant HSV1-sr39tk's expression. *J Nucl Med* 47: 706-715.
35. Green, L. A., et al. (2004). A tracer kinetic model for 18F-FHBG for quantitating herpes simplex virus type 1 thymidine kinase reporter gene expression in living animals using PET. *J Nucl Med* 45: 1560-1570.
36. Gambhir, S. S., et al. (2000). A mutant herpes simplex virus type 1 thymidine kinase reporter gene shows improved sensitivity for imaging reporter gene expression with positron emission tomography. *Proc Natl Acad Sci U S A* 97: 2785-2790.
37. Luker, G. D., et al. (2002). Noninvasive imaging of protein-protein interactions in living animals. *Proc Natl Acad Sci U S A* 99: 6961-6966.
38. Balzarini, J., Liekens, S., Solaroli, N., El Omari, K., Stammers, D. K., and Karlsson, A. (2006). Engineering of a Single Conserved Amino Acid Residue of Herpes Simplex Virus Type 1 Thymidine Kinase Allows a Predominant Shift from Pyrimidine to Purine Nucleoside Phosphorylation. *J. Biol. Chem.* 281: 19273-19279.
39. Ray, P., et al. (2002). Noninvasive quantitative imaging of protein-protein interactions in living subjects. *Proc Natl Acad Sci U S A* 99: 3105-3110.
40. Cao, F., et al. (2006). In Vivo Visualization of Embryonic Stem Cell Survival, Proliferation, and Migration After Cardiac Delivery. *Circulation* 113: 1005-1014.
41. Jacobs, A., et al. (2001). Quantitative kinetics of [124I]FIAU in cat and man. *J Nucl Med* 42: 467-475.
42. Jacobs, A., et al. (2001). Positron-emission tomography of vector-mediated gene expression in gene therapy for gliomas. *Lancet* 358: 727-729.

43. Ponomarev, V., et al. (2007). A Human-Derived Reporter Gene for Noninvasive Imaging in Humans: Mitochondrial Thymidine Kinase Type 2
10.2967/jnumed.106.036962. *J Nucl Med* 48: 819-826.
44. Eberling, J. L., Cunningham, J., Pivrotto, P., Bringas, J., Daadi, M. M., and Bankiewicz, K. S. (2003). In Vivo PET Imaging of Gene Expression in Parkinsonian Monkeys. *Mol Ther* 8: 873-875.
45. Bankiewicz, K. S., et al. (2000). Convection-Enhanced Delivery of AAV Vector in Parkinsonian Monkeys; In Vivo Detection of Gene Expression and Restoration of Dopaminergic Function Using Pro-drug Approach. *Experimental Neurology* 164: 2-14.
46. Forsayeth, J. R., et al. (2006). A Dose-Ranging Study of AAV-hAADC Therapy in Parkinsonian Monkeys. *Mol Ther* 14: 571-577.
47. Bankiewicz, K. S., et al. (2006). Long-Term Clinical Improvement in MPTP-Lesioned Primates after Gene Therapy with AAV-hAADC. *Mol Ther* 14: 564-570.
48. Doubrovin, M., et al. (2003). Development of a new reporter gene system--dsRed/xanthine phosphoribosyltransferase-xanthine for molecular imaging of processes behind the intact blood-brain barrier. *Mol Imaging* 2: 93-112.
49. MacLaren, D. C., et al. (1999). Repetitive, non-invasive imaging of the dopamine D2 receptor as a reporter gene in living animals. *Gene Ther* 6: 785-791.
50. Liang, Q., et al. (2002). Noninvasive, repetitive, quantitative measurement of gene expression from a bicistronic message by positron emission tomography, following gene transfer with adenovirus. *Mol Ther* 6: 73-82.
51. Chen, I. Y., et al. (2004). Micro-positron emission tomography imaging of cardiac gene expression in rats using bicistronic adenoviral vector-mediated gene delivery. *Circulation* 109: 1415-1420.
52. Ogawa, O., et al. (2000). In vivo imaging of adenovirus-mediated over-expression of dopamine D-2 receptors in rat striatum by positron emission tomography. *Neuroreport* 11: 743-748.
53. Umegaki, H., et al. (2002). In vivo assessment of adenoviral vector-mediated gene expression of dopamine D-2 receptors in the rat striatum by positron emission tomography. *Synapse* 43: 195-200.
54. Forrer, F., Valkema, R., Kwekkeboom, D. J., de Jong, M., and Krenning, E. P. (2007). Peptide receptor radionuclide therapy. *Best Practice & Research Clinical Endocrinology & Metabolism Neuroendocrine Tumours* 21: 111-129.
55. Ginj, M., et al. (2006). Radiolabeled somatostatin receptor antagonists are preferable to agonists for in vivo peptide receptor targeting of tumors. *PNAS* 103: 16436-16441.
56. Zinn, K. R., Buchsbaum, D. J., Chaudhuri, T. R., Mountz, J. M., Grizzle, W. E., and Rogers, B. E. (2000). Noninvasive monitoring of gene transfer using a reporter receptor imaged with a high-affinity peptide radiolabeled with Tc-99m or Re-188. *Journal of Nuclear Medicine* 41: 887-895.
57. Zinn, K. R., Chaudhuri, T. R., Buchsbaum, D. J., Mountz, J. M., and Rogers, B. E. (2001). Simultaneous evaluation of dual gene transfer to adherent cells by gamma-ray imaging. *Nucl Med Biol* 28: 135-144.
58. Zinn, K. R., et al. (2002). Gamma camera dual imaging with a somatostatin receptor and thymidine kinase after gene transfer with a bicistronic adenovirus in mice. *Radiology* 223: 417-425.
59. Rogers, B. E., Chaudhuri, T. R., Reynolds, P. N., Della Manna, D., and Zinn, K. R. (2003). Non-invasive gamma camera imaging of gene transfer using an adenoviral vector encoding an epitope-tagged receptor as a reporter. *Gene Therapy* 10: 105-114.
60. Furukawa, T., Lohith, T. G., Takamatsu, S., Mori, T., Tanaka, T., and Fujibayashi, Y. (2006). Potential of the FES-hERL PET reporter gene system -- Basic evaluation for gene therapy monitoring. *Nuclear Medicine and Biology* 33: 145-151.
61. Pareto, D., Alvarado, M., Hanrahan, S. M., and Biegon, A. (2004). In vivo occupancy of female rat brain estrogen receptors by 17[beta]-estradiol and tamoxifen. *NeuroImage* 23: 1161-1167.

62. Haberkorn, U., et al. (2001). Transfer of the Human NaI Symporter Gene Enhances Iodide Uptake in Hepatoma Cells. *J Nucl Med* 42: 317-325.
63. Boelaert, K., and Franklyn, J. (2003). Sodium iodide symporter: a novel strategy to target breast, prostate, and other cancers? *The Lancet* 361: 796-797.
64. Huang, M., et al. (2001). Ectopic expression of the thyroperoxidase gene augments radioiodide uptake and retention mediated by the sodium iodide symporter in non-small cell lung cancer. *Cancer Gene Therapy* 8: 612-618.
65. Vadysirisack, D. D., Shen, D. H., and Jhiang, S. M. (2006). Correlation of Na⁺/I⁻ Symporter Expression and Activity: Implications of Na⁺/I⁻ Symporter as an Imaging Reporter Gene. *J Nucl Med* 47: 182-190.
66. Auricchio, A., et al. (2003). In vivo quantitative noninvasive imaging of gene transfer by single-photon emission computerized tomography. *Hum Gene Ther* 14: 255-261.
67. Anton, M., et al. (2004). Use of the norepinephrine transporter as a reporter gene for non-invasive imaging of genetically modified cells. *J Gene Med* 6: 119-126.
68. Buursma, A. R., et al. (2005). The human norepinephrine transporter in combination with ¹¹C-m-hydroxyephedrine as a reporter gene/reporter probe for PET of gene therapy. *J Nucl Med* 46: 2068-2075.
69. Altmann, A., et al. (2003). Increased MIBG Uptake After Transfer of the Human Norepinephrine Transporter Gene in Rat Hepatoma. *J Nucl Med* 44: 973-980.
70. Moroz, M. A., et al. (2007). Imaging hNET Reporter Gene Expression with ¹²⁴I-MIBG 10.2967/jnumed.106.037812. *J Nucl Med* 48: 827-836.
71. Ding, Y. S., Lin, K. S., and Logan, J. (2006). PET imaging of norepinephrine transporters. *Current Pharmaceutical Design* 12: 3831-3845.
72. Zhao, H., Doyle, T. C., Coquoz, O., Kalish, F., Rice, B. W., and Contag, C. H. (2005). Emission spectra of bioluminescent reporters and interaction with mammalian tissue determine the sensitivity of detection in vivo. *J Biomed Opt* 10: 41210.
73. Lee, K. H., et al. (2003). Cell uptake and tissue distribution of radioiodine labelled D-luciferin: implications for luciferase based gene imaging. *Nucl Med Commun* 24: 1003-1009.
74. Ignowski, J. M., and Schaffer, D. V. (2004). Kinetic analysis and modeling of firefly luciferase as a quantitative reporter gene in live mammalian cells. *Biotechnol Bioeng* 86: 827-834.
75. Luker, K. E., Smith, M. C., Luker, G. D., Gammon, S. T., Piwnica-Worms, H., and Piwnica-Worms, D. (2004). Kinetics of regulated protein-protein interactions revealed with firefly luciferase complementation imaging in cells and living animals. *Proc Natl Acad Sci U S A* 101: 12288-12293.
76. Bhaumik, S., and Gambhir, S. S. (2002). Optical imaging of Renilla luciferase reporter gene expression in living mice. *Proc Natl Acad Sci U S A* 99: 377-382.
77. Zhao, H., et al. (2004). Characterization of coelenterazine analogs for measurements of Renilla luciferase activity in live cells and living animals. *Mol Imaging* 3: 43-54.
78. Bhaumik, S., Lewis, X. Z., and Gambhir, S. S. (2004). Optical imaging of Renilla luciferase, synthetic Renilla luciferase, and firefly luciferase reporter gene expression in living mice. *J Biomed Opt* 9: 578-586.
79. Paulmurugan, R., and Gambhir, S. S. (2003). Monitoring protein-protein interactions using split synthetic renilla luciferase protein-fragment-assisted complementation. *Anal Chem* 75: 1584-1589.
80. Paulmurugan, R., Massoud, T. F., Huang, J., and Gambhir, S. S. (2004). Molecular imaging of drug-modulated protein-protein interactions in living subjects. *Cancer Res* 64: 2113-2119.
81. Kim, S. B., Ozawa, T., Watanabe, S., and Umezawa, Y. (2004). High-throughput sensing and noninvasive imaging of protein nuclear transport by using reconstitution of split Renilla luciferase. *PNAS* 101: 11542-11547.
82. Paulmurugan, R., and Gambhir, S. S. (2007). Combinatorial library screening for developing an improved split-firefly luciferase fragment-assisted complementation system for studying protein-protein interactions. *Anal Chem* 79: 2346-2353.

83. Loening, A. M., Fenn, T. D., Wu, A. M., and Gambhir, S. S. (2006). Consensus guided mutagenesis of Renilla luciferase yields enhanced stability and light output. *Protein Eng Des Sel* 19: 391-400.
84. Pichler, A., Prior, J. L., and Piwnica-Worms, D. (2004). Imaging reversal of multidrug resistance in living mice with bioluminescence: MDR1 P-glycoprotein transports coelenterazine. *Proc Natl Acad Sci U S A* 101: 1702-1707.
85. Tannous B.A., Kim D.E., Fernandez J.L., Weissleder, R., and Breakefield, X. O. (2005). Codon-optimized Gaussia luciferase cDNA for mammalian gene expression in culture and in vivo. *Mol Ther* 11: 435-443.
86. Remy, I., and Michnick, S. W. (2006). A highly sensitive protein-protein interaction assay based on Gaussia luciferase. *Nat Methods* 3: 977-979.
87. Kim, D. E., Schellingerhout, D., Ishii, K., Shah, K., and Weissleder, R. (2004). Imaging of stem cell recruitment to ischemic infarcts in a murine model. *Stroke* 35: 952-957.
88. Tang, Y., Shah, K., Messerli, S. M., Snyder, E., Breakefield, X., and Weissleder, R. (2003). In vivo tracking of neural progenitor cell migration to glioblastomas. *Hum Gene Ther* 14: 1247-1254.
89. Rehemtulla, A., et al. (2000). Rapid and quantitative assessment of cancer treatment response using in vivo bioluminescence imaging. *Neoplasia* 2: 491-495.
90. Moriyama, E. H., Bisland, S. K., Lilge, L., and Wilson, B. C. (2004). Bioluminescence imaging of the response of rat gliosarcoma to ALA-PpIX-mediated photodynamic therapy. *Photochem Photobiol* 80: 242-249.
91. Burgos, J. S., et al. (2003). Time course of bioluminescent signal in orthotopic and heterotopic brain tumors in nude mice. *Biotechniques* 34: 1184-1188.
92. Uhrbom, L., Nerio, E., and Holland, E. C. (2004). Dissecting tumor maintenance requirements using bioluminescence imaging of cell proliferation in a mouse glioma model. *Nat Med* 10: 1257-1260.
93. Vooijs, M., Jonkers, J., Lyons, S., and Berns, A. (2002). Noninvasive imaging of spontaneous retinoblastoma pathway-dependent tumors in mice. *Cancer Res* 62: 1862-1867.
94. Rehemtulla, A., et al. (2002). Molecular imaging of gene expression and efficacy following adenoviral-mediated brain tumor gene therapy. *Mol Imaging* 1: 43-55.
95. Luker, G. D., Bardill, J. P., Prior, J. L., Pica, C. M., Piwnica-Worms, D., and Leib, D. A. (2002). Noninvasive bioluminescence imaging of herpes simplex virus type 1 infection and therapy in living mice. *J Virol* 76: 12149-12161.
96. Yoshimitsu, M., et al. (2004). Bioluminescent imaging of a marking transgene and correction of Fabry mice by neonatal injection of recombinant lentiviral vectors. *Proc Natl Acad Sci U S A* 101: 16909-16914.
97. Zacharias, D. A., and Tsien, R. Y. (2006). Molecular biology and mutation of green fluorescent protein. *Methods Biochem Anal* 47: 83-120.
98. Giepmans, B. N. G., Adams, S. R., Ellisman, M. H., and Tsien, R. Y. (2006). The Fluorescent Toolbox for Assessing Protein Location and Function. *Science* 312: 217-224.
99. Patterson, G. H. (2004). A new harvest of fluorescent proteins. *Nat Biotechnol* 22: 1524-1525.
100. Shaner, N. C., Campbell, R. E., Steinbach, P. A., Giepmans, B. N., Palmer, A. E., and Tsien, R. Y. (2004). Improved monomeric red, orange and yellow fluorescent proteins derived from *Discosoma* sp. red fluorescent protein. *Nat Biotechnol* 22: 1567-1572.
101. Wang, L., Jackson, W. C., Steinbach, P. A., and Tsien, R. Y. (2004). Evolution of new nonantibody proteins via iterative somatic hypermutation. *PNAS* 101: 16745-16749.
102. Baens, M., et al. (2006). The dark side of EGFP: defective polyubiquitination. *PLoS ONE* 1: e54.
103. Huang, W.-Y., Aramburu, J., Douglas, P. S., and Izumo, S. (2000). Transgenic expression of green fluorescence protein can cause dilated cardiomyopathy. *Nat Med* 6: 482-483.

104. Klein, R. L., Dayton, R. D., Leidenheimer, N. J., Jansen, K., Golde, T. E., and Zweig, R. M. (2006). Efficient neuronal gene transfer with AAV8 leads to neurotoxic levels of tau or green fluorescent proteins. *Mol Ther* 13: 517-527.
105. Hakamata, Y., Murakami, T., and Kobayashi, E. (2006). "Firefly rats" as an organ/cellular source for long-term in vivo bioluminescent imaging. *Transplantation* 81: 1179-1184.
106. Gilad, A. A., Winnard, P. T., Jr., van Zijl, P. C., and Bulte, J. W. (2007). Developing MR reporter genes: promises and pitfalls. *NMR Biomed* 20: 275-290.
107. Koretsky, A., Brosnan, M., Chen, L., Chen, J., and Dyke, T. (1990). NMR Detection of Creatine Kinase Expressed in Liver of Transgenic Mice: Determination of Free ADP Levels. *PNAS* 87: 3112-3116.
108. Auricchio, A., Zhou, R., Wilson, J. M., and Glickson, J. D. (2001). In vivo detection of gene expression in liver by P-31 nuclear magnetic resonance spectroscopy employing creatine kinase as a marker gene. *Proceedings of the National Academy of Sciences of the United States of America* 98: 5205-5210.
109. Li, Z., et al. (2005). Creatine kinase, a magnetic resonance-detectable marker gene for quantification of liver-directed gene transfer. *Hum Gene Ther* 16: 1429-1438.
110. Walter, G., Barton, E. R., and Sweeney, H. L. (2000). Noninvasive measurement of gene expression in skeletal muscle. *PNAS* 97: 5151-5155.
111. Ki, S., et al. (2006). A novel magnetic resonance-based method to measure gene expression in living cells. *Nucl. Acids Res.* 34: e51-.
112. Ki, S., Sugihara, F., Kasahara, K., Tochio, H., Shirakawa, M., and Kokubo, T. (2007). Magnetic resonance-based visualization of gene expression in mammalian cells using a bacterial polyphosphate kinase reporter gene. *Biotechniques* 42: 209-215.
113. Stegman, L. D., et al. (1999). Noninvasive quantitation of cytosine deaminase transgene expression in human tumor xenografts with in vivo magnetic resonance spectroscopy. *Proc Natl Acad Sci U S A* 96: 9821-9826.
114. Dresselaers, T., et al. (2003). Non-invasive ¹⁹F MR spectroscopy of 5-fluorocytosine to 5-fluorouracil conversion by recombinant Salmonella in tumours. *Br J Cancer* 89: 1796-1801.
115. Cui, W., Otten, P., Li, Y., Koeneman, K. S., Yu, J., and Mason, R. P. (2004). Novel NMR approach to assessing gene transfection: 4-fluoro-2-nitrophenyl-beta-D-galactopyranoside as a prototype reporter molecule for beta-galactosidase. *Magn Reson Med* 51: 616-620.
116. Louie, A. Y., et al. (2000). In vivo visualization of gene expression using magnetic resonance imaging. *Nat Biotechnol* 18: 321-325.
117. Weissleder, R., et al. (2000). In vivo magnetic resonance imaging of transgene expression. *Nat Med* 6: 351-355.
118. Moore, A., Josephson, L., Bhorade, R. M., Basilion, J. P., and Weissleder, R. (2001). Human transferrin receptor gene as a marker gene for MR imaging. *Radiology* 221: 244-250.
119. So, P. W., Hotee, S., Herlihy, A. H., and Bell, J. D. (2005). Generic method for imaging transgene expression. *Magn Reson Med* 54: 218-221.
120. Mantyla, T., Hakumaki, J. M., Huhtala, T., Narvanen, A., and Yla-Herttuala, S. (2006). Targeted magnetic resonance imaging of Scavidin-receptor in human umbilical vein endothelial cells in vitro. *Magn Reson Med* 55: 800-804.
121. Weissleder, R., Simonova, M., Bogdanova, A., Bredow, S., Enochs, W. S., and Bogdanov, A., Jr. (1997). MR imaging and scintigraphy of gene expression through melanin induction. *Radiology* 204: 425-429.
122. Alfke, H., et al. (2003). In vitro MR imaging of regulated gene expression. *Radiology* 228: 488-492.
123. Genove, G., Demarco, U., Xu, H., Goins, W. F., and Ahrens, E. T. (2005). A new transgene reporter for in vivo magnetic resonance imaging. *Nat Med* 11: 450-454.
124. Cohen, B., Dafni, H., Meir, G., Harmelin, A., and Neeman, M. (2005). Ferritin as an endogenous MRI reporter for noninvasive imaging of gene expression in C6 glioma tumors. *Neoplasia* 7: 109-117.

125. Deans, A. E., Wadghiri, Y. Z., Bernas, L. M., Yu, X., Rutt, B. K., and Turnbull, D. H. (2006). Cellular MRI contrast via coexpression of transferrin receptor and ferritin. *Magn Reson Med* 56: 51-59.
126. Cohen, B., et al. (2007). MRI detection of transcriptional regulation of gene expression in transgenic mice. *Nat Med* 13: 498-503.
127. Gilad, A. A., et al. (2007). Artificial reporter gene providing MRI contrast based on proton exchange. *Nat Biotechnol* 25: 217-229.
128. Debyser, Z. (2003). Biosafety of lentiviral vectors. *Curr Gene Ther* 3: 517-525.
129. Mitchell, R. S., et al. (2004). Retroviral DNA integration: ASLV, HIV, and MLV show distinct target site preferences. *PLoS Biol* 2: E234.
130. Manilla, P., et al. (2005). Regulatory considerations for novel gene therapy products: a review of the process leading to the first clinical lentiviral vector. *Hum Gene Ther* 16: 17-25.
131. Cavazzana-Calvo, M., and Fischer, A. (2007). Gene therapy for severe combined immunodeficiency: are we there yet? *J Clin Invest* 117: 1456-1465.
132. Naldini, L., et al. (1996). In vivo gene delivery and stable transduction of nondividing cells by a lentiviral vector. *Science* 272: 263-267.
133. Lauwers, E., Debyser, Z., Van Dorpe, J., De Strooper, B., Nuttin, B., and Baekelandt, V. (2003). Neuropathology and neurodegeneration in rodent brain induced by lentiviral vector-mediated overexpression of alpha-synuclein. *Brain Pathol* 13: 364-372.
134. Lo Bianco, C., et al. (2004). Lentiviral vector delivery of parkin prevents dopaminergic degeneration in an alpha-synuclein rat model of Parkinson's disease. *Proc Natl Acad Sci U S A* 101: 17510-17515.
135. Baekelandt, V., Eggermont, K., Michiels, M., Nuttin, B., and Debyser, Z. (2003). Optimized lentiviral vector production and purification procedure prevents immune response after transduction of mouse brain. *Gene Ther* 10: 1933-1940.
136. Kordower, J. H., et al. (2000). Neurodegeneration prevented by lentiviral vector delivery of GDNF in primate models of Parkinson's disease. *Science* 290: 767-773.
137. Kyrkanides, S., Miller, J. H., Brouxon, S. M., Olschowka, J. A., and Federoff, H. J. (2005). beta-hexosaminidase lentiviral vectors: transfer into the CNS via systemic administration. *Brain Res Mol Brain Res* 133: 286-298.
138. Mazarakis, N. D., et al. (2001). Rabies virus glycoprotein pseudotyping of lentiviral vectors enables retrograde axonal transport and access to the nervous system after peripheral delivery. *Hum Mol Genet* 10: 2109-2121.
139. Van den Haute, C., Eggermont, K., Nuttin, B., Debyser, Z., and Baekelandt, V. (2003). Lentiviral vector-mediated delivery of short hairpin RNA results in persistent knockdown of gene expression in mouse brain. *Hum Gene Ther* 14: 1799-1807.
140. Ralph, G. S., et al. (2005). Silencing mutant SOD1 using RNAi protects against neurodegeneration and extends survival in an ALS model. *Nat Med* 11: 429-433.
141. Raoul, C., et al. (2005). Lentiviral-mediated silencing of SOD1 through RNA interference retards disease onset and progression in a mouse model of ALS. *Nat Med* 11: 423-428.
142. Naldini, L., Blomer, U., Gage, F. H., Trono, D., and Verma, I. M. (1996). Efficient transfer, integration, and sustained long-term expression of the transgene in adult rat brains injected with a lentiviral vector. *Proc Natl Acad Sci U S A* 93: 11382-11388.
143. Geraerts, M., Willems, S., Baekelandt, V., Debyser, Z., and Gijssbers, R. (2006). Comparison of lentiviral vector titration methods. *BMC Biotechnol* 6: 34.
144. Zufferey, R., Nagy, D., Mandel, R. J., Naldini, L., and Trono, D. (1997). Multiply attenuated lentiviral vector achieves efficient gene delivery in vivo. *Nat Biotechnol* 15: 871-875.
145. Dull, T., et al. (1998). A third-generation lentivirus vector with a conditional packaging system. *J Virol* 72: 8463-8471.
146. Hacein-Bey-Abina, S., et al. (2003). LMO2-associated clonal T cell proliferation in two patients after gene therapy for SCID-X1. *Science* 302: 415-419.

147. Philippe, S., et al. (2006). Lentiviral vectors with a defective integrase allow efficient and sustained transgene expression in vitro and in vivo. *Proc Natl Acad Sci U S A* 103: 17684-17689.
148. De Rijck, J., Vandekerckhove, L., Christ, F., and Debyser, Z. (2007). Lentiviral nuclear import: a complex interplay between virus and host. *Bioessays* 29: 441-451.
149. Follenzi, A., Ailles, L. E., Bakovic, S., Geuna, M., and Naldini, L. (2000). Gene transfer by lentiviral vectors is limited by nuclear translocation and rescued by HIV-1 pol sequences. *Nat Genet* 25: 217-222.
150. Kingsman, S. M., Mitrophanous, K., and Olsen, J. C. (2005). Potential oncogene activity of the woodchuck hepatitis post-transcriptional regulatory element (WPRE). *Gene Ther* 12: 3-4.
151. Cronin, J., Zhang, X. Y., and Reiser, J. (2005). Altering the tropism of lentiviral vectors through pseudotyping. *Curr Gene Ther* 5: 387-398.
152. Stein, C. S., Martins, I., and Davidson, B. L. (2005). The Lymphocytic Choriomeningitis Virus Envelope Glycoprotein Targets Lentiviral Gene Transfer Vector to Neural Progenitors in the Murine Brain. *Mol Ther* 11: 382-389.
153. Kafri, T., van Praag, H., Gage, F. H., and Verma, I. M. (2000). Lentiviral vectors: regulated gene expression. *Mol Ther* 1: 516-521.
154. Ray, P., De, A., Min, J. J., Tsien, R. Y., and Gambhir, S. S. (2004). Imaging tri-fusion multimodality reporter gene expression in living subjects. *Cancer Res* 64: 1323-1330.
155. Ray, P., Tsien, R., and Gambhir, S. S. (2007). Construction and validation of improved triple fusion reporter gene vectors for molecular imaging of living subjects. *Cancer Res* 67: 3085-3093.
156. Szymczak, A. L., and Vignali, D. A. (2005). Development of 2A peptide-based strategies in the design of multicistronic vectors. *Expert Opin Biol Ther* 5: 627-638.
157. Ellis, J. (2005). Silencing and variegation of gammaretrovirus and lentivirus vectors. *Hum Gene Ther* 16: 1241-1246.
158. Ni, Y., et al. (2005). Generation of a packaging cell line for prolonged large-scale production of high-titer HIV-1-based lentiviral vector. *J Gene Med* 7: 818-834.
159. Wiznerowicz, M., and Trono, D. (2005). Harnessing HIV for therapy, basic research and biotechnology. *Trends Biotechnol* 23: 42-47.
160. Levine, B. L., et al. (2006). Gene transfer in humans using a conditionally replicating lentiviral vector. *Proc Natl Acad Sci U S A* 103: 17372-17377.
161. Bank, A., Dorazio, R., and Leboulch, P. (2005). A phase I/II clinical trial of beta-globin gene therapy for beta-thalassemia. *Ann N Y Acad Sci* 1054: 308-316.
162. McConnell, M. J., and Imperiale, M. J. (2004). Biology of adenovirus and its use as a vector for gene therapy. *Hum Gene Ther* 15: 1022-1033.
163. Meier, O., and Greber, U. F. (2004). Adenovirus endocytosis. *J Gene Med* 6 Suppl 1: S152-163.
164. Verma, I. M., and Weitzman, M. D. (2005). Gene therapy: twenty-first century medicine. *Annu Rev Biochem* 74: 711-738.
165. Vasileva, A., and Jessberger, R. (2005). Precise hit: adeno-associated virus in gene targeting. *Nat Rev Microbiol* 3: 837-847.
166. McCarty, D. M., Young, S. M., Jr., and Samulski, R. J. (2004). Integration of adeno-associated virus (AAV) and recombinant AAV vectors. *Annu Rev Genet* 38: 819-845.
167. Nakai, H., et al. (2005). Large-scale molecular characterization of adeno-associated virus vector integration in mouse liver. *J Virol* 79: 3606-3614.
168. Nakai, H., Montini, E., Fuess, S., Storm, T. A., Grompe, M., and Kay, M. A. (2003). AAV serotype 2 vectors preferentially integrate into active genes in mice. *Nat Genet* 34: 297-302.
169. Frampton, A. R., Jr., Goins, W. F., Nakano, K., Burton, E. A., and Glorioso, J. C. (2005). HSV trafficking and development of gene therapy vectors with applications in the nervous system. *Gene Ther* 12: 891-901.
170. Molnar, M. J., et al. (2004). Factors influencing the efficacy, longevity, and safety of electroporation-assisted plasmid-based gene transfer into mouse muscles. *Mol Ther* 10: 447-455.

171. Liu, F., Song, Y., and Liu, D. (1999). Hydrodynamics-based transfection in animals by systemic administration of plasmid DNA. *Gene Ther* 6: 1258-1266.
172. Yoshino, H., Hashizume, K., and Kobayashi, E. (2006). Naked plasmid DNA transfer to the porcine liver using rapid injection with large volume. *Gene Ther* 13: 1696-1702.
173. Ruiz, F. E., et al. (2001). A clinical inflammatory syndrome attributable to aerosolized lipid-DNA administration in cystic fibrosis. *Hum Gene Ther* 12: 751-761.
174. Gao, X., Kim, K. S., and Liu, D. (2007). Nonviral gene delivery: what we know and what is next. *Aaps J* 9: E92-104.
175. Baekelandt, V., et al. (2000). DNA-Dependent protein kinase is not required for efficient lentivirus integration. *J Virol* 74: 11278-11285.
176. Baekelandt, V., et al. (2002). Characterization of lentiviral vector-mediated gene transfer in adult mouse brain. *Hum Gene Ther* 13: 841-853.
177. Geraerts, M., Eggermont, K., Hernandez-Acosta, P., Garcia-Verdugo, J.-M., Baekelandt, V., and Debyser, Z. (2006). Lentiviral Vectors Mediate Efficient and Stable Gene Transfer in Adult Neural Stem Cells In Vivo. *Human Gene Therapy* 17: 635-650.
178. Consiglio, A., et al. (2004). Robust in vivo gene transfer into adult mammalian neural stem cells by lentiviral vectors. *Proc Natl Acad Sci U S A* 101: 14835-14840.
179. Chambers, A. F., Groom, A. C., and MacDonald, I. C. (2002). Dissemination and growth of cancer cells in metastatic sites. *Nat Rev Cancer* 2: 563-572.
180. Le, L. Q., Kabarowski, J. H., Wong, S., Nguyen, K., Gambhir, S. S., and Witte, O. N. (2002). Positron emission tomography imaging analysis of G2A as a negative modifier of lymphoid leukemogenesis initiated by the BCR-ABL oncogene. *Cancer Cell* 1: 381-391.
181. Chitneni, S. K., et al. (2007). Synthesis and Preliminary Evaluation of (18)F- or (11)C-Labeled Bicyclic Nucleoside Analogues as Potential Probes for Imaging Varicella-Zoster Virus Thymidine Kinase Gene Expression Using Positron Emission Tomography. *J Med Chem* 50: 1041-1049.
182. Hamacher, K., Coenen, H., and Stocklin, G. (1986). Efficient stereospecific synthesis of no-carrier-added 2-[18F]-fluoro-2-deoxy-D-glucose using aminopolyether supported nucleophilic substitution. *J Nucl Med* 27: 235-238.
183. Collisson, E. A., De, A., Suzuki, H., Gambhir, S. S., and Kolodney, M. S. (2003). Treatment of metastatic melanoma with an orally available inhibitor of the Ras-Raf-MAPK cascade. *Cancer Res* 63: 5669-5673.
184. Sienaert, R., Naesens, L., Brancale, A., De Clercq, E., McGuigan, C., and Balzarini, J. (2002). Specific Recognition of the Bicyclic Pyrimidine Nucleoside Analogs, a New Class of Highly Potent and Selective Inhibitors of Varicella-Zoster Virus (VZV), by the VZV-Encoded Thymidine Kinase. *Mol Pharmacol* 61: 249-254.
185. Zufferey, R., et al. (1998). Self-Inactivating Lentivirus Vector for Safe and Efficient In Vivo Gene Delivery. *J. Virol.* 72: 9873-9880.
186. De Rijck, J., et al. (2006). Overexpression of the lens epithelium-derived growth factor/p75 integrase binding domain inhibits human immunodeficiency virus replication. *J Virol* 80: 11498-11509.
187. De Rijck, J., and Debyser, Z. (2006). The central DNA flap of the human immunodeficiency virus type 1 is important for viral replication. *Biochem Biophys Res Commun* 349: 1100-1110.
188. Geraerts, M., Michiels, M., Baekelandt, V., Debyser, Z., and Gijssbers, R. (2005). Upscaling of lentiviral vector production by tangential flow filtration. *J Gene Med* 7: 1299-1310.
189. Loening, A. M., and Gambhir, S. S. (2003). AMIDE: a free software tool for multimodality medical image analysis. *Mol Imaging* 2: 131-137.
190. Contag, P. R., Olomu, I. N., Stevenson, D. K., and Contag, C. H. (1998). Bioluminescent indicators in living mammals. *Nat Med* 4: 245-247.
191. Gage, F. H. (2000). Mammalian neural stem cells. *Science* 287: 1433-1438.
192. Taupin, P. (2005). Adult neurogenesis in the mammalian central nervous system: functionality and potential clinical interest. *Med Sci Monit* 11: RA247-252.

193. Curtis, M. A., et al. (2007). Human Neuroblasts Migrate to the Olfactory Bulb via a Lateral Ventricular Extension. *Science* 315: 1243-1249.
194. Zhang, R. L., Zhang, Z. G., and Chopp, M. (2005). Neurogenesis in the adult ischemic brain: generation, migration, survival, and restorative therapy. *Neuroscientist* 11: 408-416.
195. Geraerts, M., Krylyshkina, O., Debysers, Z., and Baekelandt, V. (2007). Concise review: therapeutic strategies for Parkinson disease based on the modulation of adult neurogenesis. *Stem Cells* 25: 263-270.
196. Doetsch, F., Caille, I., Lim, D. A., Garcia-Verdugo, J. M., and Alvarez-Buylla, A. (1999). Subventricular zone astrocytes are neural stem cells in the adult mammalian brain. *Cell* 97: 703-716.
197. Kaplan, M. S., and Bell, D. H. (1984). Mitotic neuroblasts in the 9-day-old and 11-month-old rodent hippocampus. *J Neurosci* 4: 1429-1441.
198. Kempermann, G., Gast, D., Kronenberg, G., Yamaguchi, M., and Gage, F. H. (2003). Early determination and long-term persistence of adult-generated new neurons in the hippocampus of mice. *Development* 130: 391-399.
199. Kempermann, G., Kuhn, H. G., and Gage, F. H. (1997). More hippocampal neurons in adult mice living in an enriched environment. *Nature* 386: 493-495.
200. Bruel-Jungerman, E., Laroche, S., and Rampon, C. (2005). New neurons in the dentate gyrus are involved in the expression of enhanced long-term memory following environmental enrichment. *Eur J Neurosci* 21: 513-521.
201. Meshi, D., et al. (2006). Hippocampal neurogenesis is not required for behavioral effects of environmental enrichment. *Nat Neurosci* 9: 729-731.
202. Santarelli, L., et al. (2003). Requirement of hippocampal neurogenesis for the behavioral effects of antidepressants. *Science* 301: 805-809.
203. Bischofberger, J. (2007). Young and excitable: new neurons in memory networks. *Nat Neurosci* 10: 273-275.
204. Kee, N., Teixeira, C. M., Wang, A. H., and Frankland, P. W. (2007). Preferential incorporation of adult-generated granule cells into spatial memory networks in the dentate gyrus. *Nat Neurosci* 10: 355-362.
205. Lois, C., Garcia-Verdugo, J. M., and Alvarez-Buylla, A. (1996). Chain migration of neuronal precursors. *Science* 271: 978-981.
206. Saghatelian, A., Carleton, A., Lagier, S., de Chevigny, A., and Lledo, P. M. (2003). Local neurons play key roles in the mammalian olfactory bulb. *J Physiol Paris* 97: 517-528.
207. Hoglinger, G. U., et al. (2004). Dopamine depletion impairs precursor cell proliferation in Parkinson disease. *Nat Neurosci* 7: 726-735.
208. Freundlieb, N., Francois, C., Tande, D., Oertel, W. H., Hirsch, E. C., and Hoglinger, G. U. (2006). Dopaminergic substantia nigra neurons project topographically organized to the subventricular zone and stimulate precursor cell proliferation in aged primates. *J Neurosci* 26: 2321-2325.
209. Bengel, F. M., Schachinger, V., and Dimmeler, S. (2005). Cell-based therapies and imaging in cardiology. *European Journal of Nuclear Medicine and Molecular Imaging* V32: S404-S416.
210. Kirik, D., Breyse, N., Björklund, T., Besret, L., and Hantraye, P. (2005). Imaging in cell-based therapy for neurodegenerative diseases. *European Journal of Nuclear Medicine and Molecular Imaging* V32: S417-S434.
211. Sykova, E., and Jendelova, P. (2006). Magnetic resonance tracking of transplanted stem cells in rat brain and spinal cord. *Neurodegener Dis* 3: 62-67.
212. Weissleder, R., Cheng, H. C., Bogdanova, A., and Bogdanov, A., Jr. (1997). Magnetically labeled cells can be detected by MR imaging. *J Magn Reson Imaging* 7: 258-263.
213. Adonai, N., et al. (2002). Ex vivo cell labeling with ⁶⁴Cu-pyruvaldehyde-bis(N4-methylthiosemicarbazone) for imaging cell trafficking in mice with positron-emission tomography. *Proc Natl Acad Sci U S A* 99: 3030-3035.

214. Hofmann, M., et al. (2005). Monitoring of Bone Marrow Cell Homing Into the Infarcted Human Myocardium. *Circulation* 111: 2198-2202.
215. Blocklet, D., et al. (2006). Myocardial Homing of Nonmobilized Peripheral-Blood CD34+ Cells After Intracoronary Injection. *Stem Cells* 24: 333-336.
216. Hoehn, M., et al. (2002). Monitoring of implanted stem cell migration in vivo: a highly resolved in vivo magnetic resonance imaging investigation of experimental stroke in rat. *Proc Natl Acad Sci U S A* 99: 16267-16272.
217. Modo, M., et al. (2004). Mapping transplanted stem cell migration after a stroke: a serial, in vivo magnetic resonance imaging study. *Neuroimage* 21: 311-317.
218. Shyu, W. C., Chen, C. P., Lin, S. Z., Lee, Y. J., and Li, H. (2007). Efficient tracking of non-iron-labeled mesenchymal stem cells with serial MRI in chronic stroke rats. *Stroke* 38: 367-374.
219. Ben-Hur, T., et al. (2007). Serial in vivo MR tracking of magnetically labeled neural spheres transplanted in chronic EAE mice. *Magn Reson Med* 57: 164-171.
220. Zhang, Z., et al. (2004). In vivo magnetic resonance imaging tracks adult neural progenitor cell targeting of brain tumor. *Neuroimage* 23: 281-287.
221. Shah, K., et al. (2005). Glioma therapy and real-time imaging of neural precursor cell migration and tumor regression. *Ann Neurol* 57: 34-41.
222. Kim, D. E., et al. (2006). Neural stem cell transplant survival in brains of mice: assessing the effect of immunity and ischemia by using real-time bioluminescent imaging. *Radiology* 241: 822-830.
223. Pineda, J. R., et al. (2007). Neuroprotection by GDNF-secreting stem cells in a Huntington's disease model: optical neuroimage tracking of brain-grafted cells. *Gene Ther* 14: 118-128.
224. Miletic, H., et al. (2007). Bystander Killing of Malignant Glioma by Bone Marrow-derived Tumor-Infiltrating Progenitor Cells Expressing a Suicide Gene. *Mol Ther* 15: 1373-1381.
225. Munoz, J. R., Stoutenger, B. R., Robinson, A. P., Spees, J. L., and Prockop, D. J. (2005). Human stem/progenitor cells from bone marrow promote neurogenesis of endogenous neural stem cells in the hippocampus of mice. *PNAS* 102: 18171-18176.
226. Wu, J. C., Sundaresan, G., Iyer, M., and Gambhir, S. S. (2001). Noninvasive optical imaging of firefly luciferase reporter gene expression in skeletal muscles of living mice. *Mol Ther* 4: 297-306.
227. Blomer, U., Naldini, L., Kafri, T., Trono, D., Verma, I. M., and Gage, F. H. (1997). Highly efficient and sustained gene transfer in adult neurons with a lentivirus vector. *J Virol* 71: 6641-6649.
228. Shai, E., et al. (2005). Prolonged transgene expression in murine salivary glands following non-primate lentiviral vector transduction. *Mol Ther* 12: 137-143.
229. Lin, A. H., et al. (2005). Global analysis of Smad2/3-dependent TGF-beta signaling in living mice reveals prominent tissue-specific responses to injury. *J Immunol* 175: 547-554.
230. Troy, T., Jekic-McMullen, D., Sambucetti, L., and Rice, B. (2004). Quantitative comparison of the sensitivity of detection of fluorescent and bioluminescent reporters in animal models. *Mol Imaging* 3: 9-23.
231. Wang, G., Li, Y., and Jiang, M. (2004). Uniqueness theorems in bioluminescence tomography. *Med Phys* 31: 2289-2299.
232. Pan, D., et al. (2002). Biodistribution and Toxicity Studies of VSVG-Pseudotyped Lentiviral Vector after Intravenous Administration in Mice with the Observation of in Vivo Transduction of Bone Marrow. *Mol Ther* 6: 19-29.
233. Kobayashi, H., et al. (2005). Neonatal Gene Therapy of MPS I Mice by Intravenous Injection of a Lentiviral Vector. *Mol Ther* 11: 776-789.
234. Gambhir, S. S. (2002). Molecular imaging of cancer with positron emission tomography. *Nat Rev Cancer* 2: 683-693.
235. Yu, Y., et al. (2000). Quantification of target gene expression by imaging reporter gene expression in living animals. *Nat Med* 6: 933-937.

236. Adams, J. Y., et al. (2002). Visualization of advanced human prostate cancer lesions in living mice by a targeted gene transfer vector and optical imaging. *Nat Med* 8: 891-897.
237. Collisson, E. A., et al. (2003). Atorvastatin prevents RhoC isoprenylation, invasion, and metastasis in human melanoma cells. *Mol Cancer Ther* 2: 941-948.
238. Paulus, M. J., Gleason, S. S., Kennel, S. J., Hunsicker, P. R., and Johnson, D. K. (2000). High resolution X-ray computed tomography: an emerging tool for small animal cancer research. *Neoplasia* 2: 62-70.
239. Paulus, M. J., Gleason, S. S., Easterly, M. E., and Foltz, C. J. (2001). A review of high-resolution X-ray computed tomography and other imaging modalities for small animal research. *Lab Anim (NY)* 30: 36-45.
240. Weber, S. M., et al. (2004). Imaging of murine liver tumor using microCT with a hepatocyte-selective contrast agent: accuracy is dependent on adequate contrast enhancement. *J Surg Res* 119: 41-45.
241. Berger, F., et al. (2002). Whole-body skeletal imaging in mice utilizing microPET: optimization of reproducibility and applications in animal models of bone disease. *Eur J Nucl Med Mol Imaging* 29: 1225-1236.
242. Nakai, M., Mundy, G. R., Williams, P. J., Boyce, B., and Yoneda, T. (1992). A synthetic antagonist to laminin inhibits the formation of osteolytic metastases by human melanoma cells in nude mice. *Cancer Res* 52: 5395-5399.
243. Hiraga, T., Nakajima, T., and Ozawa, H. (1995). Bone resorption induced by a metastatic human melanoma cell line. *Bone* 16: 349-356.
244. Giavazzi, R., et al. (1990). Interleukin 1-induced augmentation of experimental metastases from a human melanoma in nude mice. *Cancer Res* 50: 4771-4775.
245. Seftor, R. E., Seftor, E. A., and Hendrix, M. J. (1999). Molecular role(s) for integrins in human melanoma invasion. *Cancer Metastasis Rev* 18: 359-375.
246. Kang, K. W., Min, J. J., Chen, X., and Gambhir, S. S. (2005). Comparison of [(14)C]FMAU, [(3)H]FEAU, [(14)C]FIAU, and [(3)H]PCV for Monitoring Reporter Gene Expression of Wild Type and Mutant Herpes Simplex Virus Type 1 Thymidine Kinase in Cell Culture. *Mol Imaging Biol* 7: 296-303.
247. Kondo, S., et al. (2004). Use of FDG-microPET for detection of small nodules in a rabbit model of pulmonary metastatic cancer. *Ann Nucl Med* 18: 51-57.
248. Seemann, M. D. (2004). Human PET/CT scanners: feasibility for oncological in vivo imaging in mice. *Eur J Med Res* 9: 468-472.
249. Jenkins, D. E., et al. (2003). Bioluminescent imaging (BLI) to improve and refine traditional murine models of tumor growth and metastasis. *Clin Exp Metastasis* 20: 733-744.
250. Edinger, M., Cao, Y. A., Verneris, M. R., Bachmann, M. H., Contag, C. H., and Negrin, R. S. (2003). Revealing lymphoma growth and the efficacy of immune cell therapies using in vivo bioluminescence imaging. *Blood* 101: 640-648.
251. Minn, A. J., et al. (2005). Distinct organ-specific metastatic potential of individual breast cancer cells and primary tumors. *J Clin Invest* 115: 44-55.
252. Smith, M. C., et al. (2004). CXCR4 regulates growth of both primary and metastatic breast cancer. *Cancer Res* 64: 8604-8612.
253. Ntziachristos, V., Ripoll, J., Wang, L. V., and Weissleder, R. (2005). Looking and listening to light: the evolution of whole-body photonic imaging. *Nat Biotechnol* 23: 313-320.
254. Kang, Y., et al. (2005). Breast cancer bone metastasis mediated by the Smad tumor suppressor pathway. *Proc Natl Acad Sci U S A* 102: 13909-13914.
255. Miyagawa, M., et al. (2004). PET of Cardiac Transgene Expression: Comparison of 2 Approaches Based on Herpesviral Thymidine Kinase Reporter Gene. *J Nucl Med* 45: 1917-1923.
256. Koehne, G., et al. (2003). Serial in vivo imaging of the targeted migration of human HSV-TK-transduced antigen-specific lymphocytes. *Nat Biotechnol* 21: 405-413.
257. Kim, S. J., et al. (2006). Quantitative micro positron emission tomography (PET) imaging for the in vivo determination of pancreatic islet graft survival. *Nat Med* 12: 1423-1428.

258. Deroose, C. M., et al. (2007). Multimodality Imaging of Tumor Xenografts and Metastasis in Mice with Combined Micro Positron Emission Tomography, Small Animal Computed Tomography and Bioluminescence Imaging. *The Journal of Nuclear Medicine* 48: 295-303.
259. Green, L. A., et al. (2002). Indirect monitoring of endogenous gene expression by positron emission tomography (PET) imaging of reporter gene expression in transgenic mice. *Mol Imaging Biol* 4: 71-81.
260. Richard, J. C., et al. (2004). Quantitation of pulmonary transgene expression with PET imaging. *J Nucl Med* 45: 644-654.
261. Chaudhuri, T. R., Rogers, B. E., Buchsbaum, D. J., Mountz, J. M., and Zinn, K. R. (2001). A Noninvasive Reporter System to Image Adenoviral-Mediated Gene Transfer to Ovarian Cancer Xenografts. *Gynecologic Oncology* 83: 432-438.
262. Rogers, B. E., Parry, J. J., Andrews, R., Cordopatis, P., Nock, B. A., and Maina, T. (2005). MicroPET Imaging of Gene Transfer with a Somatostatin Receptor-Based Reporter Gene and ^{94m}Tc-Demotate 1. *J Nucl Med* 46: 1889-1897.
263. Groot-Wassink, T., Aboagye, E. O., Glaser, M., Lemoine, N. R., and Vassaux, G. (2002). Adenovirus biodistribution and noninvasive imaging of gene expression in vivo by positron emission tomography using human sodium/iodide symporter as reporter gene. *Hum Gene Ther* 13: 1723-1735.
264. McGuigan, C., et al. (1999). Potent and selective inhibition of varicella-zoster virus (VZV) by nucleoside analogues with an unusual bicyclic base. *J Med Chem* 42: 4479-4484.
265. McGuigan, C., et al. (2000). Highly potent and selective inhibition of varicella-zoster virus by bicyclic furopyrimidine nucleosides bearing an aryl side chain. *J Med Chem* 43: 4993-4997.
266. Balzarini, J., et al. (2002). Lack of susceptibility of bicyclic nucleoside analogs, highly potent inhibitors of varicella-zoster virus, to the catabolic action of thymidine phosphorylase and dihydropyrimidine dehydrogenase. *Mol Pharmacol* 61: 1140-1145.
267. Toelen, J., et al. (2007). Fetal gene transfer with lentiviral vectors: long-term in vivo follow-up evaluation in a rat model. *Am J Obstet Gynecol* 196: 352 e351-356.
268. Borst, P., et al. (2004). The potential impact of drug transporters on nucleoside-analog-based antiviral chemotherapy. *Antiviral Res* 62: 1-7.
269. Deroose, C., et al. (2006). Imaging of lentiviral vector-mediated gene transfer to mouse muscle with micro positron emission tomography (PET) and bioluminescence imaging (BLI). *J Nucl Med* 47: 341P.
270. Balzarini, J., and McGuigan, C. (2002). Chemotherapy of varicella-zoster virus by a novel class of highly specific anti-VZV bicyclic pyrimidine nucleosides. *Biochim Biophys Acta* 1587: 287-295.
271. Balzarini, J., and McGuigan, C. (2002). Bicyclic pyrimidine nucleoside analogues (BCNAs) as highly selective and potent inhibitors of varicella-zoster virus replication. *J Antimicrob Chemother* 50: 5-9.
272. Kokoris, M. S., and Black, M. E. (2002). Characterization of herpes simplex virus type 1 thymidine kinase mutants engineered for improved ganciclovir or acyclovir activity. *Protein Sci* 11: 2267-2272.
273. Vercammen, L., et al. (2006). Parkin protects against neurotoxicity in the 6-hydroxydopamine rat model for Parkinson's disease. *Mol Ther* 14: 716-723.
274. Polymeropoulos, M. H., et al. (1997). Mutation in the {alpha}-Synuclein Gene Identified in Families with Parkinson's Disease. *Science* 276: 2045-2047.
275. Singleton, A. B., et al. (2003). alpha-Synuclein Locus Triplication Causes Parkinson's Disease. *Science* 302: 841-.
276. John Hardy, H. C., Mark R. Cookson, Katrina Gwinn-Hardy, Andrew Singleton, (2006). Genetics of Parkinson's disease and parkinsonism. *Annals of Neurology* 60: 389-398.
277. Hacein-Bey-Abina, S., et al. (2002). Sustained Correction of X-Linked Severe Combined Immunodeficiency by ex Vivo Gene Therapy. *N Engl J Med* 346: 1185-1193.

278. Woods, N. B., Bottero, V., Schmidt, M., von Kalle, C., and Verma, I. M. (2006). Gene therapy: therapeutic gene causing lymphoma. *Nature* 440: 1123.
279. Ott, M. G., et al. (2006). Correction of X-linked chronic granulomatous disease by gene therapy, augmented by insertional activation of MDS1-EV11, PRDM16 or SETBP1. *Nat Med* 12: 401-409.
280. Editorial (2006). One of three successfully treated CGD patients in a Swiss-German gene therapy trial died due to his underlying disease. *The Journal of Gene Medicine* 8: 1435.
281. Mavilio, F., et al. (2006). Correction of junctional epidermolysis bullosa by transplantation of genetically modified epidermal stem cells. *Nat Med* 12: 1397-1402.
282. Kaplitt, M. G., et al. (2007). Safety and tolerability of gene therapy with an adeno-associated virus (AAV) borne GAD gene for Parkinson's disease: an open label, phase I trial. *Lancet* 369: 2097-2105.
283. Snyder, E. Y., Deitcher, D. L., Walsh, C., Arnold-Aldea, S., Hartweg, E. A., and Cepko, C. L. (1992). Multipotent neural cell lines can engraft and participate in development of mouse cerebellum. *Cell* 68: 33-51.
284. Shapiro, E. M., Gonzalez-Perez, O., Manuel Garcia-Verdugo, J., Alvarez-Buylla, A., and Koretsky, A. P. (2006). Magnetic resonance imaging of the migration of neuronal precursors generated in the adult rodent brain. *NeuroImage* 32: 1150-1157.
285. Bhowmick, N. A., Neilson, E. G., and Moses, H. L. (2004). Stromal fibroblasts in cancer initiation and progression. *Nature* 432: 332-337.
286. Becher, O. J., Holland, E. C., Sausville, E. A., and Burger, A. M. (2006). Genetically Engineered Models Have Advantages over Xenografts for Preclinical Studies. *Cancer Res* 66: 3355-3359.
287. Killion, J. J., Radinsky, R., and Fidler, I. J. (1998). Orthotopic models are necessary to predict therapy of transplantable tumors in mice. *Cancer Metastasis Rev* 17: 279-284.
288. Lyons, S. K., Meuwissen, R., Krimpenfort, P., and Berns, A. (2003). The generation of a conditional reporter that enables bioluminescence imaging of Cre/loxP-dependent tumorigenesis in mice. *Cancer Res* 63: 7042-7046.
289. Safran, M., Kim, W. Y., Kung, A. L., Horner, J. W., DePinho, R. A., and Kaelin, W. G., Jr. (2003). Mouse reporter strain for noninvasive bioluminescent imaging of cells that have undergone Cre-mediated recombination. *Mol Imaging* 2: 297-302.

